CONCEPTS FOR A THEORETICAL AND EXPERIMENTAL STUDY OF LIFTING ROTOR RANDOM LOADS AND VIBRATIONS

(Effects of Blade Torsion, of Blade Flap Bending Flexibility and of Rotor Support Flexibility on Rotor Stability and Random Response)

Phase VI-A Report under Contract NAS2-4151

by

Kurt H. Hohenemser

and

S. K. Yin

Department of Mechanical and Aerospace Engineering

Washington University
School of Engineering and Applied Science
St. Louis, Missouri

June, 1972

CONCEPTS FOR A THEORETICAL AND EXPERIMENTAL STUDY OF LIFTING ROTOR RANDOM LOADS AND VIBRATIONS

(Effects of Blade Torsion, of Blade Flap Bending Flexibility and of Rotor Support Flexibility on Rotor Stability and Random Response)

Phase VI-A Report under Contract NAS2-4151

Prepared for the Ames Directorate, AMRDL,
at Ames Research Center, Moffett Field, California

by Kurt H. Hohenemser

Kurt H. Hohenemser

and Sheng K. Yin

S. K. Yin

Washington University
School of Engineering and Applied Science
St. Louis, Missouri

June, 1972

Scope of Contract NAS2-4151

Work under Contract NAS2-4151 started on February 1, 1967. Phase I Report of September 1967 develops analytical concepts for a random loads and vibration analysis of lifting rotors. Phase II Report of August 1968 presents a perturbation solution method for random blade flapping. Phase III Report of June 1969 develops a more general method to include high rotor advance ratios and makes use of a specific atmospheric turbulence model. Phase IV Report of June 1970 extends the method to the computation of threshold crossing statistics for random blade flapping and introduces non-uniformity of the vertical turbulence velocity in the longitudinal direction. Phase V-A Report of June 1971 treats the effects of torsional blade flexibility on single blade random gust response statistics. Phase V-B Report of June 1971 presents a multiblade coordinate analysis of coupled blade dynamic stability and random response, studying various gust alleviation methods. Phase V-C Report of June 1971 describes the development of experimental methods of substantiating the random loads and vibration analysis.

During FY 1972 the work was extended in two directions, resulting in two separate Phase VI reports. Phase VI-A Report covers three refinements of the preceding analysis. The effects of blade torsion on dynamic stability and random

response has been analyzed beyond Phase V-A Report, adding new insights into this subject matter. The effects of blade flap bending flexibility on rotor stability and random response have been studied leading to a simple method of correcting the rigid blade analysis. Finally the effects of rotor support flexibility have been analyzed, solving the problem of whirl flutter in high advance ratio oblique flow. Phase VI-B Report covers the experimental work performed in FY 1972 to substantiate the analysis. The work summarized in Phase VI-A and Phase VI-B Reports was performed under Modification 7 to subject contract, which covers also FY 1973. The scope of the work planned for FY 1973 is to further remove limitations to the present analytical model and at the same time to simplify the methods of analysis, and to conduct further tests in support of the analysis.

The following is a list of publications sponsored under subject research contract issued to date.

1. Gaonkar, G. H. and Hohenemser, K. H., "Flapping Response of Lifting Rotor Blades to Atmospheric Turbulence", Journal of Aircraft, Vol. 6, No. 6, Nov.-Dec. 1969, pp. 496-503. First presented as AIAA Paper 69-206 at the AIAA/AHS VTOL Meeting, Atlanta, Georgia, February 1969.

2. Gaonkar, G. H. and Hohenemser, K. H., "Stochastic Properties of Turbulence Excited Rotor Blade Vibrations", AIAA Journal, Vol. 9, No. 3, March 1971, pp. 419-424. First presented as AIAA Paper 70-548 at the AIAA Atmospheric Flight Mechanics Conference, Tullahoma, Tennessee, May 1970.

3. Gaonkar, G. H. and Hohenemser, K. H., "Comparison of Two Stochastic Models for Threshold Crossing Studies of Rotor Blade Flapping Vibrations", Presented as AIAA Paper 71-389 at the AIAA/ASME 12th Structures Conference, Anaheim, California, April 1971.

4. Gaonkar, G. H. and Hohenemser, K. H., "An Advanced Stochastic Model for Threshold Crossing Studies of Rotor Blade Vibrations", AIAA Journal, Vol. 10, No. 6, July 1972.

5. Yin, S. K. and Hohenemser, K. H., "The Method of Multiblade Coordinates in the Linear Analysis of Lifting Rotor Dynamic Stability and Gust Response", Presented as AHS Preprint No. 512 at the 27th Annual National Forum of the AHS, Washington, D. C., May 1971.

6. Hohenemser, K. H. and Yin, S. K., "Some Applications of the Method of Multiblade Coordinates", Journal of the American Helicopter Society, Vol. 17, No. 3, July 1972.

CONCEPTS FOR A THEORETICAL AND EXPERIMENTAL STUDY OF LIFTING ROTOR RANDOM LOADS AND VIBRATIONS

Phase VI-A

(Effects of Blade Torsion, of Blade Flap Bending Flexibility and of Rotor Support Flexibility on Rotor Stability and Random Response)

by

Kurt H. Hohenemser
and
S. K. Yin

Washington University
St. Louis, Missouri

Organization of Report

Because of the relative independence of the three subject matters treated in this report, each of the three parts has its own abstract, nomenclature, introduction, list of references, figure captions and appendices. For the sake of completeness the first part includes in abbreviated form also material from Phase V-A Report of June 1971. The remainder of Part I and Parts II and III contain new results obtained in FY 1972. The addendum by D. A. Prelewicz*, though not sponsored by subject contract, has been stimulated by the contract research and is presented here because it views the various applied stochastic methods in a broader frame of reference.

*Assistant Professor, Dept. Applied Math & Computer Sciences, Washington University, St. Louis, Missouri

CONCEPTS FOR A THEORETICAL AND EXPERIMENTAL STUDY OF LIFTING ROTOR RANDOM LOADS AND VIBRATIONS

Phase VI-A

(Effects of Blade Torsion, of Blade Flap Bending Flexibility and of Rotor Support Flexibility on Rotor Stability and Random Response)

Table of Contents

Part I

Random Gust Response Statistics for Coupled Torsion-Flapping Rotor Blade Vibrations

Abstract

An analysis of coupled torsion-flapping rotor blade vibrations in response to atmospheric turbulence revealed that at high rotor advance ratios anticipated for future high speed pure or convertible rotorcraft both flapping and torsional vibrations can be severe. While appropriate feedback systems can alleviate flapping, they have little effect on torsion. Dynamic stability margins have also no substantial influence on dynamic torsion loads. The only effective means found to alleviate turbulence caused torsional vibrations and loads at high advance ratio was a substantial margin with respect to static torsional divergence of the retreating blade.

Nomenclature

$A(t)$	state matrix
$A^T(t)$	transpose of $A(t)$
$a = 2\mu/(L/R)$	nondimensional turbulence parameter
B	tip-loss factor
$C(t), C_\delta(t), C_{\theta_o}(t)$	aerodynamic damping
c	blade chord
$E[\ . \ . \ .]$	mathematical expectation of $[\ . \ . \ .]$
$E[N_{+x_j}(\zeta,t)]$	time variable expected number of positive crossings per unit time of threshold ζ for response component X_j
$F = (I_1/I_f)(c/4R)^2$	nondimensional quantity
$f\Omega$	blade torsional frequency
I	identity matrix
I_1	flapping mass moment of inertia
I_f	feathering mass moment of inertia
$K(t), K_\delta(t)$	aerodynamic stiffness
K_f	flapping feedback gain
K_o	coning feedback gain
L	scale of longitudinal turbulence
$l_{r\beta}(t), l_{r\dot{\beta}}(t), l_{r\theta_o}(t), l_{r\lambda}(t)$	aerodynamic lift, reversed flow region
$m_{\theta_o}(t), m_{\theta_1}(t), m_\lambda(t)$	aerodynamic flapping moments
N	number of blades per rotor
$n(t)$	white noise input vector
$P\Omega$	blade flapping frequency

$Q = (I_l/I_f)(c/4R)$	nondimensional quantity
R	rotor radius
$R_{xx}(t_1,t_2)$	correlation matrix of $X(t)$
$R_{xx}(t,t) = P(t)$	variance matrix of $X(t)$
t	nondimensional time, time unit $1/\Omega$
V	flight velocity
w	vertical turbulence velocity
$X(t)$	state or output vector
$X^T(t)$	transpose of $X(t)$
β	blade flapping angle
γ	blade Lock inertia number
δ	torsional elastic deflection from root to blade tip
$\delta(...)$	Dirac delta function
ζ	response value exceeded in a threshold crossing
θ_o	blade root pitch angle
$\lambda = w/\Omega R$	nondimensional vertical turbulence velocity
$\mu = V/\Omega R$	rotor advance ratio
ξ	real part of characteristic value
$\sigma_{x_j}(t) = [R_{x_j x_j}(t)]^{1/2}$	standard deviation of $x_j(t)$
σ_β	standard deviation of β
σ_δ	standard deviation of δ
τ	nondimensional time, time unit $1/\Omega$
$\phi(t,\tau)$	state transition matrix
Ω	angular rotor speed

Introduction

The problem of random rotor blade flapping vibrations caused by atmospheric turbulence has been studied earlier.[1] It was found that at high rotor advance ratios anticipated for future high speed pure or convertible rotorcraft, severe random vibrations and dynamic loads can occur, unless flapping or hub moment feedback systems are applied.[2] The blade representation used in these studies was a rigid straight blade flexibly attached at the rotor center, using quasi-steady linear aerodynamics including reversed flow effects but excluding non-uniform inflow, stall and compressibility effects.[3] Extensive wind-tunnel tests have shown that this representation gives useful approximations to the flapping response for low lift high advance ratio conditions, if the root flexibility is appropriately selected to represent the actual blade.[4] Even if the elastic center, the center of gravity and the aerodynamic center of the rotor blade cross-section coincide, as they usually approximately do in practical blade designs, large blade torsional moments occur in the region of reversed flow, because the aerodynamic center is then shifted from the quarter chord point to the three quarter chord point.[5] It is, therefore of interest to study the effects of atmospheric turbulence on the coupled torsion-flapping rotor blade vibrations.

Blade Representation and Method of Analysis

It is assumed that the blade torsion mode is a straight line through the rotor center, that in regions of normal flow direction the aerodynamic center, the center of gravity and the shear center of blade cross-section coincide, and that linear quasi-static aerodynamics are used. Because of the higher frequency of the torsional vibrations the last assumption is more questionnable than for the flapping case and as yet no tests are available to substantiate the analysis of Reference 5. Though quantitatively the results to be presented here may require some corrections due to over simplified aerodynamic assumptions the established important trends should remain valid, if reversed flow stall flutter is avoided.[6]

When the dynamic equations of blade flapping and blade torsion, given in Reference (5), are extended to include the effect of root pitch angle θ_o, one obtains

$$(2/\gamma)\ddot{\beta} + C(t)\dot{\beta} + [(2P^2/\gamma) + K(t)]\beta - m_{\theta_1}(t)\delta = m_\lambda(t)\lambda + m_{\theta_o}(t)\theta_o \tag{1}$$

$$(1/3\gamma)\ddot{\delta} + FC_\delta(t)\dot{\delta} + [(f^2/3\gamma) + QK_\delta(t)]\delta + Q\ell_{r\dot{\beta}}(t)\dot{\beta} + Q\ell_{r\beta}(t)\beta + (1/2\gamma)\ddot{\theta}_o + FC_{\theta_o}(t)\dot{\theta}_o = -Q[\ell_{r\lambda}(t)\lambda + \ell_{r\theta_o}(t)\theta_o] \tag{2}$$

The flapping feedback is assumed to occur without producing a mechanical flapping moment. The only periodic coefficient not defined in either Reference (3) or (5) is $\ell_{r\theta_o}$ with the value in the normal flow region,

$$\ell_{r\theta_o} = 0$$

$$l_{r\theta_o} = \mu^4[-(1/32) + (1/24)\cos 2t - (1/96)\cos 4t]$$

in the mixed flow region, and

$$l_{r\theta_o} = -[(B^4/4) + (B^2\mu^4/4)] - (2/3)B^3\mu\sin t + (B^2\mu^2/4)\cos 2t$$

in the reversed flow region.

For the blade without feedback, $\theta_o = 0$. In case of pitch-flap coupling, θ_o is to be replaced by

$$\theta_o = -K_f\beta \tag{3a}$$

In case of coning angle feedback, θ_o is to be replaced by

$$\theta_o = -K_o\left((1/N)\sum_{K=1}^{N}\beta_k\right) \tag{3b}$$

where all blades are assumed to perform the same flapping motion except for appropriate phase shifts.

In order to obtain from Eqs. (1) to (3) the response to the random vertical gust velocity λ, it is assumed that this gust velocity at a point in time is uniformly distributed over the rotor disk, an assumption which has been proven approximately valid for current ratios of turbulence scale L over rotor radius R.[7] If one approximates the widely used von Kármán-Taylor Turbulence spectrum by one with exponential autocorrelation function,[1] the dimensionless vertical turbulence velocity λ is determined from[7,8]

$$\dot{\lambda} + a\lambda = \sigma_\lambda(2a)^{1/2}n(t) \tag{4}$$

where n(t) has the autocorrelation function

$$R_n(\tau) = \delta(\tau) \tag{5}$$

We now express the dynamic equations (1) to (4) in state variable form

$$\dot{X}(t) = A(t)\ X(t) + B(t)\ n(t) \tag{6}$$

The response variance P(t) can then be determined from the matrix equation[8,9,10]

$$\dot{P}(t) = A(t)\ P(t) + P(t)\ A^T(t) + B(t)\ B^T(t) \tag{7}$$

with zero initial state, and the response covariance matrix is obtained from

$$\begin{aligned} R_{xx}(t_1,t_2) &= \phi(t_1,t_2)\ P(t_2) \quad \text{for } t_1 \geqslant t_2 \\ &= P(t_1)\ \ \phi^T(t_2,t_1) \quad \text{for } t_1 \leqslant t_2 \end{aligned} \tag{8}$$

where the state transition matrix is defined by

$$\dot{\phi}(t,\tau) = A(t)\ \phi(t,\tau),\ \phi(\tau,\tau) = I \tag{9}$$

Once the response covariance matrix is known, the threshold crossing expectations can be determined from expressions given in the literature.[7]

For an alternative method[1] the covariance matrix is

$$R_{xx}(t_1,t_2) = \int_{-\infty}^{\infty} H^*(\omega,t_1)\ S_\lambda(\omega)\ H^T(\omega,t_2)\,d\omega \tag{10}$$

with

$$S_\lambda(\omega)/\sigma_\lambda^2 = a/\pi(a^2+\omega^2) \tag{11}$$

and $H(\omega,t)$ the response vector to the input $\lambda(t) = u(t)\exp i\omega t$, $u(t)$ being the unit step function. The numerical examples were computed with the second method, truncating $S_\lambda(\omega)$ at $|\omega| > 3$. The first method gives slightly different results with about one third the computational effort.

Numerical Results

As before[1], the numerical data are for a lifting rotor operating with a rotor advance ratio of $\mu = 1.6$, which corresponds at a flight speed of 280 Knots to a blade tip speed of $\Omega R = 300$ fps. In the stochastic analysis the standard deviation of the dimensionless vertical turbulence velocity $\lambda = w/\Omega R$ is assumed to be $\sigma_\lambda = 1$, which results in Eq. (4). 8 fps is a representative value[1] for the standard deviation of the vertical turbulence velocity, occurring at low altitudes with .1% probability. Using this value and $\Omega R = 300$ fps we have $\sigma_\lambda = 1.5°$. The non-dimensional standard deviations σ_β, σ_δ for flapping and elastic blade twist respectively, and the thresholds ζ shown in the figures must then be multiplied by 1.5 to obtain the dimensional values of these quantities in degrees. The remaining rotor parameters are also the same as before[1]: Tip loss factor $B = .97$, Lock number $\gamma = 4$ and turbulence scale over rotor radius $L/R = 12$, which corresponds for a rotor radius of 33 ft to 400 ft turbulence scale length, typical of low altitude turbulence. The flapping frequency ratio is assumed as $P = 1.3$. Further assumed is a flapping over feathering inertia ratio of $I_1/I_f = 940$ and a radius over blade chord ratio of 15.6, resulting in $F = .24$ and $Q = 15$. The torsional blade frequency is assumed to vary between $f = 8$ and $f = 12$. In addition to the response data of Figs. 3 to 8 dynamic stability data for the blade are shown in Figs. 1 and

2. These figures give the real part ξ of the characteristic values of the Floquet state transition matrix[2] vs. pitch-flap coupling gain K_f. The curves indicated by crosses represent conjugate complex characteristic values; the curves indicated by circles represent a single characteristic value. Figure 1 is for f = 8. The blade is very stable (negative ξ) up to about K_f = .5, has a minimum of stability of about K_f = 1.5, reaches a relative stability maximum of K_f = 2.0 and becomes unstable at K_f = 2.4. Figure 2 is for f = 10. The stability is almost unchanged up to K_f = .5 and at K_f = 2.0, but is improved at K_f = 1.5, and the stability limit is raised to K_f = 3.0. The dash-dash line indicates that an increase in Lock number is destabilizing, the dash-dot line indicates that for a pure flapping blade without elastic flapping restraint (P = 1) the blade reaches almost its stability limit at K_f = 1.7.

Figures 3 and 4 show the time variable standard deviations of the basic blade with torsional frequency ratio f = 8 for zero feedback, for flapping feedback with K_f = .4 and for coning angle feedback with K_o = .4. The flapping maximum standard deviation is reduced by either of the feedbacks from 2.3 to 1.5, the torsion maximum standard deviation is very high - about 6 - and not much affected by feedback. The figures show the second revolution after imposing the turbulence excitation, when the response standard deviations are almost stabilized and periodic. The blade is in the aft position at

$t = 0, 2\pi, 4\pi$, etc. The maximum flapping standard deviation occurs when the blade is approximately in the forward position, the maximum torsion standard deviation occurs, when the blade is in the region of maximum reversed flow.

Figures 5 and 6 show for the basic blade without feedback the effect of torsional frequency ratio f on the standard deviations. From Fig. 5 it is seen that flapping is little affected by a variation in f. Fig. 6 shows a very large effect of f on the torsional standard deviation, much more than would be expected from the increase in torsional stiffness. For example this increase would account for a reduction factor of .64 when changing from $f = 8$ to $f = 10$. The actual reduction factor for the maximum standard deviation is .37. It was found that for constant feathering moment of inertia the blade experiences static torsional divergence in the reversed flow region at $f = 6.6$. Though dynamic instability would not occur at $f = 6.6$, the torsional deflections would be extremely high. The closeness to the static torsional divergence limit is presumably the reason why an increase in torsional stiffness from $f = 8$ to $f = 10$ causes a decrease in torsional maximum standard deviation substantially larger than normally expected from the torsional stiffness increase, see also the discusion of Fig. 21 in Ref. 11.

Figure 7 shows the responses β and δ of the basic blade with $f = 10$ to a step gust input $\lambda = 1$ at $t = 0$, when the blade is in the aft position. The dash line is obtained when the coupling terms in Eqs. (1) and (2) are omitted. Flapping is

hardly affected, however, the torsional response is much reduced without the coupling terms. While qualitatively the torsional response to turbulence could be studied without coupling with flapping, the results would be quite unconservative.

Figures 8 and 9 show the expected number of upcrossings per unit of time of the positive levels $\zeta = 2$ and $\zeta = 3$ for flapping and torsion respectively. The solid lines are for $f = 10$, the dash lines for $f = 8$. Note for torsion the very large reduction in the number of crossings when changing from $f = 8$ to $f = 10$ (Fig. 9), while this change hardly affects the number of crossings for flapping (Fig. 8).

Unlike the configuration $f = 8$, the torsionally stiffer blade with $f = 10$ shows upcrossings of the levels $\zeta = 2$ and 3 only within a short time period of the order of the period of the natural torsional mode. One can, therefore conclude that in most cases an upcrossing will lead to a single peak value within a revolution. The number of peaks per revolution above the level ζ can then be approximated by integrating the curves of Fig. 9 over one revolution. This method is not applicable at the shown ζ levels for $f = 8$. For flapping with its natural period close to 2π this method of obtaining the number of peaks per revolution exceeding the level $\zeta=2$ or $\zeta=3$ is justified both for $f = 8$ and $f = 10$, as is seen from Fig. 8. The crossing expectations for the levels $\zeta=-2$ and $\zeta=-3$ are similar to those

shown in Figs. 8 and 9, except that the curves are somewhat shifted on the time scale.

The case of f = 10 and an advance ratio of μ = .8 has also been computed. In this case the torsion response is quite small, since the torsional divergence limit is reduced from f = 6.6 to f = 1.4, so that a very large torsional stiffness margin exists.

Conclusion

In summary, it can be concluded from the numerical examples that blade torsional response to atmospheric turbulence at high rotor advance ratio (μ = 1.6) can be very severe unless the torsional blade stiffness is several times greater than that for the static torsional divergence limit in the region of maximum reversed flow. Flapping-torsion coupling has little effect on flapping but has a large detrimental effect on torsion. The preceding analysis of blade responses to atmospheric turbulence is for rigid rotor support omitting higher blade modes. The effects of elastic rotor supports, of second mode blade bending and of random rotorcraft motions due to turbulence remain to be determined.

References

1. Gaonkar, G. H. and Hohenemser, K. H., "Stochastic Properties of Turbulence Excited Rotor Blade Vibrations", AIAA Journal, Vol. 9, No. 3, March 1971, pp. 419-424.

2. Yin, S. K. and Hohenemser, K. H., "The Method of Multiblade Coordinates in the Linear Analysis of Lifting Rotor Dynamic Stability and Gust Response", 27th Annual National Forum of the American Helicopter Society, Paper No. 512, May 1971.

3. Sissingh, G. J., "Dynamics of Rotors Operating at High Advance Ratios", Journal American Helicopter Society, Vol. 13, No. 3, July 1968, pp. 56-63.

4. Kuczynski, W. A., Sharpe, D. L. and Sissingh, G. J., "Hingeless Rotor - Experimental Frequency Response and Dynamic Characteristics with Hub Moment Feedback Controls", 28th Annual National Forum of the American Helicopter Society, Paper No. 612, May 1972.

5. Sissingh, G. J. and Kuczynski, W. A., "Investigation on the Effects of Torsion on the Dynamics of the Flapping Motion", Journal of American Helicopter Society, Vol. 15, No. 2, April 1970, pp. 2-9.

6. White, R. P. Jr., "Instabilities Associated with a Rotor Blade Stopped in Flight", 24th Annual Forum of the American Helicopter Society, Paper No. 229, May 1968.

7. Gaonkar, G. H. and Hohenemser, K. H., "Comparison of Two Stochastic Models for Threshold Crossing Studies of Rotor Blade Flapping Vibrations", AIAA/ASME 12th Structures Conference, AIAA Paper No. 71-389, April 1971.

8. Wan, F. Y. M. and Lakshmikantham, C., "Rotor Blade Response to Random Loading: A Direct Time Domain Approach", AIAA 10th Aerospace Science Meeting, AIAA Paper No. 72-169, January 1972.

9. Van Trees, H. L., Detection, Estimation and Modulation Theory, John Wiley & Sons, New York, 1968.

10. Gaonkar, G. H., "Interpolation of Aerodynamic Damping of Lifting Rotors in Forward Flight from Measured Response Variance", Journal of Sound and Vibrations, Vol. 18 (3), 1971, pp. 381-389.

11. Wachs, M. A. and Rabbott, J. P. Jr., "Rotary Wing Aircraft Design Trends", Journal of American Helicopter Society, Vol. 9, No. 2, April 1964, pp. 1-16.

Figure Captions

Fig. 1 Real Part ξ of Characteristic Value vs. Flapping Feedback Gain K_f, f = 8

Fig. 2 Real Part ξ of Characteristic Value vs. Flapping Feedback Gain K_f, f = 10

Fig. 3 Flapping Standard Deviation $\sigma_\beta(t)$ for zero feedback, K_f = .4 and K_o = .4, f = 8

Fig. 4 Torsion Standard Deviation $\sigma_\delta(t)$ for zero feedback, K_f = .4 and K_o = .4, f = 8

Fig. 5 Flapping Standard Deviation $\sigma_\beta(t)$ for f = 8, 10, 12, No feedback

Fig. 6 Torsion Standard Deviation $\sigma_\delta(t)$ for f = 8, 10, 12, No feedback

Fig. 7 Flapping and Torsion Response $\beta(t)$, $\delta(t)$ for unit gust Input (Dash lines: no torsion-flapping coupling)

Fig. 8 Expected Number of Flapping Upcrossings per Unit Time of Levels ζ=2 and ζ=3, No feedback

Fig. 9 Expected Number of Torsion Upcrossings per Unit Time of Levels ζ=2 and ζ=3, No feedback

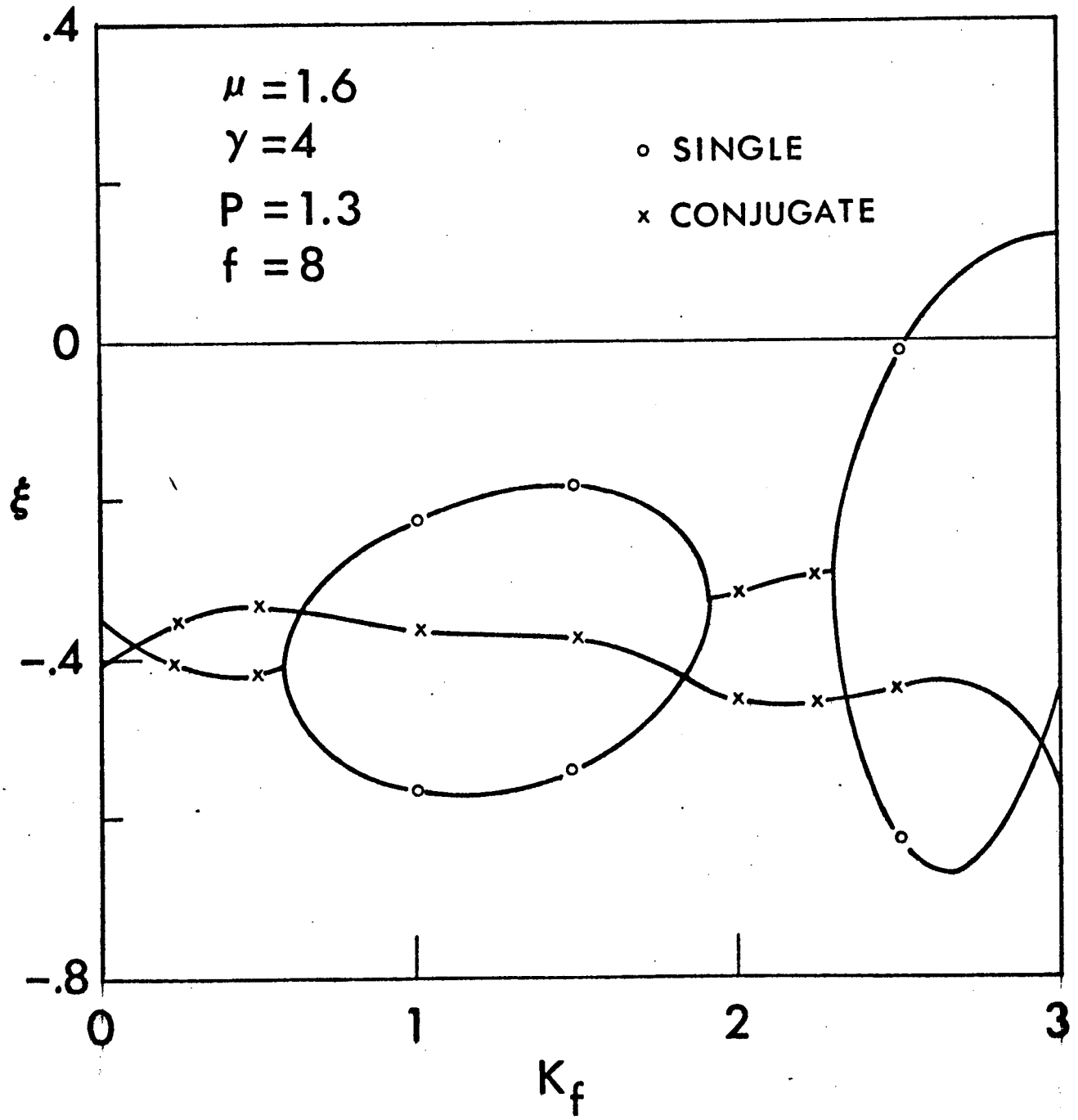

FIG. 1

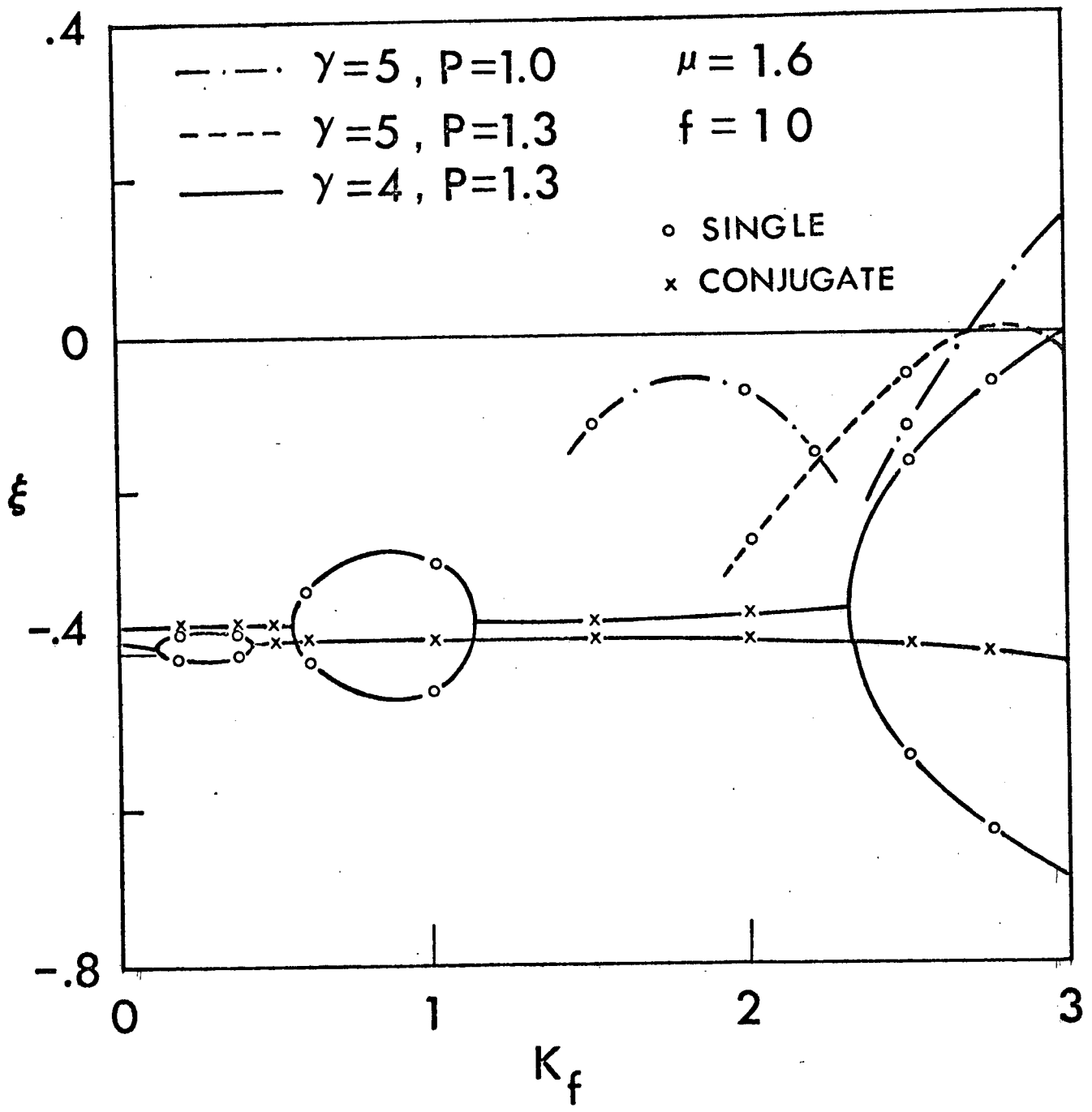

FIG. 2

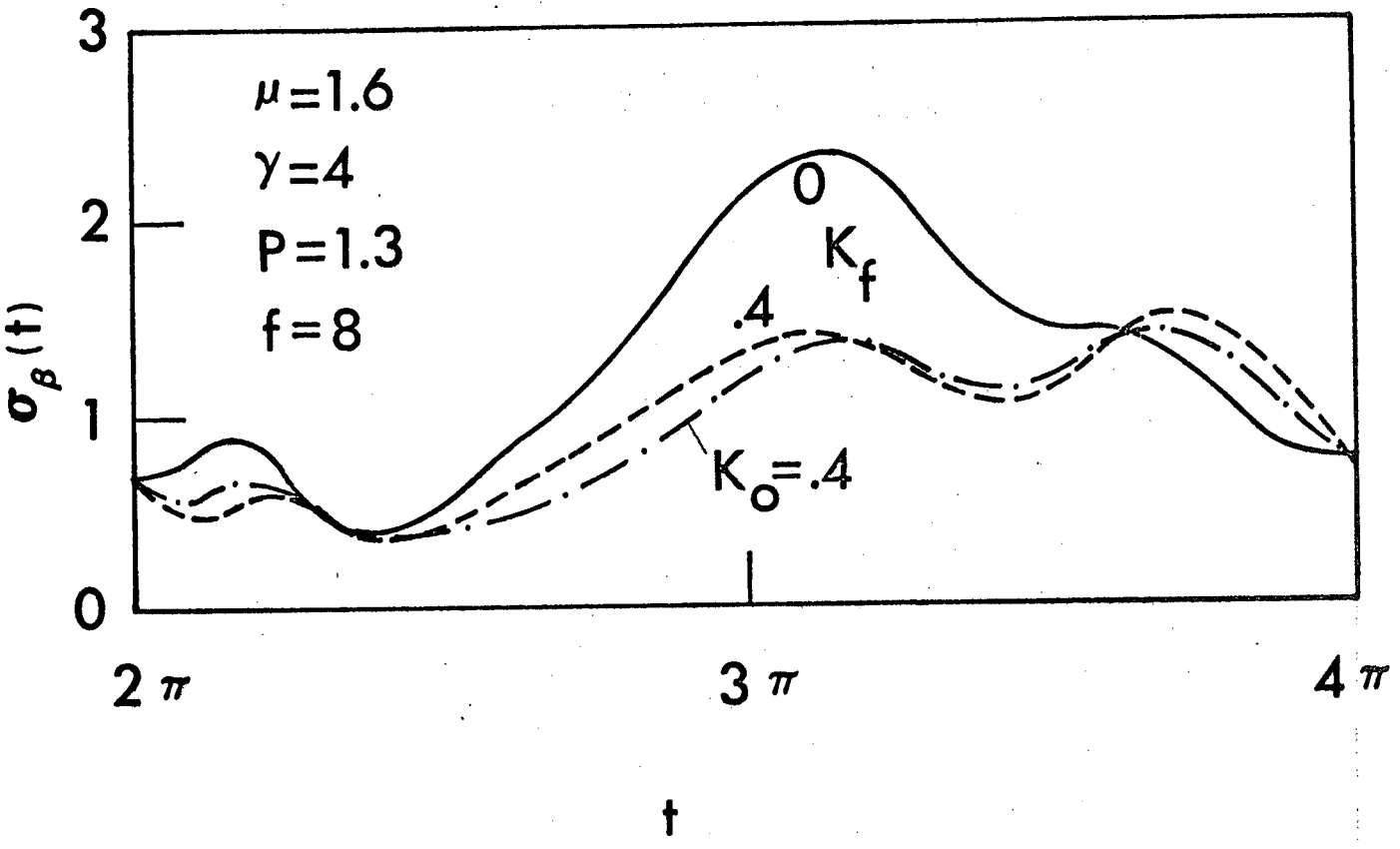

FIG. 3

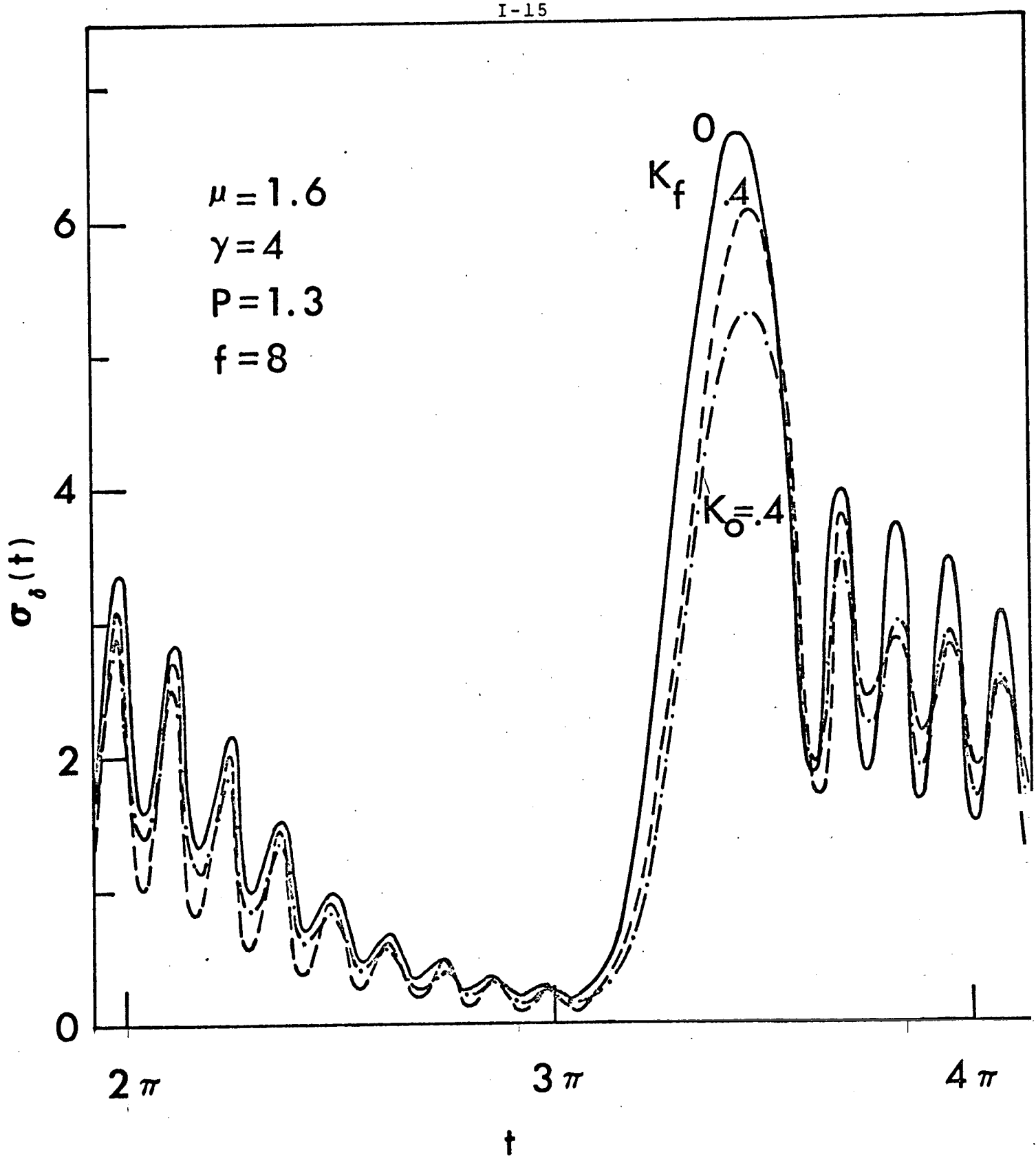

FIG. 4

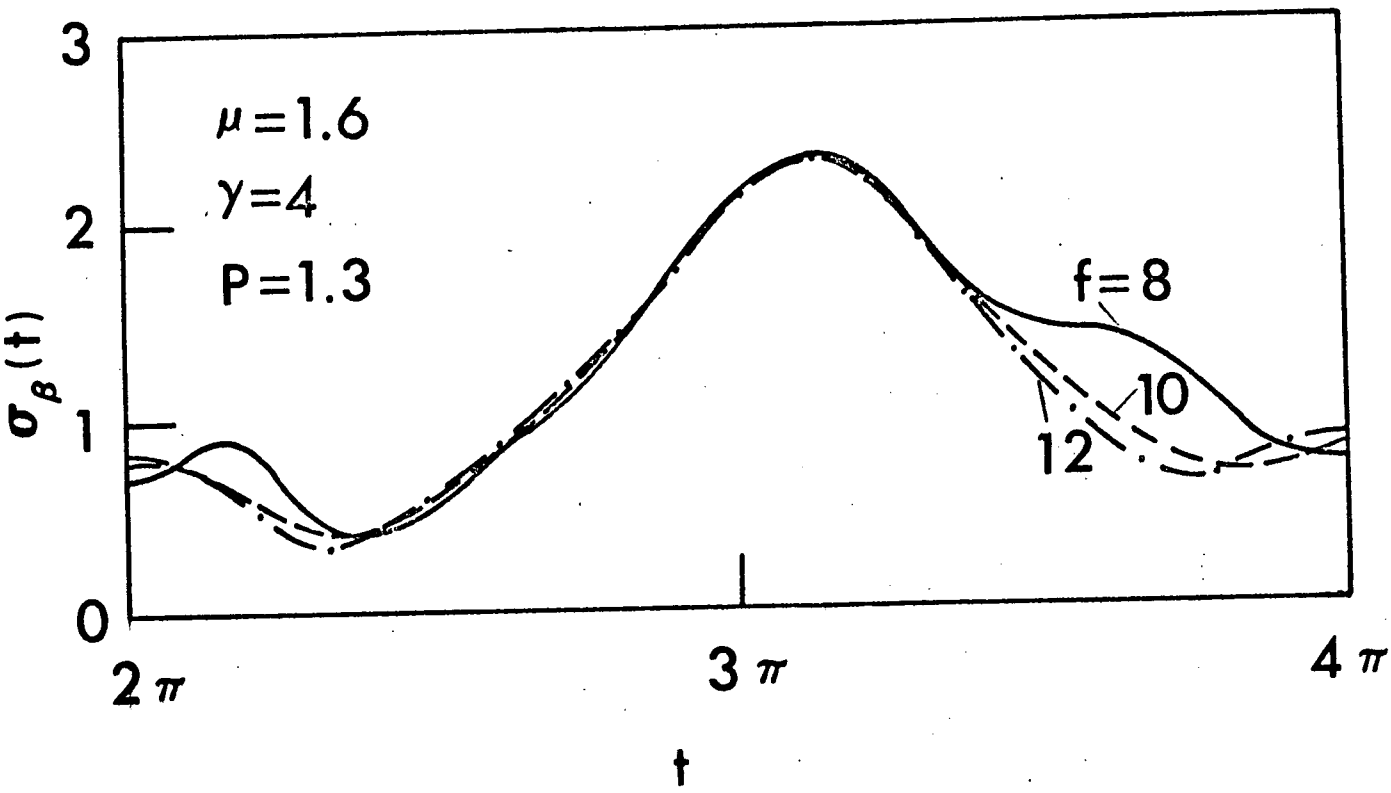

FIG. 5

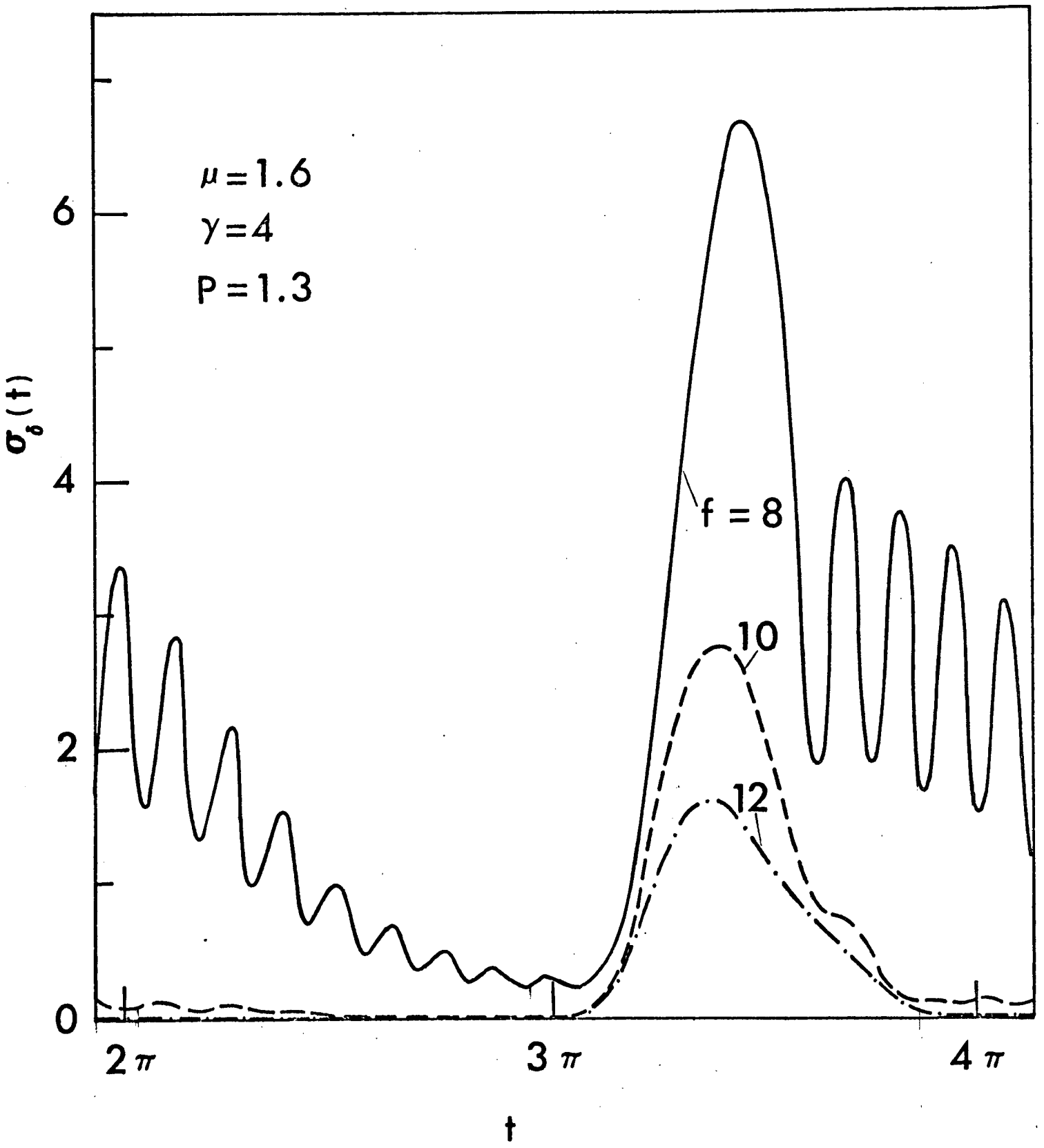

FIG. 6

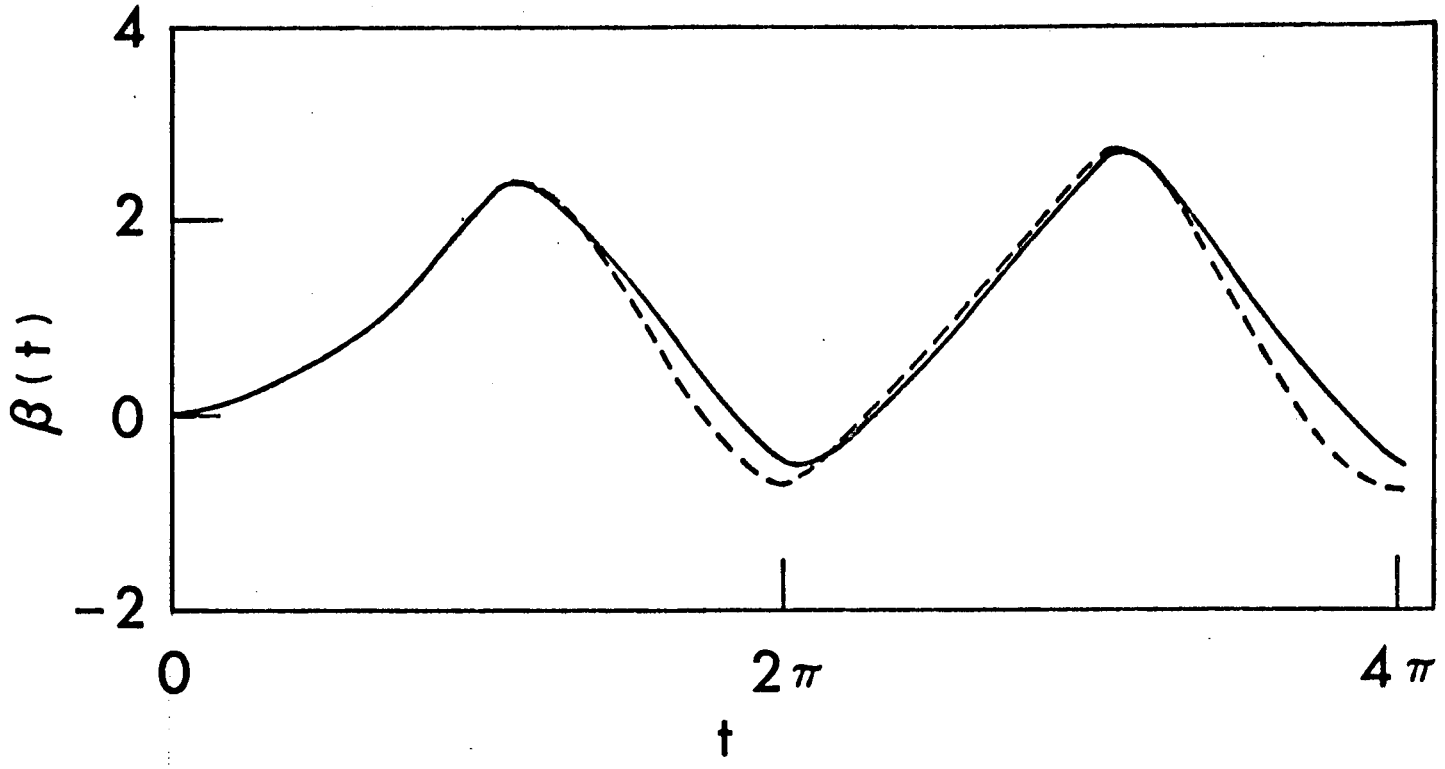

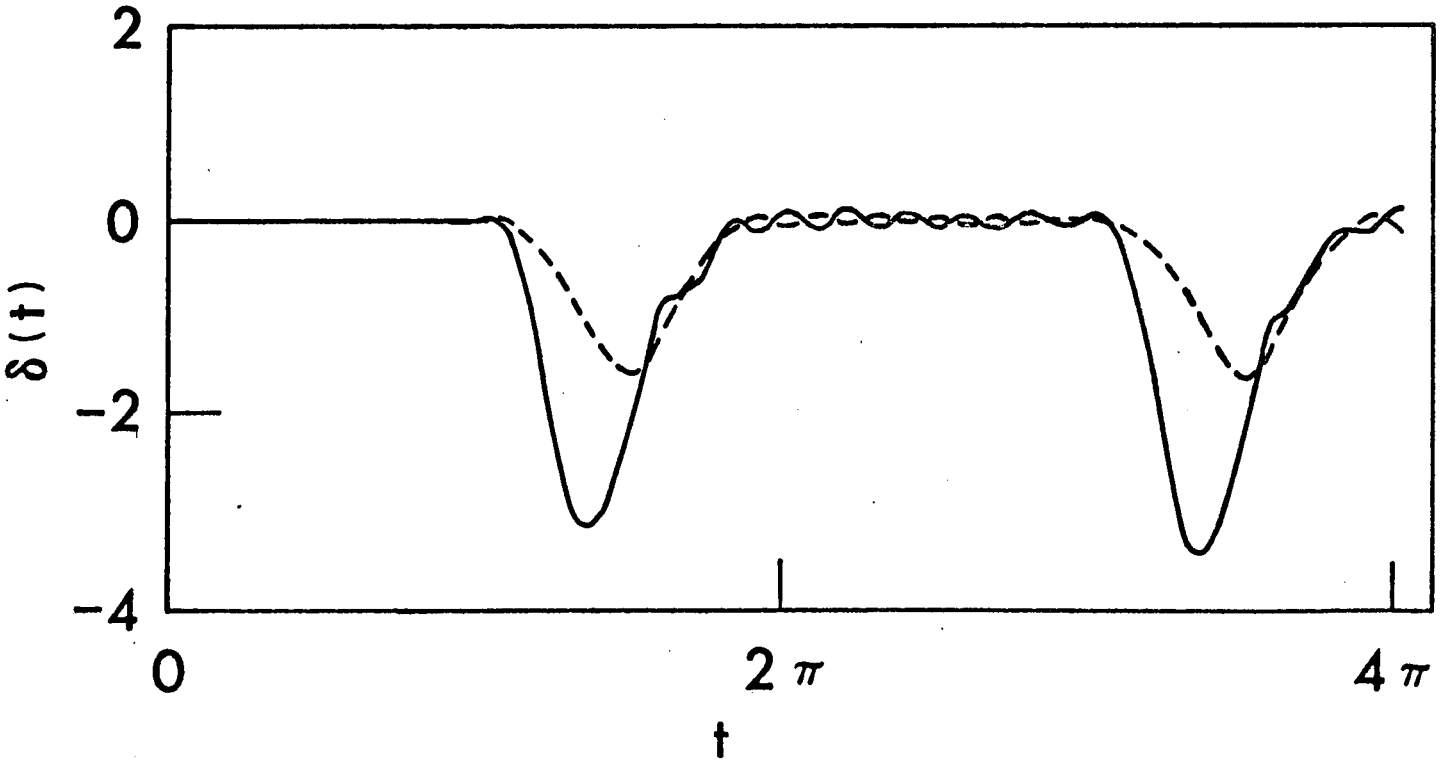

FIG. 7

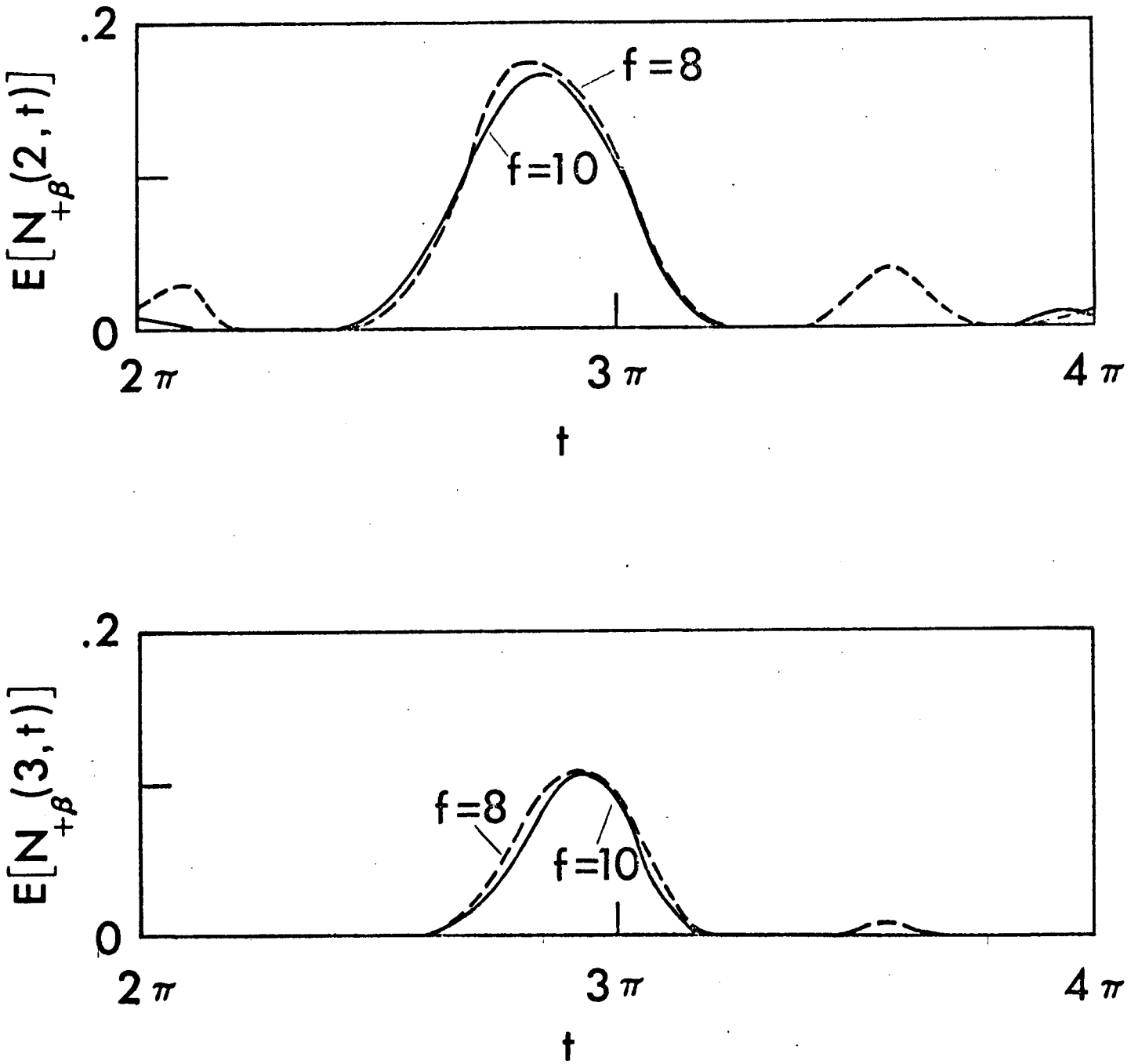

FIG. 8

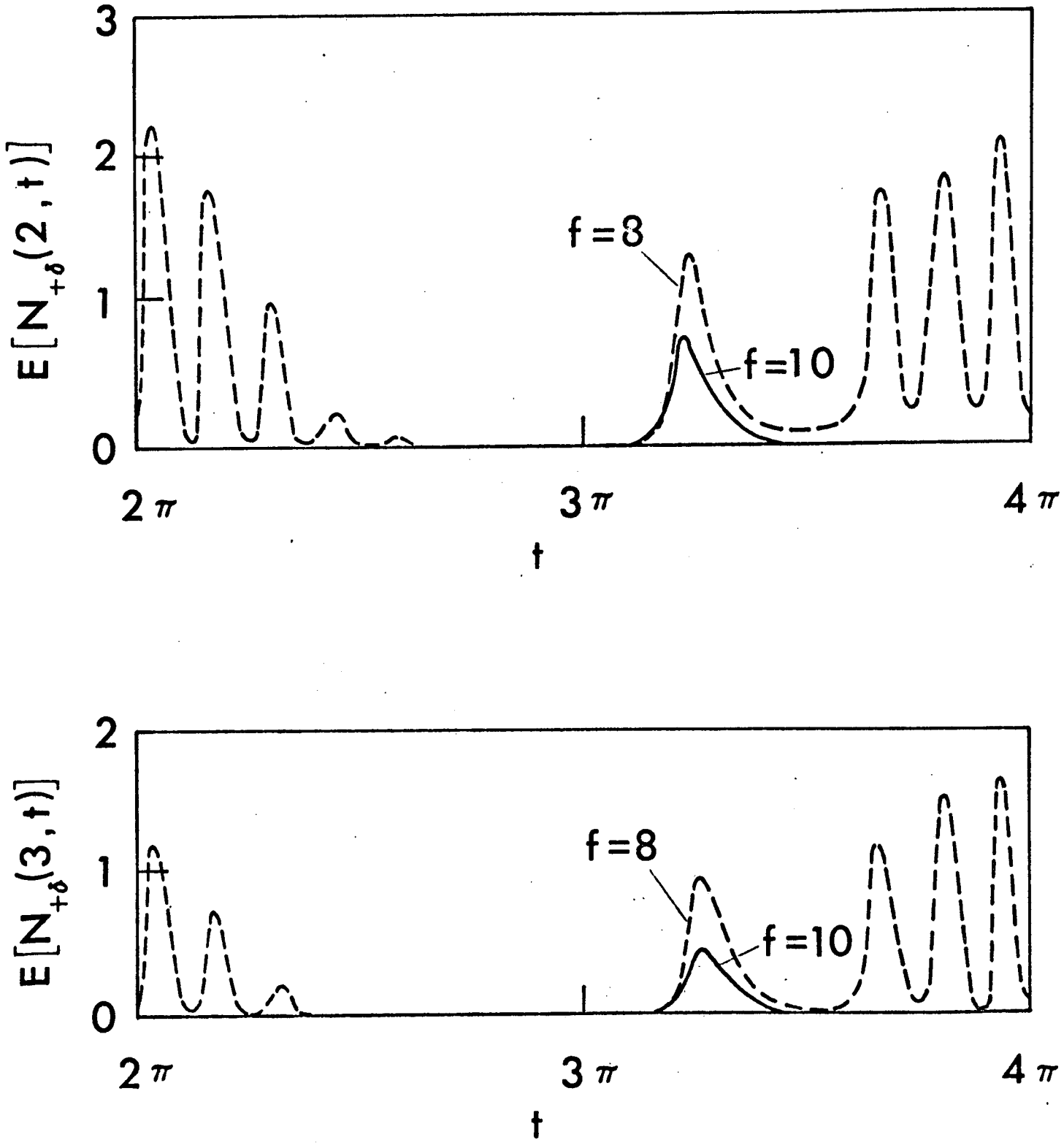

FIG. 9

Part II

Flap Bending Corrections to the Rigid Blade Analysis of Lifting Rotors

Abstract

A modal analysis was performed using the undamped natural modes of the rotating blade. Two types of mass and stiffness distributions were assumed: a uniform one, and one corresponding to a blade strongly tapered in thickness. The response to cyclic pitch input at low and high advance ratio could be reasonably well approximated by a simple analysis using a single elastic mode whereby all moments are balanced about the rotor center. This result is different from recently published single mode analyses without moment balance about the rotor center, where under certain conditions larger errors were found. The difference is attributed to the use of rotating blade modes rather than the non-rotating modes used in the previous work. The single elastic mode model is then applied to the problem of dynamic stability and random loads at high advance ratio which had previously been solved with the help of a rigid blade model. Substantial corrections were found due to the flap bending flexibility of the blades.

Nomenclature

a	lift slope
b	number of blades per rotor
c	blade chord
$C_T = T/\rho\pi R^4\Omega^2$	rotor thrust coefficient
$C_\ell = L/\rho\pi R^5\Omega^2$	rotor rolling moment coefficient, positive to right
$C_m = M/\rho\pi R^5\Omega^2$	rotor pitching moment coefficient, positive up
$C_M = M_b/\rho\pi R^5\Omega^2$	blade flapping moment coefficient, positive down
C, C_1, C_2, C_{ij}	aerodynamic damping coefficients
EI	flap bending stiffness of blade
EI_o	reference stiffness of blade
$f(x,t)$	nondimensional blade load per unit length, positive up
K, K_1, K_2, K_{ij}	aerodynamic stiffness coefficients
L	rotor rolling moment
M	rotor pitching moment
M_b	blade flapping moment
m	blade mass per unit length, or flap moment
m_λ, m_θ, m_{θ_1}	flap moment derivatives
m_o	reference blade mass per unit length
$q = EI_o/m_oR^4\Omega^2$	nondimensional reference stiffness of blade
R	rotor radius
r	radius at blade station

$r_{\beta_I \beta_{II}}$	cross correlation coefficient
t	nondimensional time, time unit $1/\Omega$
T	tension or rotor thrust
T_b	blade thrust
U_T	nondimensional tangential velocity component
U_p	nondimensional normal velocity component
$x = r/R$	nondimensional radius of blade station
$y(x,t)$	nondimensional flapwise deflection of blade, length unit R
$\beta_i(t)$	generalized coordinate
ψ_i	nondimensional generalized force, or azimuth
$\gamma = \rho acR^2/\int x^2 dm$	rigid blade Lock number
$\gamma_i = \rho acR^2/\int \eta_i^2 dm$	modal Lock number
$\gamma_m = \rho acR^2/\int x\eta dm$	Lock number for first mode moment equation
κ	adaptation factor for first mode representation: $\eta = x + \kappa\eta_h$
λ	inflow ratio, positive up
μ	advance ratio
Ω	rotor angular speed
ω	nondimensional frequency of harmonic blade motion, frequency unit Ω
ρ	air density
$\sigma = bc/\pi R$	rotor solidity ratio
$\sigma_1 = c/\pi R$	blade solidity ratio
σ_{β_I}, $\sigma_{\beta_{II}}$	standard deviations
θ	blade pitch setting

θ_1	blade linear twist
$\eta_i(x)$	blade natural mode
η_h	first elastic mode of uniform hinged-free beam
ξ	real part of characteristic value

Introduction

A rigid blade dynamic rotor analysis provides a reasonable approximation for many purposes and has been applied both to articulated and hingeless rotors. In the latter case the rigid blade model involves an elastically restrained hinge. Because of our present uncertainties regarding the rotor wake structure particularly at low advance ratio,[1] it is difficult to assess the errors from the rigid blade analysis by a comparison between analytical and test results. Errors in the assumed rotor wake structure may well mask the effects of blade flap-bending elasticity. Though good correlation between a rigid blade analysis and tests with a 7.5 ft. hingeless rotor model was found at .79 advance ratio for hub moment response to harmonic cyclic pitch input,[2] the omitted wake effects may have been substantial,[3] casting doubts on the claimed accuracy of the rigid blade analytical model.

There is a rather extensive literature on flap bending effects of both articulated and hingeless rotors. Leone[4] showed that flap bending of an articulated blade in forward flight produces compared to the rigid blade analysis sizeable corrections to lateral flapping and to retreating blade tip angle of attack. Daughaday et al[5] showed for zero advance ratio experimentally with a mechanically excited articulated rotor blade and theoretically, that the first flap bending

mode has a very high load amplification factor which can be substantially reduced by coupling with the carefully tuned torsion mode with the help of a forwardly located blade tip weight. Perisho[6] showed for an articulated blade with δ_3 hinge that the rigid blade high advance ratio flapping instability is substantially modified when including elastic torsion and elastic first mode flap bending. Curtiss and Shupe[7] found for hingeless rotors surprisingly large differences in analytical hub moments between a one mode and a two mode elastic analysis. With one or two elastic modes used they also found significant differences between hub moments computed from the elastic bending moments and from the moments of the airloads. Ormiston and Peters[3] compared hingeless rotor moment and thrust changes from cyclic pitch inputs computed with elastically restrained rigid blades with and without hinge off-set to those computed with the first elastic flap-bending mode and with the first two elastic modes. Up to about .4 advance ratio the rigid blade analyses agree well with the two types of flexible blade analysis. At an advance ratio of one rather large differences between the results of these four methods of analysis were found. It should be noted that Curtiss and Shupe[7] neglect the aerodynamic coupling between elastic modes. Both Curtiss and Shupe[7] and Ormiston and Peters[3] use elastic natural blade modes at zero rotor speed. Particularly the first elastic flap bending mode is substantially affected

by rotation, and the relatively large differences of the one mode and two mode analysis found in References 3 and 7 for low first mode natural frequencies point toward the possibility that the error in the single mode analysis may in part be due to the assumption of a non-rotating first mode rather than a rotating first mode. The use of non-rotating modes may also have contributed to the surprisingly large differences between elastic and airload hub moments shown in Reference 7.

In order to clarify the questions raised by References 3 and 7 and in order to provide a basis for a flap bending correction of the multiblade dynamic stability and random loads analysis of Reference 8, a linear flap bending modal analysis was performed with the natural modes of the rotating blade, including the aerodynamic coupling terms and including reversed flow effects.

Problem Formulation

One way of determining the effects of blade flap bending is to formulate a finite element analysis as was done, for example, by Blankenship and Harvey[9] which included large angle effects and coupling with chordwise and torsional blade motions. Each blade is subdivided into several rigid segments connected to each other by appropriate flexures. Although this has not been done as yet one could perform for the linearized problem, after transformation to state variable form, a normal mode analysis by extracting eigen values and eigen vectors from the Floquet state transition matrix. At a zero advance ratio natural mode the various finite elements will oscillate with the same frequency but with different phase angles. At a non-zero advance ratio natural mode the various finite elements will oscillate with a product of a periodic function with period 2π and a harmonic function with the natural frequency ω_k. Both factors will differ between finite elements, except that all harmonic factors of one mode will have the same ω_k but different phase angles. In addition there will be a third factor, common to all finite elements, consisting of a real exponential function $\exp \xi_\kappa t$.

A modal analysis of this type has been suggested[10] but work performed since then has shown that under certain conditions basic difficulties arise in performing a normal mode

expansion for a periodic system. We will, therefore, use here the conventional approach, 3, 5, 6, 7 of a modal analysis, not with the actual uncoupled natural modes but rather with a set of normal modes which are natural uncoupled modes only under very restricted circumstances: at zero advance ratio and neglecting aerodynamic or other damping. Such modes reflect the elastic and kinetic energies of the system and the effects of centrifugal loads. They become coupled in the presence of aerodynamic loads although the coupling terms are sometimes neglected.[6] The problem can be formulated now in terms of generalized coordinates associated with the elastic modes. A state variable form is again required and eigen values and eigen vectors can be extracted from the Floquet state transition matrix. If a sufficient number of elastic modes is used, the natural frequencies ω_κ and real exponents ξ_κ of the natural modes should be the same as in a finite element analysis with sufficient numbers of elements. Usually only 2, at most 3 elastic blade modes suffice at least as far as dynamic stability studies are concerned. The ratio of elastic energy over the energy of the aerodynamic springlike or damperlike forces increases very rapidly for the higher elastic modes, so that they become almost uncoupled from the lower modes, thus contributing almost nothing to the dynamic stability problem. Of course, for the purpose of evaluating noise and high

frequency vibrations from rotor induced turbulence, the high elastic blade modes are of significance and cannot be disregarded.

For hingeless rotors - but also to a lesser degree for articulated rotors - there are elastic and inertial coupling terms between flap bending, lag bending and torsion modes, whereby mean flapping or lagging displacements of hingeless blades are particularly effective in causing couplings. At high advance ratio there also is in the reversed flow region an aerodynamic coupling between torsion and flap bending. If torsional divergence and flutter margins for torsion-bending flutter as well as margins for chordwise motion instabilities are adequate and if inertial torsion-flap bending coupling is kept small by design (coinciding section c.g. and a.c.), the low frequency flap-bending dynamics can be expected to be only mildly affected by torsion or lag coupling terms. With respect to torsion coupling this expectation is supported among others by References 6 and 11, with respect to chordwise coupling by Reference 12.

The following then is a linear flap bending type of analysis of lifting rotors with constant chord blades using generalized coordinates associated with the undamped elastic modes of the blades rotating in vacuum. Quasi-steady aerodynamics is used and wake effects are neglected.

In view of the steady wake effects revealed among others in References 1 and 3, the latter assumption is likely

to require corrections. However, as of now there exist neither a theory nor systematic tests which would allow the inclusion of unsteady wake effects in the analysis of lifting rotors.

Outline of Modal Analysis

Though basically of the same type as the modal analyses used in References 3, 5 and 7, the following analysis differs from the references in essential details. As compared to Daughaday et al[5] it is in part less general since torsion is omitted, in part more general since it is not limited to zero advance ratio. As compared to Curtiss and Shupe[7] the following analysis is more general since aerodynamic coupling between modes and reversed flow are included. As compared to both Curtiss and Shupe[7] and Ormiston and Peters[3] the following analysis is, for a given number of modes more accurate since modes of the rotating blade rather than those of the non-rotating blade are used. While in References 3 and 7 the emphasis is on first harmonic excitation of the blades to determine rotor derivatives, the purpose of the following analysis is to provide the basis for a flap bending correction of the multi-blade dynamic stability and random load analysis previously performed with the rigid blade model.[8]

The basic units for the non-dimensional quantities are: Time unit $1/\Omega$, length unit R, mass unit $\pi\rho R^3$. The derived

units are: velocity unit ΩR and linear acceleration unit $\Omega^2 R$. The force unit would be $\pi\rho R^4\Omega^2$. However, since all aerodynamic forces have the factor $a\sigma$, we include this factor in the definition of the force unit, which then is

$$\pi\rho R^4\Omega^2 a\sigma = \rho acR^3\Omega^2 b \tag{1}$$

The moment unit is

$$\pi\rho R^5\Omega^2 a\sigma = \rho acR^4\Omega^2 b \tag{2}$$

The selection of these units results in non-dimensional blade thrust and flapping moment values

$$C_T/a\sigma_1 = T_b/\rho acR^3\Omega^2 \tag{3}$$

$$C_M/a\sigma_1 = M_b/\rho acR^4\Omega^2 \tag{4}$$

The elastic natural flap-bending modes and natural frequencies of the blade in a rotating frame of reference are determined from the equation

$$(EIy'')'' - (Ty')' - m\Omega^2\omega^2 y = 0 \tag{5}$$

Instead of solving this differential equation, the blade is replaced by a number of point masses connected by massless flexible beam segments. Following Myklestad,[13] a state transition matrix is established which relates the state vector at one end of an elastic segment to that at the other end. At the outer end of the blade the shear and bending moment are zero, deflection and slope are unknown. The state vector at the blade root is related to that at the blade tip by the product of the state transition matrices of all blade segments. The inner state vector is computed for

2 values of the tip state vector, corresponding to tip deflection one and tip slope zero and tip deflection zero and tip slope one. The inner boundary conditions of zero deflection and slope result in a two by two frequency determinant which is solved by iteration of the entire process. For each natural frequency the modal deflections, slopes, bending moments and shear forces can then be determined. The dimensionless natural frequencies depend only on

$$q = EI_o/m_o R^4 \Omega^2 \tag{6}$$

The natural modes η_j are normalized such that the blade tip deflection or a certain fraction of it is unity. A non-dimensional deflection $y(x,t)$ of the blade can now be represented by a linear combination of natural modes

$$y(x,t) = \sum_{j=1}^{\infty} \eta_j(x)\, \beta_j(t) \tag{7}$$

Both the η_j and the β_j are nondimensional. This separation of variables is possible because of the general expansion theorem according to which any arbitrary deflection can be represented by a convergent series of eigen functions. The $\beta_j(t)$ are generalized coordinates. Because of the orthogonality relations

$$\int \eta_i\, \eta_j\, dm = 0 \qquad i \neq j \tag{8}$$

one obtains from Eq. (7)

$$\beta_i = \int y\, \eta_i\, dm / \int \eta_i^2 dm \tag{7a}$$

For the nondimensional airloads df there exists the

expansion

$$df(x,t) = \sum_{j=1}^{\infty} \eta_j(x)\, dm\, \psi_j(t) / \int \eta_j^2\, dm \qquad (9)$$

The generalized forces ψ_i are obtained because of Eq. (8) by

$$\psi_i = \int \eta_i\, df \qquad (9a)$$

Because of Eq. (8) the Lagrange equations in generalized coordinates β_i and generalized forces ψ_i read

$$\ddot{\beta}_i \int \eta_i^2\, dm + \beta_i\, \omega_i^2 \Omega^2 \int \eta_i^2\, dm = \rho a c R^2 \Omega^2 \psi_i \qquad (10)$$

The integrals are to be taken in the Stieltjes sense to include discrete masses. The dimensions of each term are force per unit length. The right hand side is obtained by multiplying the non-dimensional generalized forces ψ_i by the unit for force per unit length. The mass and stiffness matrices are diagonal because of the orthogonality relation Eq. (8). The set of Lagrange equations (10) can be written in the non-dimensional form (time unit $1/\Omega$)

$$(1/\gamma_i)(\ddot{\beta}_i + \omega_i^2 \beta_i) = \psi_i,\ i = 1, 2, \ldots \qquad (11)$$

The lift force on a blade element c R dx is

$$(1/2)\rho(\Omega R)^2\, a c\ \ U_T^2\ (U_P/U_T + \Theta + x\,\theta_1)\, R\, dx$$

The non-dimensional elemental lift force is with Eq. (1)

$$df = (1/2)\, U_T^2\, (U_P/U_T + \Theta + x\,\theta_1)\, dx \qquad (12)$$

where

$$U_T = x + \mu \sin t \qquad (13)$$

$$U_P = \lambda - \mu y' \cos t - \dot{y} = \lambda - \sum_j (\mu\, \eta_j'\, \beta_j \cos t + \eta_j\, \dot{\beta}_j) \qquad (14)$$

The non-dimensional generalized forces are

$$\psi_i = \int \eta_i df = (1/2) \int U_T^2 \, \eta_i (U_P/U_T + \theta + x\theta_1) dx \qquad (15)$$

Writing

$$2\psi_i = \lambda\psi_{\lambda i} + \theta\psi_{\theta i} + \theta_1\psi_{\theta_1 i} - \sum_j (K_{ij}\,\beta_j + C_{ij}\,\dot{\beta}_j) \qquad (16)$$

we have

$$\psi_{\lambda i} = \int U_T \eta_i dx \qquad K_{ij} = \mu \int (\cos t)\, U_T \eta_i \eta_j' dx$$

$$\psi_{\theta i} = \int U_T^2 \eta_i dx \qquad C_{ij} = \int U_T \eta_i \eta_j dx \qquad (17)$$

$$\psi_{\theta_1 i} = \int U_T^2 \eta_i x dx$$

Inserting Eq. (16) into Eq. (11):

$$(1/\gamma_i)\,\ddot{\beta}_i + (1/2) \sum_j C_{ij}\,\dot{\beta}_j + (1/\gamma_i)\,\omega_i^2 \beta_i + (1/2) \sum_j K_{ij}\,\beta_j$$

$$= (1/2)(\lambda\psi_{\lambda i} + \theta\psi_{\theta i} + \theta_1\psi_{\theta_1 i}) \qquad (18)$$

In order to include the effects of tip loss, root cut-out and reversed flow, the integrals in the three regions of normal flow, mixed flow and reversed flow are respectively[14]

$$\int_A^B \ldots , \int_A^B \ldots -2\int_A^{-\mu\sin\psi} , -\int_A^B \ldots \qquad (19)$$

The region limits are defined by azimuth angles of 0 to π for normal flow, π to $\pi + \varepsilon$, and $2\pi - \varepsilon$ to 2π for mixed flow and $\pi + \varepsilon$ to $2\pi - \varepsilon$ for reversed flow, ε being obtained from $\sin\varepsilon = B/\mu$.

Hub Moments

For studies of hub moment feedback stability or whirl stability[8] expressions for the hub moment are needed and the question arises, how many modes are required to obtain a reasonably accurate hub moment. In a rotating reference system the dimensionless hub moment for a single blade is

$$C_M/a\sigma_1 = -\int x df + R^2(\int \ddot{x} y dm + \int \Omega^2 x y dm)/\rho a c R^4 \Omega^2 \qquad (20)$$

The first integral represents the moment of the aerodynamic loads, the second the inertia moment and the third the centrifugal force moment about the rotor center. Inserting Eqs. (7) and introducing γ_j:

$$C_M/a\sigma_1 = -\int x df + \sum_{j=1}^{\infty} (1/\gamma_j)(\ddot{\beta}_j + \beta_j)\int x\eta_j dm/\int \eta_j^2 dm \qquad (21)$$

A simpler expression can be obtained by computing the elastic bending moment at the rotor center as the sum of the inertia moments and centrifugal force moments for each natural mode. This is the infinite sum in Eq. (21) for

$$\ddot{\beta}_j + \omega_j^2 \beta_j = 0 \qquad (22)$$

Inserting $\ddot{\beta}_j$ from Eq. (22) into the infinite sum of Eq. (21):

$$C_M/a\sigma_1 = -\sum_{j=1}^{\infty} (1/\gamma_j)(\omega_j^2 - 1)\beta_j \int x\eta_j dm/\int \eta_j^2 dm \qquad (23)$$

In both Eqs. (21) and (23) the hub moment is positive down.

As pointed out by Curtiss and Shupe,[7] the series in Eq. (21) converges faster than the series in Eq. (23). For

example, for harmonic oscillation of β_i with frequency of unity (once per rev.)

$$\ddot{\beta}_j + \beta_j = 0 \tag{24}$$

and Eq. (21) reduces to

$$C_M/a\sigma_1 = -\int x\, df \tag{25}$$

Truncating this equation, one omits the aerodynamic effects of the neglected $\dot{\beta}_j$, β_j terms, however one includes all of the aerodynamic terms not dependent on $\dot{\beta}_j$ or β_j. Eq. (23), because of Eq. (11), can also be written

$$C_M/a\sigma_1 = -\sum_{j=1}^{\infty} \psi_j \int x\eta_j\, dm \Big/ \int \eta_j^2\, dm \tag{26}$$

Truncating this equation, one omits in addition to the neglected $\dot{\beta}_j$, β_j terms in ψ_j also the terms in ψ_j not dependent on $\dot{\beta}_j$ or β_j. Thus the truncated Eq. (23) is less accurate than the truncated Eq. (21). This does not mean that the simpler Eq. (23) cannot be used to advantage. The series of Eq. (23) also converges quite rapidly and its somewhat reduced accuracy as compared to the truncated expression Eq. (21) appears to have been overstated in Reference 7. For the case of one per rev excitation of the blade, $C_M/a\sigma_1$ is periodic with 2π. One then determines the Fourier coefficients C_{Mc} and C_{Ms} of cos t and sin t respectively and obtains pitching and rolling moment in a space fixed reference system by

$$\begin{aligned} C_m/a\sigma &= C_{Mc}/2a\sigma_1 \\ C_c/a\sigma &= C_{Ms}/2a\sigma_1 \end{aligned} \tag{27}$$

where σ is the solidity of the entire rotor.

Single Mode Analysis

In Reference 3, Fig. 4 it is shown that for values of the first natural frequency of $\omega_1 = 1.4$ and above the second mode has only a small effect on the hub moment from longitudinal cyclic pitch. The case refers to a uniform beam representation of the hingeless blade at an advance ratio of unity. For values $\omega_1 < 1.4$ Reference 3 indicates for this case substantial effects of the second mode, particularly on the hub pitching moment. As will be shown later, the second mode effects are smaller if rotating modes are used instead of the non-rotating modes. For many purposes if would then appear adequate to consider only first mode elastic bending effects. This can be done in a rather simple way by replacing the generalized force expressions of Eq. (10) by moments about the rotor center. Leaving out the subscript j for β and η we have instead of Eq. (7)

$$y(x,t) = \eta(x)\,\beta(t) \tag{28}$$

and instead of Eq. (10)

$$\ddot{\beta}\int x\eta dm + \beta\omega_1{}^2\Omega^2\int x\eta dm = \rho acR^2\Omega^2\int x df \tag{29}$$

or in non-dimensional form

$$(1/\gamma_m)(\ddot{\beta} + \omega_1{}^2\beta) = \int x df \tag{30}$$

Eq. (15) now becomes

$$m = \int x df = (1/2)\int U_T{}^2\, x(U_P/U_T + \theta + x\theta_1)dx \tag{31}$$

Writing

$$2m = \lambda m_\lambda + \theta m_\theta + \theta_1 m_{\theta_1} - K\beta - C\dot{\beta} \tag{32}$$

we have

$$m_\lambda = \int U_T x \, dx \qquad K = \mu \int (\cos t)\, U_T \, x \, \eta' \, dx$$

$$m_\theta = \int U_T^2 \, x \, dx \qquad C = \int U_T \, x \, \eta \, dx \tag{33}$$

$$m_{\theta_1} = \int U_T^2 \, x^2 \, dx$$

Inserting Eq. (32) into Eq. (30):

$$(1/\gamma_m)\ddot{\beta} + (1/2)\, C\dot{\beta} + (1/\gamma_m)\omega_1^2\beta + (1/2)\, K\beta =$$

$$(1/2)(\lambda\, m_\lambda + \theta m_\theta + \theta_1\, m_{\theta_1}) \tag{34}$$

m_λ, m_θ, m_{θ_1} are the same as in Reference (14) for rigid blades, C and K are different.

Since Eq. (34) represents the moment balance about the rotor center, the elastic moment is equal to the sum of aerodynamic moments, inertia moments and centrifugal force moment. Instead of Eqs. (21) and (23) which resulted in different hub moments after truncation, we now have a single equation for the hub moment

$$C_M/a\sigma_1 = -(1/\gamma_m)(\omega_1^2 - 1)\beta \tag{35}$$

This follows from Eq. (23) when only the first term is used and γ_1 is replaced by γ_m.

In many cases one can replace the actual first mode by the following closed form expression

$$\eta = x + \kappa[\sinh(3.93x)/2 \sinh 3.93 + \sin(3.93x)/2 \sin 3.93] \tag{36}$$

The term in brackets represents the second mode of a uniform hinged-free beam normalized for unit tip deflection. κ is an adaptation factor selected for best fit. For a wide variety of blades the fit was found to be excellent. Using the mode shape Eq. (36) the straight line $\eta=x$ for the rigid blade analysis passes through the .73 point of the mode shape, see Fig. 3 and 5. The closed form mode has the advantage that the airloads can also be expressed in closed form. Writing Eq. (36) as

$$\eta = x + \kappa\, \eta_h \tag{37}$$

we have

$$K = \mu \int (\cos t)\, U_T\, x(1 + \kappa\eta_h)dx = K_1 + \kappa\, K_2 \tag{38}$$

$$C = \int U_T\, x(x + \kappa\eta_h)dx = C_1 + \kappa\, C_2 \tag{39}$$

The coefficients K_1 and C_1 are the same as K and C for rigid blades in Reference (14). For reversed flow neglected, zero root cutout and .97 tip loss factor the coefficients defined in Eqs. (33), (38) and (39) are

$$\left.\begin{aligned}
m_\lambda &= .304 + .470\,\mu \sin t \\
m_\theta &= .221 + .608\,\mu \sin t + .470\,\mu^2 \sin^2 t \\
m_{\theta_1} &= .172 + .442\,\mu \sin t + .304\,\mu^2 \sin^2 t \\
K_1 &= \mu \cos t\,(.304 + .470\,\mu \sin t) \\
K_2 &= \mu \cos t\,(.886 + 1.070\,\mu \sin t) \qquad K = K_1 + \kappa\, K_2 \\
C_1 &= .221 + .304\,\mu \sin t \\
C_2 &= .028 - .028\,\mu \sin t \qquad C = C_1 + \kappa\, C_2
\end{aligned}\right\} \tag{40}$$

For uniform mass $\int x\, \eta_h\, dm = 0$, therefore $\gamma_m = \gamma$.

For reversed flow it is more convenient to present the Fourier coefficients of the periodic functions. This is done for $\mu = .8$ and 1.6 in Appendix B. If the first mode cannot be represented by Eq. (37), K and C must be obtained by evaluation of the expressions in Eq. (33).

Hub Moment Derivatives

Before applying the analysis of the preceding sections to stability and random loads problems, we will use the computation of some hub moment derivatives at advance ratio one as a test case to check the accuracy of the various analytical models against each other. We will use two types of blades for this check: First a blade with uniform mass and stiffness distribution, second a blade with tapered thickness characterized by the mass and thickness distributions of Fig. 1. The first two natural frequencies of the uniform blade vs. nondimensional rotor speed $q^{-1/2}$ are shown in Fig. 2. The ordinates, $\omega q^{-1/2}$ must be multiplied by $(EI/R^4 m)^{1/2}$ to obtain the dimensional circular frequencies. The straight lines represent $\omega = 1$, $\omega = 2$, etc. The first mode shape for $\omega_1 = 1.2$ to 1.4 are shown in Fig. 3. The difference in mode shape between $\omega_1 = 1.2$ and 1.4 is too small to be shown in Fig. 3. The difference between the actual mode shape and the closed form $x + \kappa \eta_h$ is also negligible. The first two natural frequencies of the tapered in thickness blade vs. nondimensional rotor speed $q^{-1/2}$

are shown in Fig. 4, the first mode shape of this blade at $\omega_1 = 1.47$ in Fig. 5. Again actual and closed form mode shape are indistinguishable.

We first assume uniform mass and flap-bending stiffness of the blade and determine the dimensionless pitching and rolling moments $C_m/a\sigma_1, C_\ell/a\sigma$ due to unit longitudinal cyclic pitch input. The parameters, same as in Fig. 4 of Reference (3) are: $\gamma = 5$, $B = .97$, $\mu = 1.0$, zero root cutout. When using two modes it was found that there is little difference in the results between rotating or non-rotating modes. It was also found that in case of two modes there is little difference between using the elastic moment Eq. (23) or the air moment Eq. (25). The two mode solution is considered to be the "exact" solution, against which the others are checked. With respect to the single mode analysis it was found that there is almost no difference between using the actual mode or using the closed form mode of Eq. (37) with an appropriate value of κ.

However, there were some differences of results in the single mode analysis between the generalized force approach of Eq. (18) leading either to the hub moment expression of Eq. (23) or of Eq. (25), and the moment approach of Eq. (34) leading to the hub moment expression Eq. (35). In all of the analytical models the first natural frequency of the rotating blade was $\omega_1 = 1.2$ or $\omega_1 = 1.4$. The following is

a list of the methods used:

A Rigid blade elastically hinged at rotor center

B Single non-rotating mode with generalized force balance, hub moment from Eq. (25). This is the single mode method of Reference (3).

C Single rotating mode with generalized force balance, elastic hub moments from Eq. (23)

D Single rotating mode with generalized force balance, airload hub moment from Eq. (25)

E Single rotating mode with moment balance about rotor center, hub moment from Eq. (35)

F Two rotating or non-rotating modes with generalized force balance, hub moment from either Eq. (23) or (25)

The following table shows the results:

Table 1

Uniform Blade Mass and Stiffness

$\gamma = 5$, $B = .97$, $\mu = 1.0$, $\theta_s = 1$

ω_1		A	B	C	D	E	F
1.2	$C_m/a\sigma$	.111	.158	.139	.136	.139	.126
	$C_\ell/a\sigma$	.028	.019	.018	.023	.019	.025
1.4	$C_m/a\sigma$	.103	.142	.133	.134	.137	.131
	$C_\ell/a\sigma$	.086	.081	.080	.081	.080	.081

The last column in the table can be considered to give the "correct" values. The rigid blade model, column A exhibits errors up to about 12% for $\omega_1 = 1.2$ and up to 20% for $\omega_1 = 1.4$. Considering the uncertainties of the omitted wake effect, this represents a reasonable engineering accuracy. The single non-rotating mode model used in References (3) and (7), column B, exhibits errors up to 25% in $c_m/a\sigma$ for $\omega_1 = 1.2$, which is worse than the rigid blade model. For $\omega_1 = 1.4$ the error is only 9%. The columns C and D for the single rotating blade model show a considerable improvement over column B for the non-rotating single mode, whereby Eq. (25) used in column D is clearly superior to Eq. (23) used in column C. This corresponds to the trend found in Reference (7). Column E computed from the moment balance about the rotor center with the rotating first mode is identical to column D for $\omega_1 = 1.4$ and somewhat less accurate for $\omega_1 = 1.2$. In view of the greater simplicity of the moment balance method, reflected in Eqs. (34) and (35), the accuracy of column E is considered to be adequate, certainly for the higher values of ω_1.

In order to check on the accuracy of the various methods for other hub moment derivatives, the response to collective pitch $\theta_o = 1$, to lateral cyclic pitch $\theta_c = 1$, to inflow $\lambda = 1$ and to blade twist $\theta_1 = 1$ was determined

and presented in Table 2. Only cases A (rigid blade), E (single mode moment balance) and F (2 modes) were computed. Again the single mode method yields satisfactory results, while the rigid blade method is in general not reliable.

Table 2

Uniform Blade Mass and Stiffness

$\gamma = 5$, $B = .97$, $\mu = 1.0$, $\omega_1 = 1.40$, $\omega_2 = 6.08$

INPUT	RESPONSE	A	E	F
$\theta_o = 1$	$C_m/a\sigma$	.137	.175	.168
	$C_\ell/a\sigma$	.108	.100	.102
$\theta_c = 1$	$C_m/a\sigma$	.062	.066	.065
	$C_\ell/a\sigma$	.025	.025	.025
$\lambda = 1$	$C_m/a\sigma$	.084	.109	.102
	$C_\ell/a\sigma$	.051	.045	.047
$\theta_1 = 1$	$C_m/a\sigma$	.096	.124	.125
	$C_\ell/a\sigma$	.075	.069	.068

Next we assume the tapered in thickness blade with mass and stiffness distribution of Fig. 1. By comparing Figs. 2 and 4 it is seen that the two first natural frequencies are spread less apart than for the uniform blade. By comparing Figs. 3 and 5 it is seen that the first mode shape is stronger curved than for the uniform blade, indicated by a higher value of κ. The effects of flap-bending flexibility should, therefore, be larger than for the uniform blade. The closed form mode, Eq. (36), is again indistinguishable from the actual mode. Only the case of $\omega_1 = 1.47$ was considered for which, according to Fig. 4, $q^{-1/2} = 7.15$, and only the cases A, E and F are shown in the following table.

Table 3

Tapered in Thickness Blade

$\gamma = 5$, $B = .97$, $\mu = 1.0$, $\omega_1 = 1.47$, $\omega_2 = 3.90$

Input	Response	A	E	F
$\theta_s = 1$	$C_m/a\sigma$	.093	.176	.163
	$C_\ell/a\sigma$	.097	.071	.073
$\theta_o = 1$	$C_m/a\sigma$	.124	.218	.200
	$C_\ell/a\sigma$	.123	.088	.091
$\theta_c = 1$	$C_m/a\sigma$	.066	.068	.060
	$C_\ell/a\sigma$	.022	.026	.026
$\lambda = 1$	$C_m/a\sigma$	.077	.138	.119
	$C_\ell/a\sigma$	.060	.037	.041
$\theta_1 = 1$	$C_m/a\sigma$	.087	.154	.159
	$C_\ell/a\sigma$	.085	.060	.057

Assuming as before, that the column F represents the "exact" values, it is seen that, as expected, the rigid blade analysis is much less accurate than for the uniform blade. However, the single mode analysis using moment balance about the rotor center, Eq. (35), is very much better than the rigid blade analysis and appears to provide adequate engineering accuracy, at least for $\omega_1 = 1.47$. From Tables 1 and 2 one can expect, that the accuracy of method E will improve for higher values of ω_1, which is also evident from Fig. 4 indicating that the ratio ω_2/ω_1 increases with increasing ω_1. Method E will be used throughout the remainder of this report.

Multiblade Analysis

The multiblade analysis with generalized coordinates follows the same pattern set up in Reference 8. Letting the subscript k refer to the kth blade and assuming a single elastic mode in the form $\eta = x + \kappa\, \eta_h$, the generalized coordinate β_k represents now the angle of the straight line through the .73 point of the mode shape, see Figs. 3 and 5, so that β_k can be interpreted as the "equivalent" flapping angle of the kth blade. The relation of the multiblade coordinates β_o, β_d, β_I, β_{II}, etc. to the individual blade coordinate β_k is given by

$$\beta_k = \beta_o + \beta_d(-1)^k + \beta_I \cos \psi_k + \beta_{II} \sin \psi_k + \beta_{III} \cos 2\psi_k + \beta_{IV} \sin 2\psi_k + \ldots \qquad (41)$$

$$k = 1, 2, \ldots b$$

C.2.

with the inverse

$$\left.\begin{aligned} \beta_o &= (1/b)\sum_{k=1}^{b}\beta_k \quad , & \beta_d &= (1/b)\sum_{k=1}^{b}\beta_k(-1)^k \\ \beta_I &= (2/b)\sum_{k=1}^{b}\beta_k \cos\psi_k \quad , & \beta_{II} &= (2/b)\sum_{k=1}^{b}\beta_k \sin\psi_k \\ \beta_{III} &= (2/b)\sum_{k=1}^{b}\beta_k \cos 2\psi_k \quad , & \beta_{IV} &= (2/b)\sum_{k=1}^{b}\beta_k \sin 2\psi_k \end{aligned}\right\} \quad (42)$$

The first of the multiblade equations is obtained by inserting Eq. (41) into Eq. (34) for each individual blade and adding the b blade equations under consideration of

$$\sum_{k=1}^{b}\cos m\psi_k = \begin{cases} 0, \text{ if } m \text{ is not a multiple of } b \\ b\cos mt, \text{ if } m = sb,\ s = 1,2\ldots \end{cases}$$

$$\sum_{k=1}^{b}\sin m\psi_k = \begin{cases} 0, \text{ } m \text{ is not a multiple of } b \\ b\sin mt, \text{ if } m = sb,\ s = 1,2\ldots \end{cases} \quad (43)$$

If b is even, the second of the multiblade equations is obtained by adding the equations for even blade number k and subtracting the equations for odd k, again making use of Eq. (43). The remaining multiblade equations are obtained by multiplying each individual blade equation by cos ψ_k and adding them, by sin ψ_k and adding the, by cos $2\psi_k$ and adding, by sin $2\psi_k$ and adding etc., always considering Eq. (43).

For neglected reversed flow one then obtains in the case of a 4 bladed rotor Equations (9) to (12) of Reference 8 plus terms originating from the elastic blade bending corrections to the rigid blade analysis. The equations are given in Appendix C with terms from the elastic blade bending effects underlined. In the numerical examples reversed flow is included. The periodic coefficients become then non-analytic and are given in the form of truncated Fourier series (see Appendix B for the single blade), whereby the truncation is selected in such a way that the error is 1 per cent or less. The effect of blade elasticity can be determined by comparing the solution for $\kappa = 0$ (rigid blade) with the solution for the value of κ corresponding to the first elastic blade mode.

Applications to Stability Problems

Lagged tilting feedback, described by

$$\dot{\theta}_I + L\,\theta_I = -K_i\,\beta_I$$

$$\dot{\theta}_{II} + L\,\theta_{II} = -K_i\,\beta_{II}$$

is assumed, whereby L remains fixed at $L = .1$ as K_i is increased to the stability limit. Two blade types are assumed: the blade with uniform mass and stiffness distribution with $\omega_1 = 1.40$ and the tapered in thickness blade with $\omega_1 = 1.47$. Two advance ratios have been studied,

μ = .8 and μ = 1.6, and two blade numbers, b = 3 and b = 4. In each case the stability analysis was performed for the rigid blade, κ = 0, and for the flexible blade with κ = .13 (uniform blade) and κ = .27 (tapered blade). Figs. 6 to 13 show the characteristic values of the Floquet state transition matrix, whereby the frequencies were selected as explained in Reference 8. The dash lines refer to κ = 0 - rigid blade - the solid lines to κ = .13 or .27. It is seen that stability suffers from inclusion of blade elasticity in all cases. For the uniform blade at μ = .8 the effect of blade elasticity is quite small, for the tapered in thickness blade at μ = .8 the elastic effect is much larger, while for μ = 1.6 the destabilizing effect of blade elasticity for both types of blades is very substantial.

Applications to Random Loads Problems

The time variable response covariance matrix with the components σ_{β_I}, $\sigma_{\beta_{II}}$, $r_{\beta_I\beta_{II}}$ has been determined using Eqs. (4) and (7) to (9) of Part I for the tapered thickness blade with ω_1 = 1.47, b = 3, μ = 1.6, γ = 5, comparing the rigid blade result with the flexible blade result for zero feedback and for lagged moment feedback with K_i = .2. The scale of longitudinal turbulence over rotor radius has been assumed as L/R = 12, and the standard deviation of λ as σ_λ = 1. Figs. 14, 15 and 16 show the components of the

response covariance matrix for zero feedback. The large unfavorable influence of blade flexibility is evident. Figs. 17, 18, 19 show the components of the covariance matrix for $K_i = .2$ lagged feedback gain. The values are lower, however the unfavorable effect of blade flexibility is greater than the favorable effect of the feedback. In order to substantiate this surprising result with a much simpler and independent case, the deterministic responses of β_I and β_{II} to a step gust $\lambda = 1$ were determined and are presented in Figs. 20 and 21 for $K_i = 0$ and in Figs. 22 and 23 for $K_i = .2$. It is seen that for $K_i = 0$ similar order of the effects of blade flexibility exist as for the standard deviations σ_{β_I} and $\sigma_{\beta_{II}}$. For $K_i = .2$ the feedback is very effective, contrary to the random gust case.

Conclusions

A variety of methods of applying blade flap bending corrections to the rigid blade analysis of hingeless lifting rotors were checked out with regard to the problem of hub moment response to longitudinal cyclic pitch input at rotor advance ratio of unity, leading to the following conclusions:

1. Using two elastic blade modes, the result is insensitive to assuming either the modes of the non-rotating or those of the rotating blade. In the latter case the result is also insensitive to computing the hub moment either

from the air loads or from the elastic blade root bending moment.

2. Using one elastic mode of the non-rotating blade, the error in the result can be even larger than for the rigid blade analysis.
3. Using one elastic mode of the rotating blade the error in the result is substantially less, whereby the air load hub moment is more accurate than the elastic blade root bending moment.
4. Using one elastic mode of the rotating blade with the moment balance about the rotor center rather than the generalized force balance as in conventional analyses, air load hub moment and elastic blade root bending moment are equal and the result is almost as accurate as that for the best of the previously listed single mode methods.
5. The single mode method with moment balance about the rotor center is sufficiently accurate also for hub moments from lateral cyclic pitch, from collective pitch, from blade twist and from inflow changes, assuming both a uniform blade and a strongly thickness tapered blade. The rigid blade method in the latter case results in large hub moment errors.
6. A closed form expression for the first rotating blade mode was found which includes an empirical factor

allowing to accurately represent the first rotating blade mode for blades with widely varying stiffness and mass distributions. Closed form aerodynamic coefficients are given to account for the aerodynamic effects of blade elastic flap bending.

The method of using the moment balance about the rotor center for the first mode in closed form was then applied to the problem of multiblade dynamic stability and random loads of a lifting rotor with lagged hub moment feedback, leading to the following conclusions:

7. The rigid blade analysis is unconservative with respect to multiblade dynamic stability. Particularly for a tapered in thickness blade large reductions in stability margins are obtained from the elastic blade flap-bending corrections.
8. The time variable standard deviations of the hub moments as a result of random gust inputs are substantially increased by considering elastic blade flap bending corrections.
9. While lagged hub tilting moment feedback is very effective in alleviating step gust responses , it is little effective in alleviating random gust responses.

References

1. Harris, I. D., Articulated Rotor Blade Flapping Motion at Low Advance Ratio, Journal American Helicopter Society, Vol. 17, No. 1, January 1972, pp. 41-48.

2. Kuczynski, W. A., Sharpe, D. L., and Sissingh, G. J., "Hingeless Rotor, Experimental Frequency Response and Dynamic Characteristics with Hub Moment Feedback Control", 28th Annual National Forum American Helicopter Society, Preprint No. 612, May 1972.

3. Ormiston, R. A. and Peters, D. A., "Hingeless Rotor Response with Non-uniform Inflow and Elastic Blade Bending", AIAA 10th Aerospace Science Meeting, San Diego, AIAA Paper No. 72-65, January 1972.

4. Leone, P. F., "A Note on Effects of Longitudinal Cyclic Pitch Control Variations on the Forced Aero-Elastic Response of a Helicopter Blade", Journal American Helicopter Society, Vol. 4, No. 4, October 1959.

5. Daughaday, H., DuWaldt, F. and Gates, C., "Investigation of Helicopter Blade Flutter and Load Amplification Problems", Journal American Helicopter Society, Vol. 2, No. 3, July 1957, pp. 27-45.

6. Perisho, C. H., "Analysis of the Stability of a Flexible Rotor Blade at High Advance Ratio", Journal American Helicopter Society, Vol. 4, No. 2, April 1959.

7. Curtiss, H. C. Jr., and Shupe, N. K., "A Stability and Control Theory for Hingeless Rotors", Proceedings 27th Annual National V/STOL Forum, American Helicopter Society, Preprint No. 541, May 1971.

8. Hohenemser, K. H., and Yin, S. K., "Some Applications of the Method of Multiblade Coordinates", Journal American Helicopter Society, Vol. 17, No. 3, July 1972.

9. Blankenship, B. L. and Harvey, K. W., "A Digital Analysis for Helicopter Performance and Rotor Blade Bending Moments", Journal American Helicopter Society, Vol. 7, No. 4, October 1962, pp. 55-68.

10. Peters, D. A. and Hohenemser, K. H., "Application of the Floquet Transition Matrix to Problems of Lifting Rotor Stability", Appendix I, Journal American Helicopter Society, Vol. 16, No. 2, April 1971, p. 33.

11. Sissingh, G. J. and Kuczynski, W. A., "Investigations on the Effect of Blade Torsion on the Dynamics of the Flapping Motion", Journal American Helicopter Society, Vol. 15, No. 2, April 1970, pp. 2-9.

12. Johnson, R. C., and Hohenemser, K. H., "On the Dynamics of Lifting Rotors with Thrust or Tilting Moment Feedback Controls", Journal American Helicopter Society, Vol. 15, No. 1, January 1970, pp. 42-58.

13. Myklestad, N. O., Fundamentals of Vibration Analysis, McGraw-Hill, New York, 1956.

14. Sissingh, G. J., "Dynamics of Rotors Operating at High Advance Ratios", Journal American Helicopter Society, Vol. 13, No. 3, July 1968, pp. 56-63.

Figure Captions

Fig. 1 Mass and Stiffness Distribution of Tapered in Thickness Blade

Fig. 2 First and Second Natural Frequencies of Uniform Blade vs. Rotor Speed

Fig. 3 First Mode Shape of Uniform Blade for $\omega_1 = 1.2$ to 1.4

Fig. 4 First and Second Natural Frequencies of Tapered in Thickness Blade vs. Rotor Speed

Fig. 5 First Mode Shape of Tapered in Thickness Blade for $\omega_1 = 1.47$

Fig. 6 Stability for Lagged Moment Feedback, $\mu = .8$, $b = 3$, Uniform Blade

Fig. 7 Stability for Lagged Moment Feedback, $\mu = .8$, $b = 4$, Uniform Blade

Fig. 8 Stability for Lagged Moment Feedback, $\mu = .8$, $b = 3$, Tapered Thickness Blade

Fig. 9 Stability for Lagged Moment Feedback, $\mu = .8$, $b = 4$, Tapered Thickness Blade

Fig. 10 Stability for Lagged Moment Feedback, $\mu = 1.6$, $b = 3$, Uniform Blade

Fig. 11 Stability for Lagged Moment Feedback, $\mu = 1.6$, $b = 4$, Uniform Blade

Fig. 12 Stability for Lagged Moment Feedback, $\mu = 1.6$, $b = 3$, Tapered Thickness Blade

Fig. 13 Stability for Lagged Moment Feedback, $\mu = 1.6$, $b = 4$, Tapered Thickness Blade

Fig. 14 Effect of Blade Flexibility on σ_{β_I}, $K_i = 0$

Fig. 15 Effect of Blade Flexibility on $\sigma_{\beta_{II}}$, $K_i = 0$

Fig. 16 Effect of Blade Flexibility on $r_{\beta_I \beta_{II}}$, $K_i = 0$

Fig. 17 Effect of Blade Flexibility on σ_{β_I}, $K_i = .2$

Fig. 18 Effect of Blade Flexibility on $\sigma_{\beta_{II}}$, $K_i = .2$

Fig. 19 Effect of Blade Flexibility on $r_{\beta_I \beta_{II}}$, $K_i = .2$

Fig. 20 Effect of Blade Flexibility on Step Gust Response β_I, $K_i = 0$

Fig. 21 Effect of Blade Flexibility on Step Gust Response β_{II}, $K_i = 0$

Fig. 22 Effect of Blade Flexibility on Step Gust Response β_I, $K_i = .2$

Fig. 23 Effect of Blade Flexibility on Step Gust Response β_{II}, $K_i = .2$

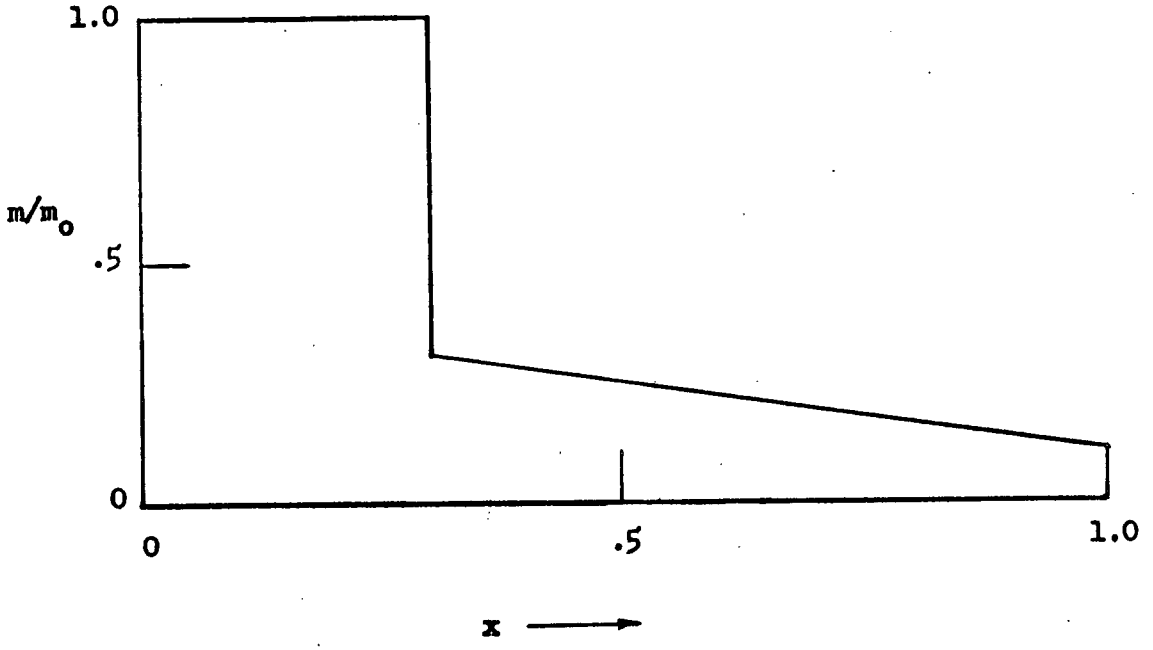

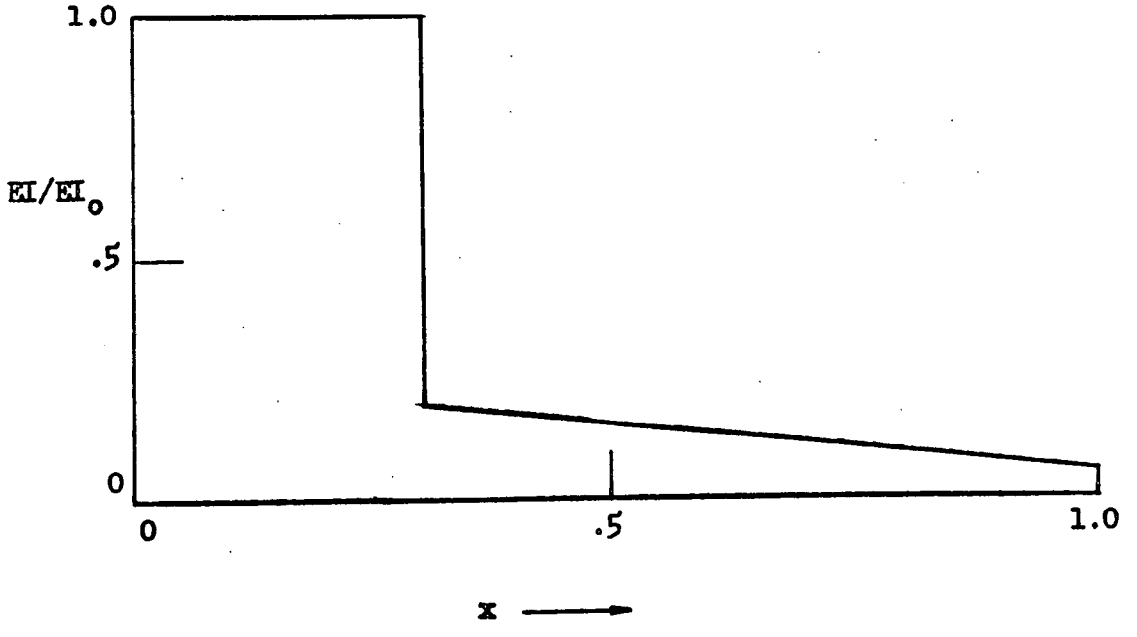

Fig. 1

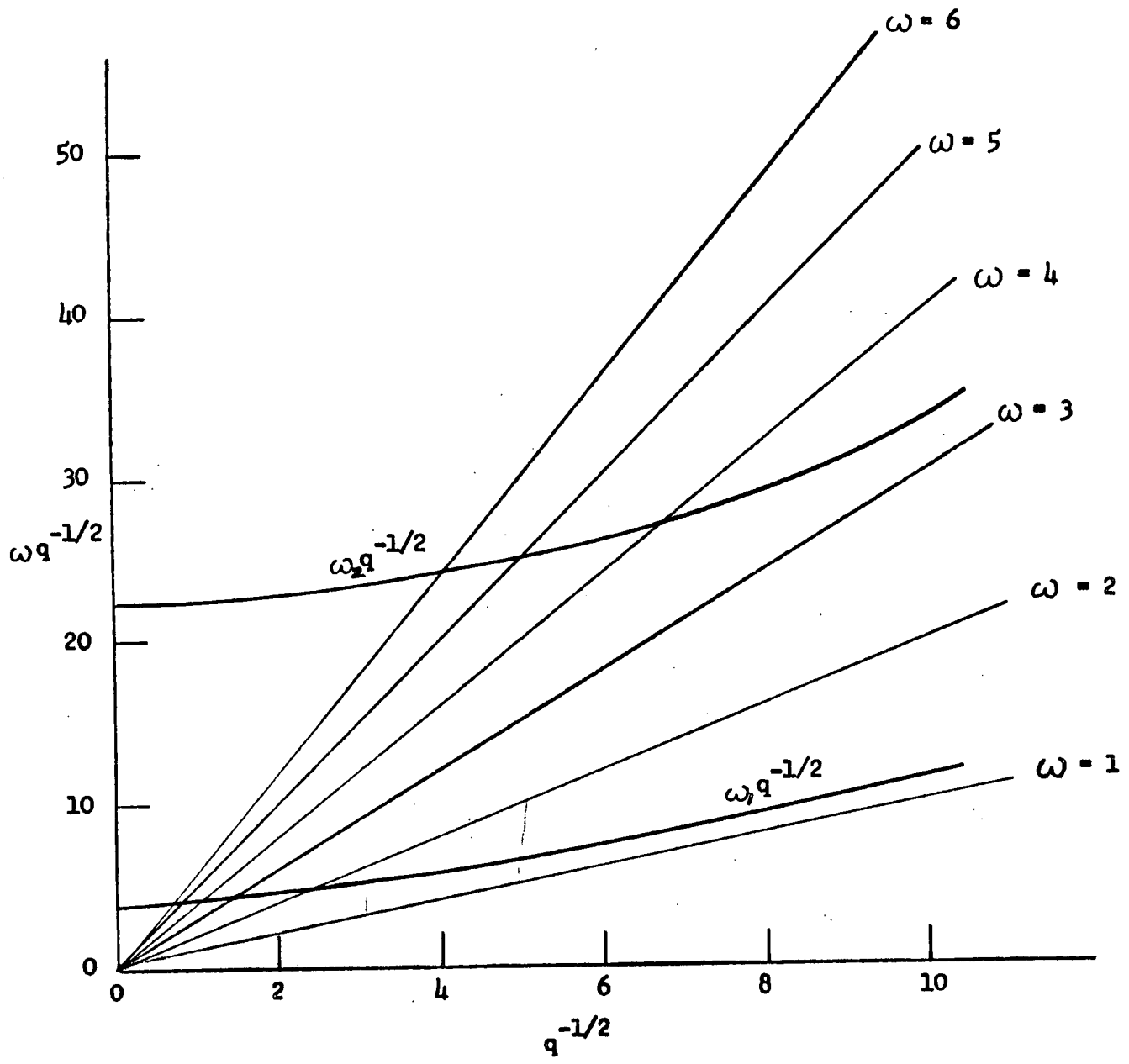
ω = 6
ω = 5
ω = 4
ω = 3
ω = 2
ω = 1
50
40
30
20
10
0
$\omega q^{-1/2}$
$\omega_2 q^{-1/2}$
$\omega_1 q^{-1/2}$
0
2
4
6
8
10
$q^{-1/2}$

Fig. 2

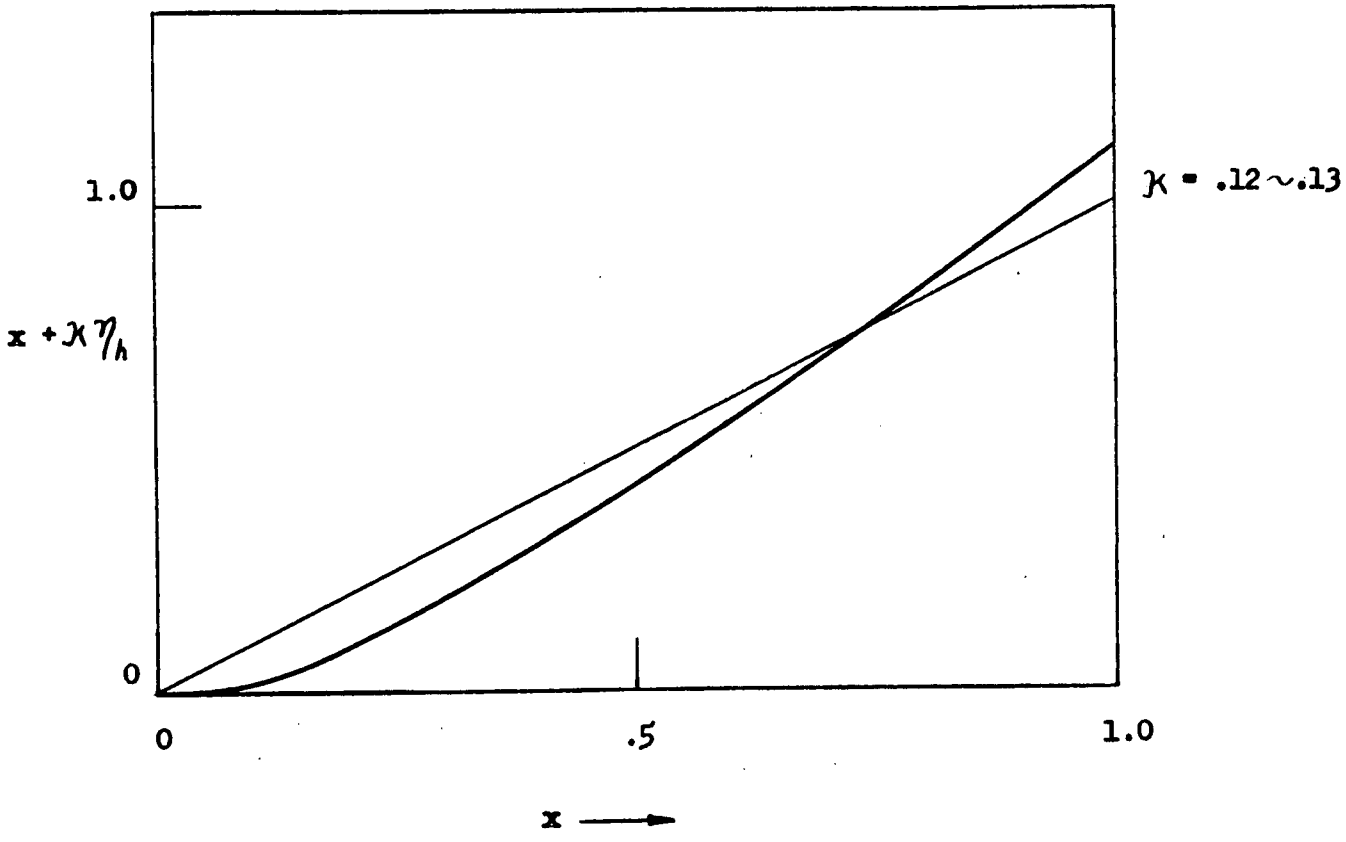

Fig. 3

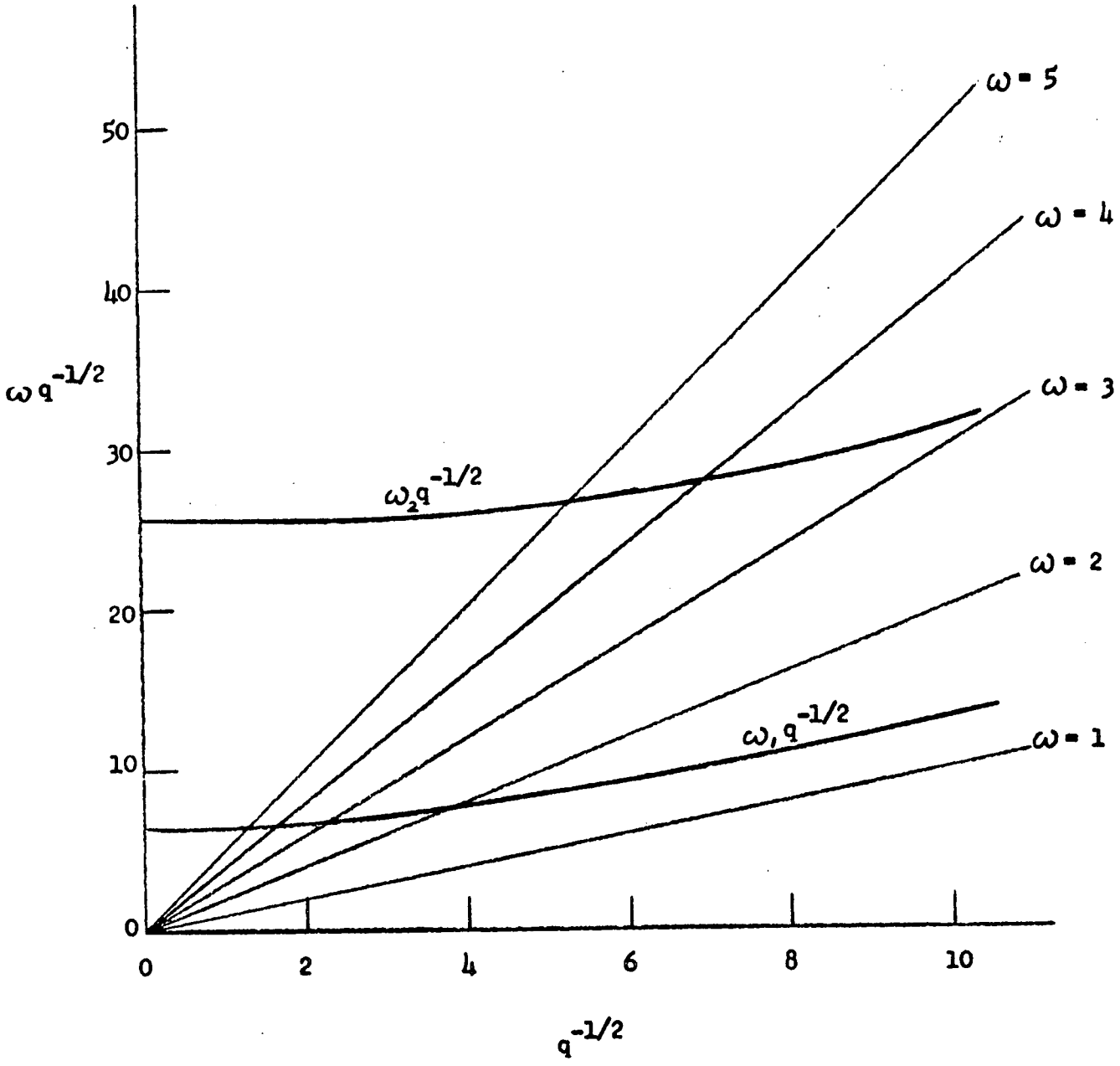
ω = 5
ω = 4
ω = 3
ω = 2
ω = 1
50
40
30
20
10
0
$\omega q^{-1/2}$
$\omega_2 q^{-1/2}$
$\omega_1 q^{-1/2}$
0
2
4
6
8
10
$q^{-1/2}$

Fig. 4

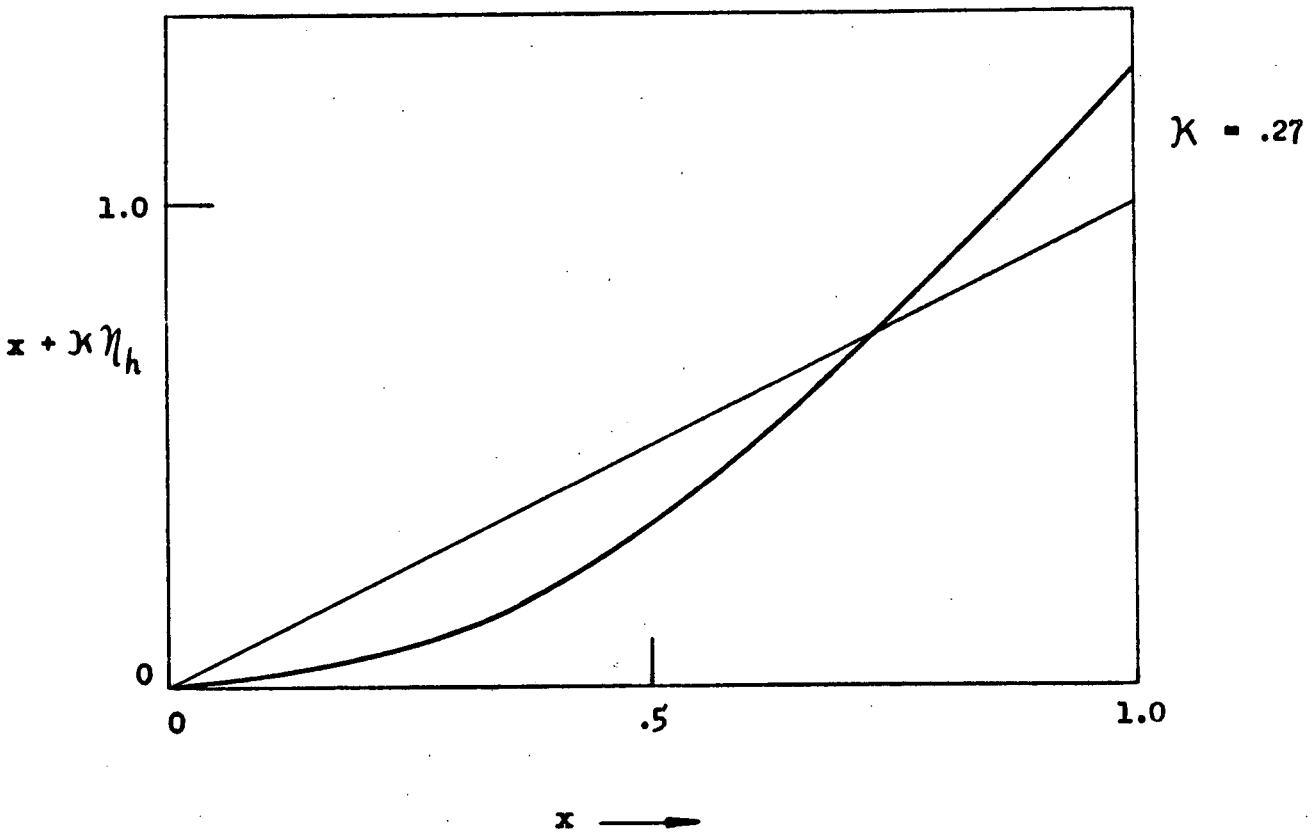

Fig. 5

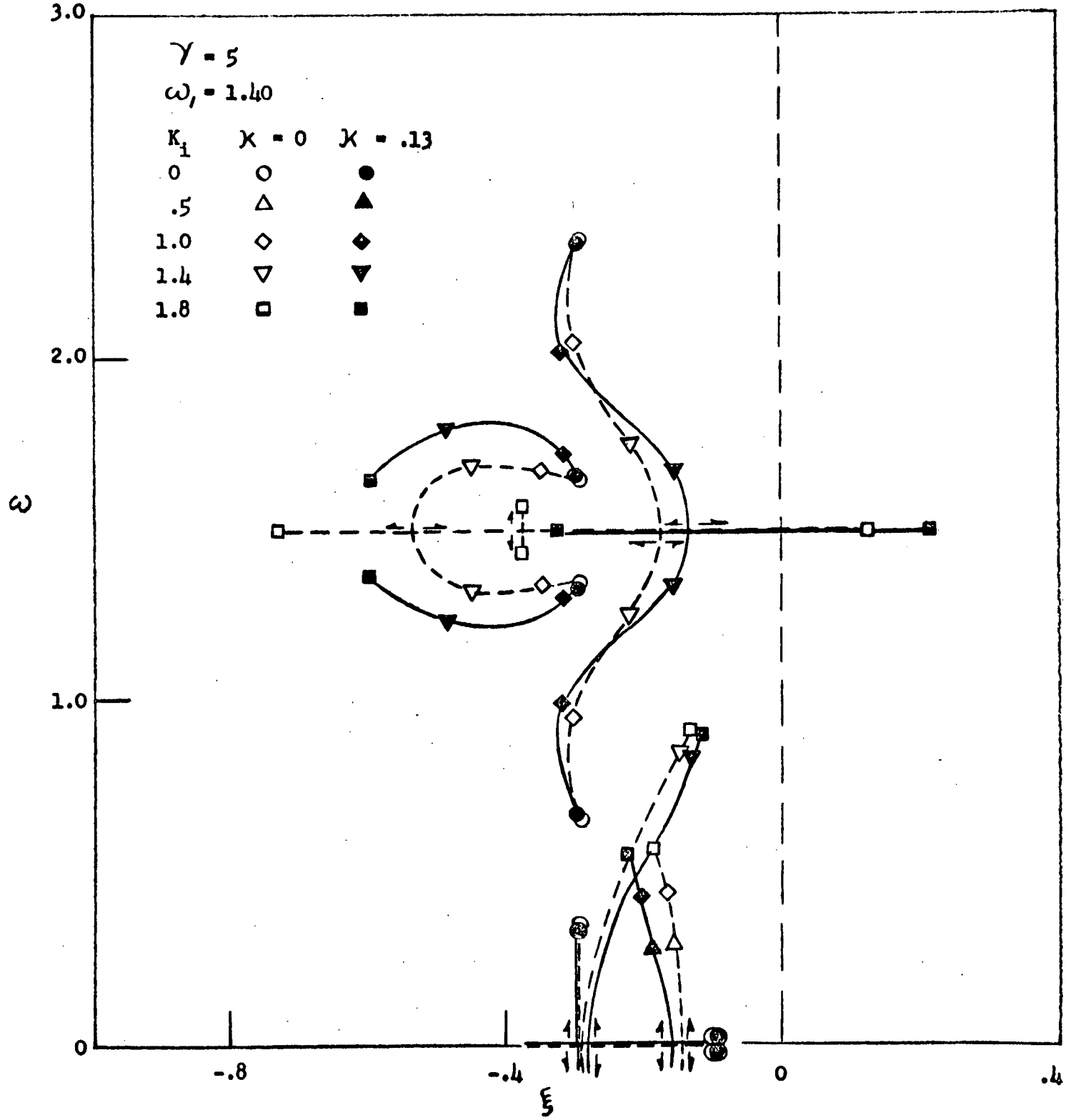

Fig. 6

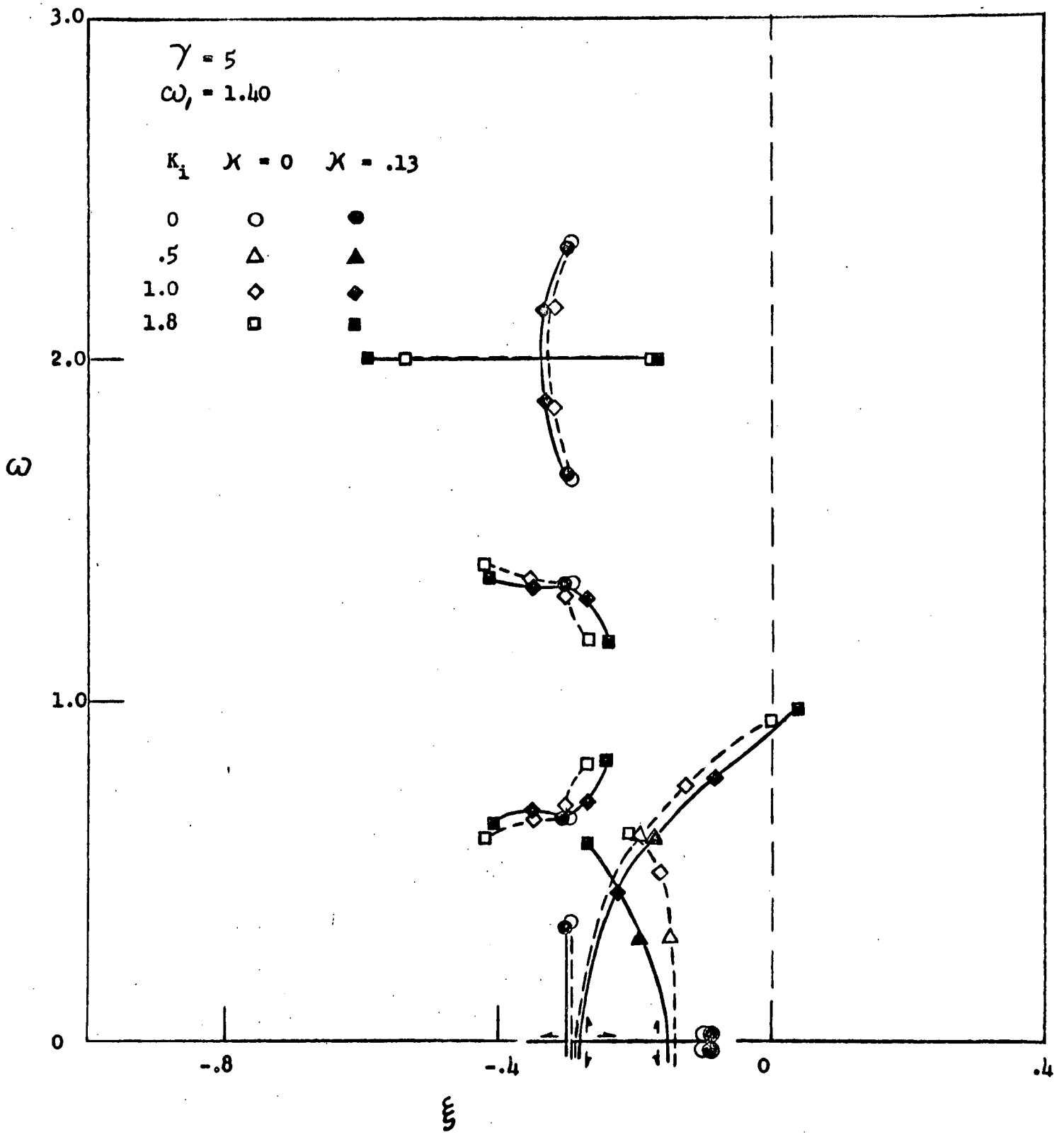

Fig. 7

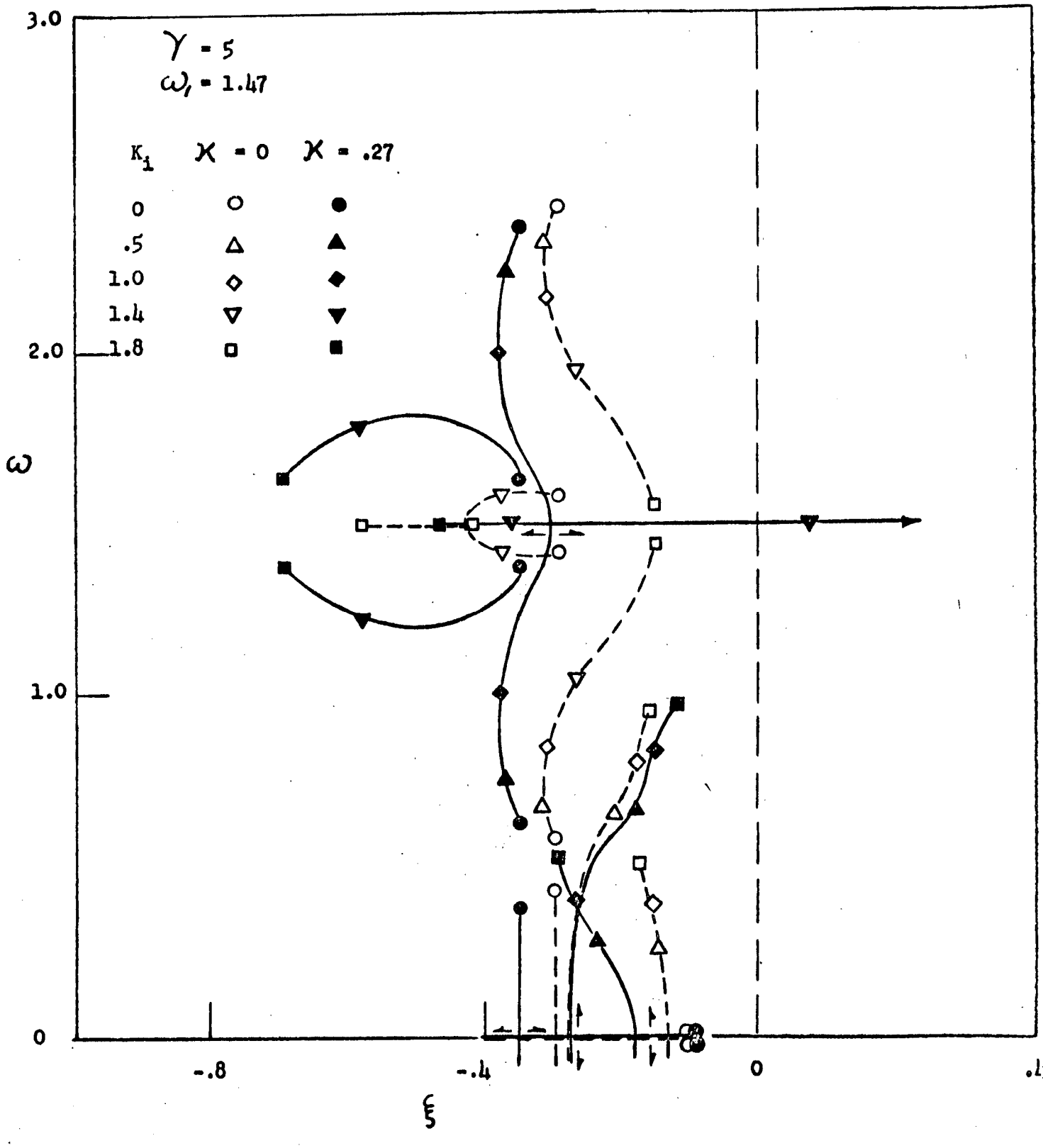

Fig. 8

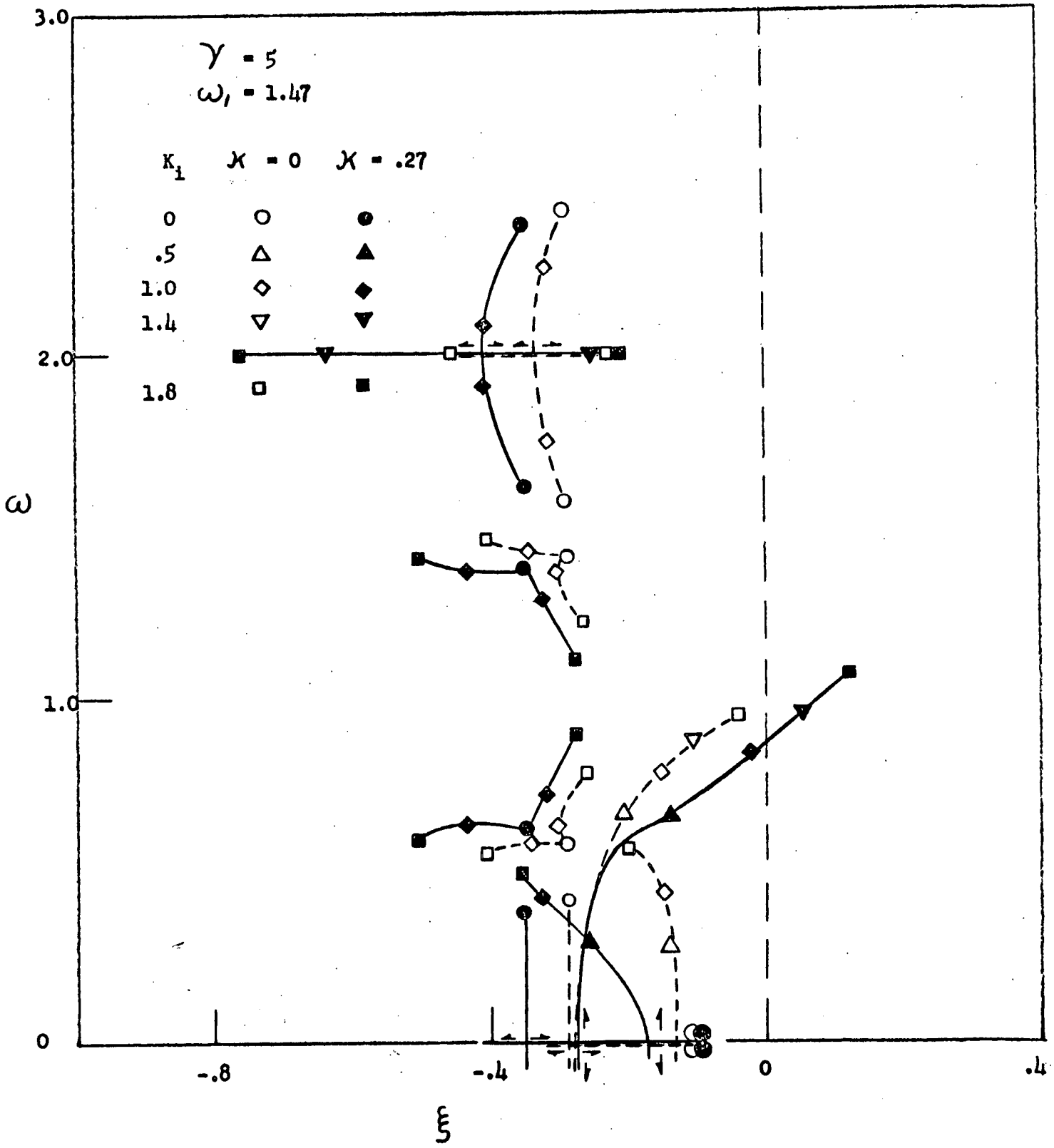

Fig. 9

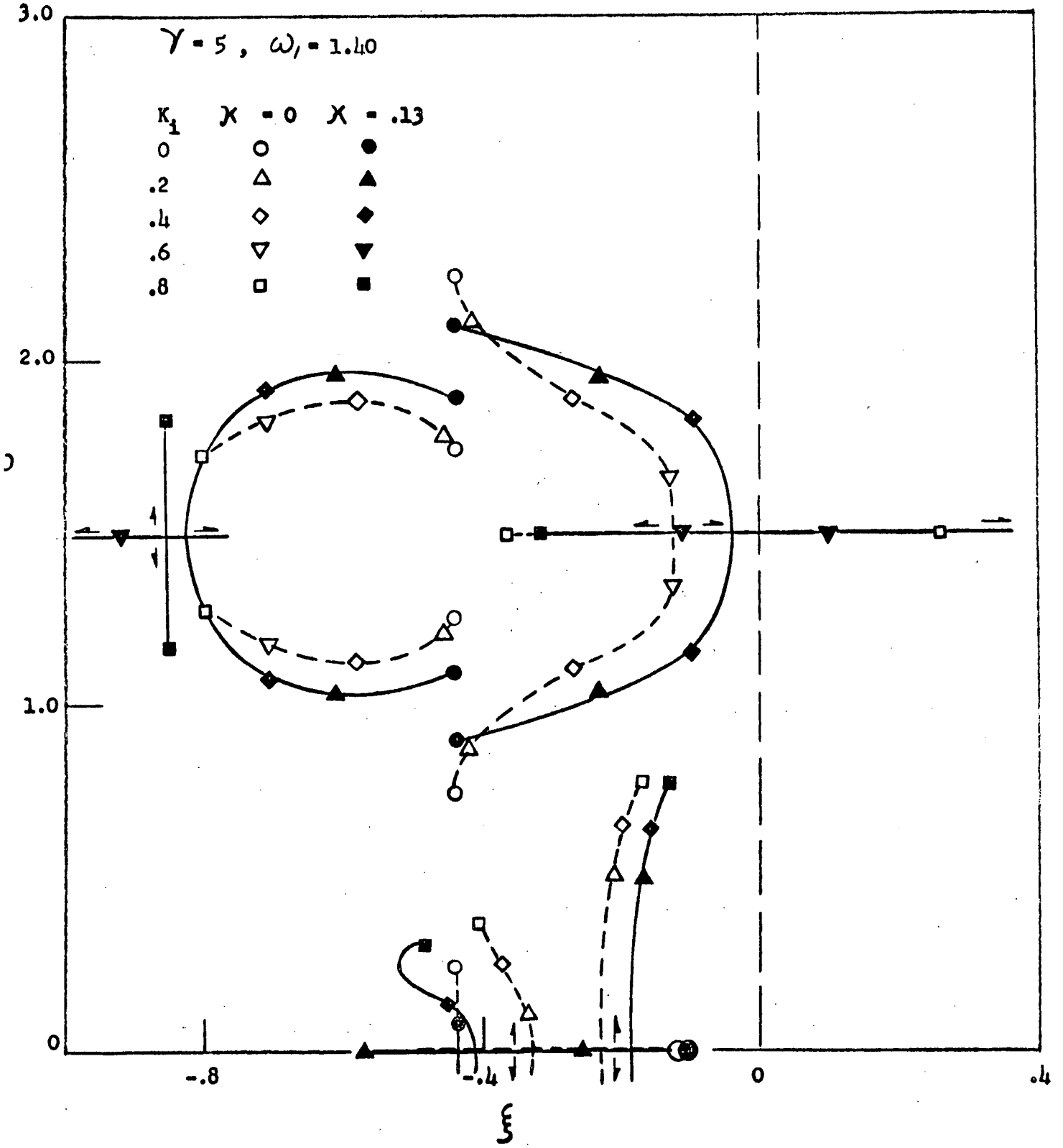

Fig. 10

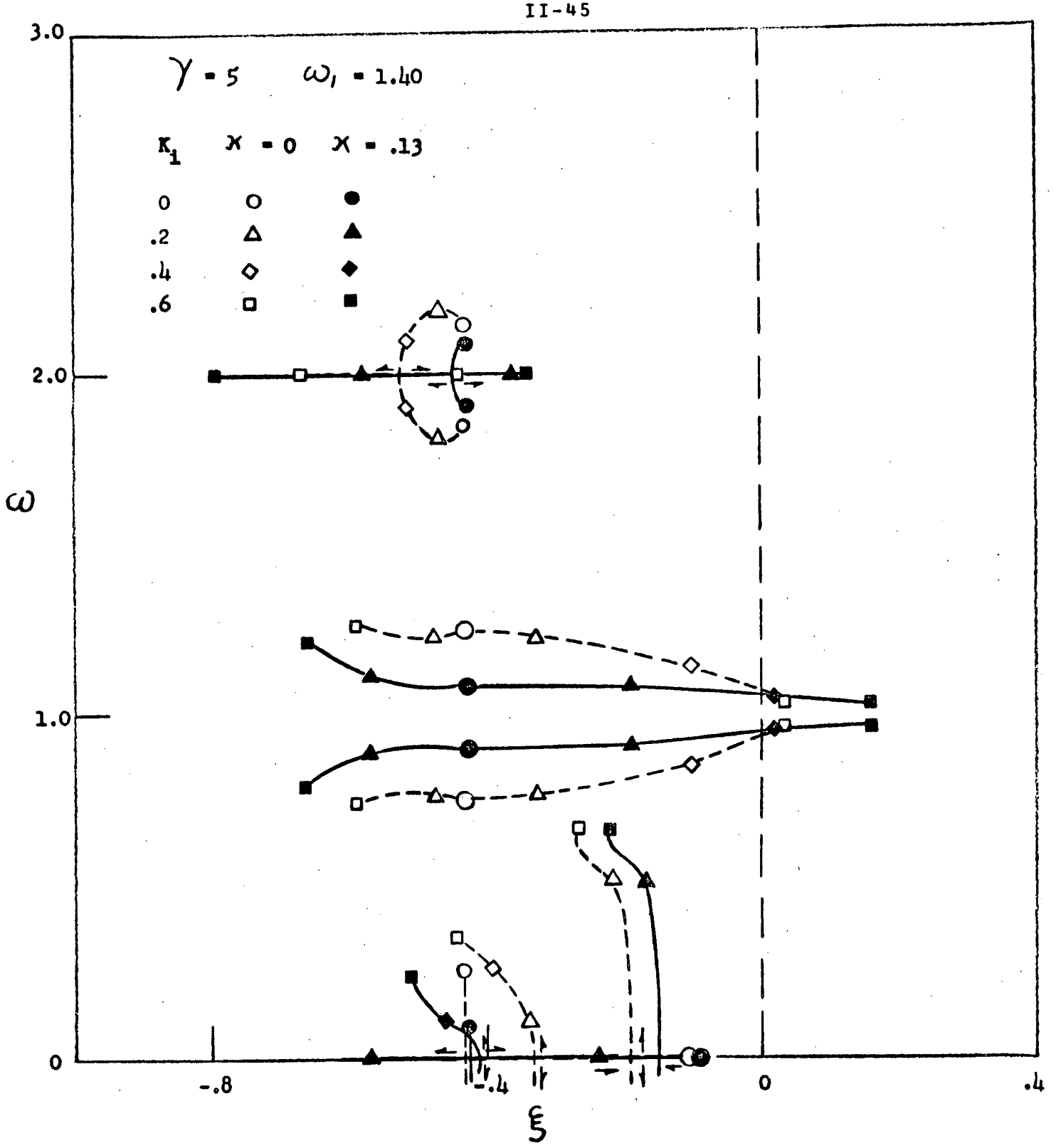

Fig. 11

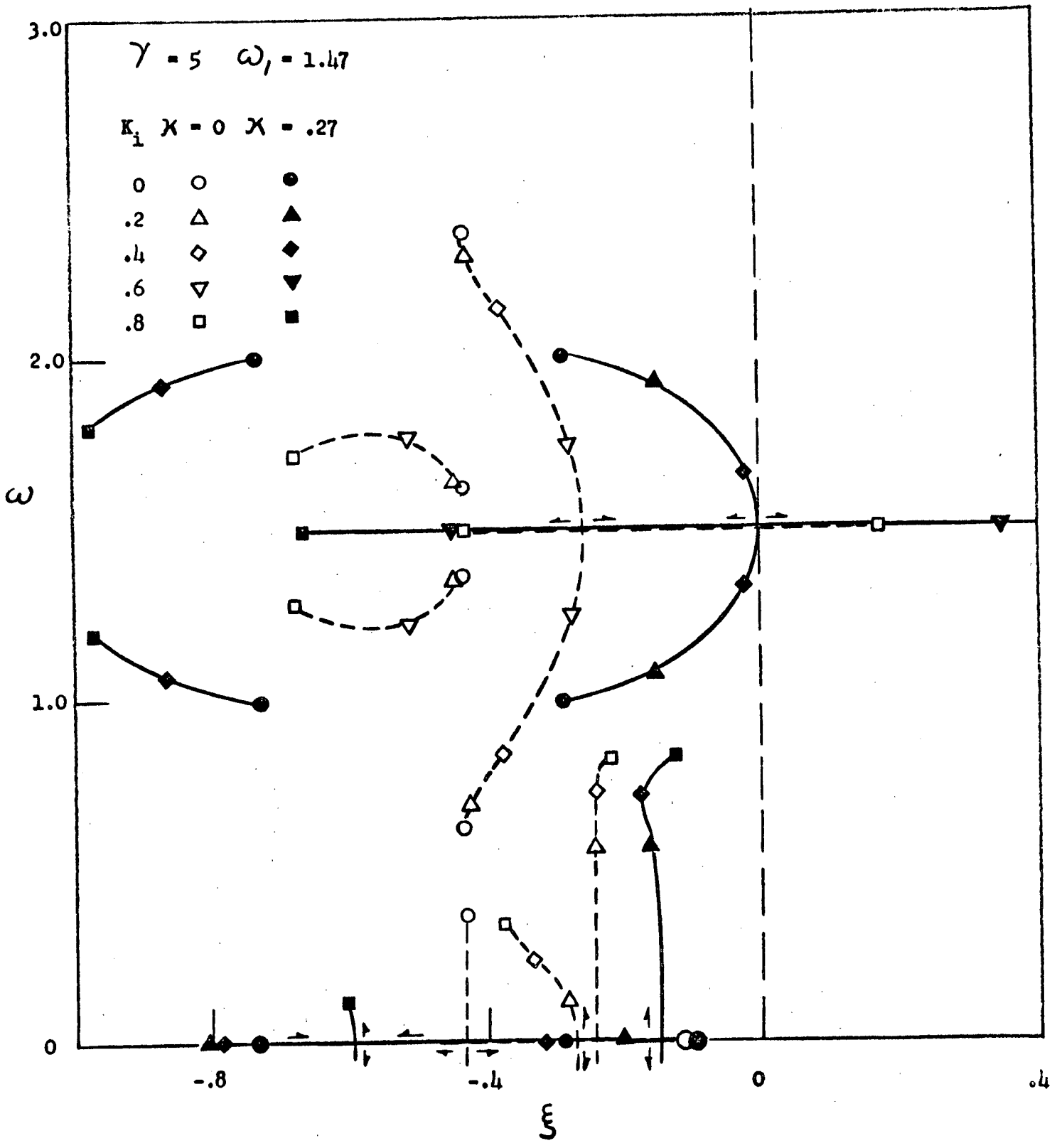

Fig. 12

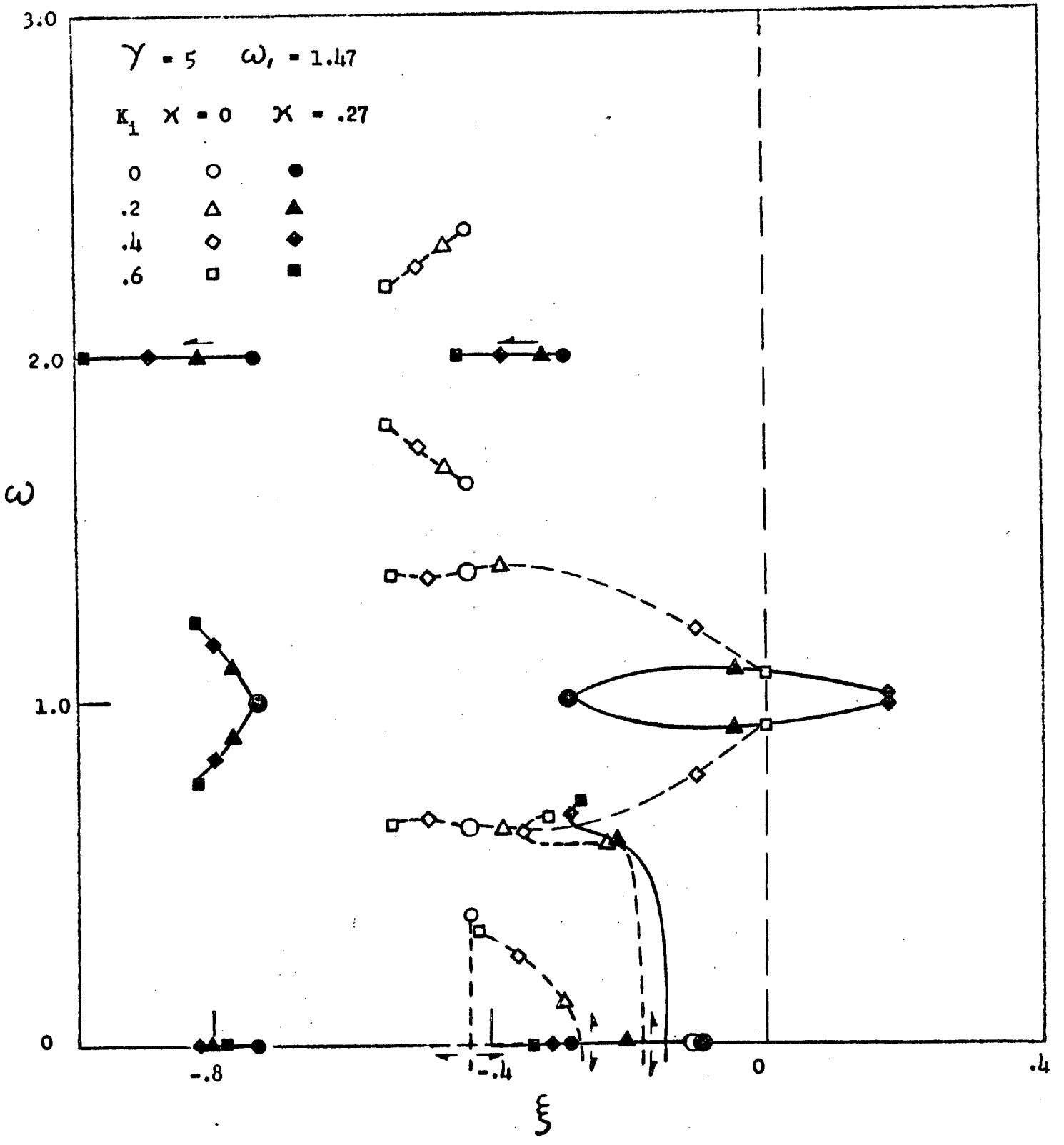

Fig. 13

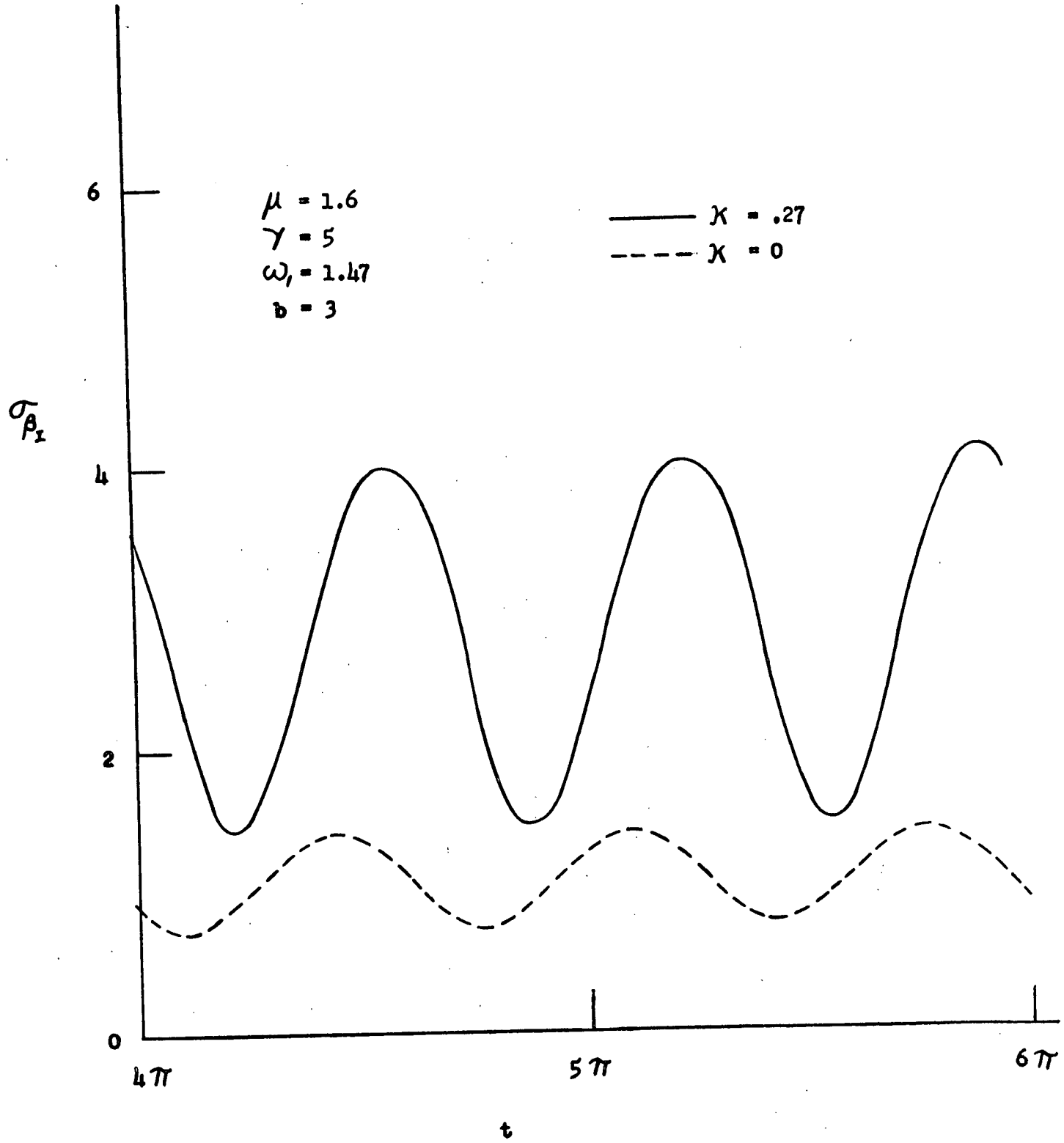
6
4
2
0
μ = 1.6
γ = 5
ω_1 = 1.47
b = 3
κ = .27
κ = 0
σ_{β_x}
4π
5π
6π
t

Fig. 14

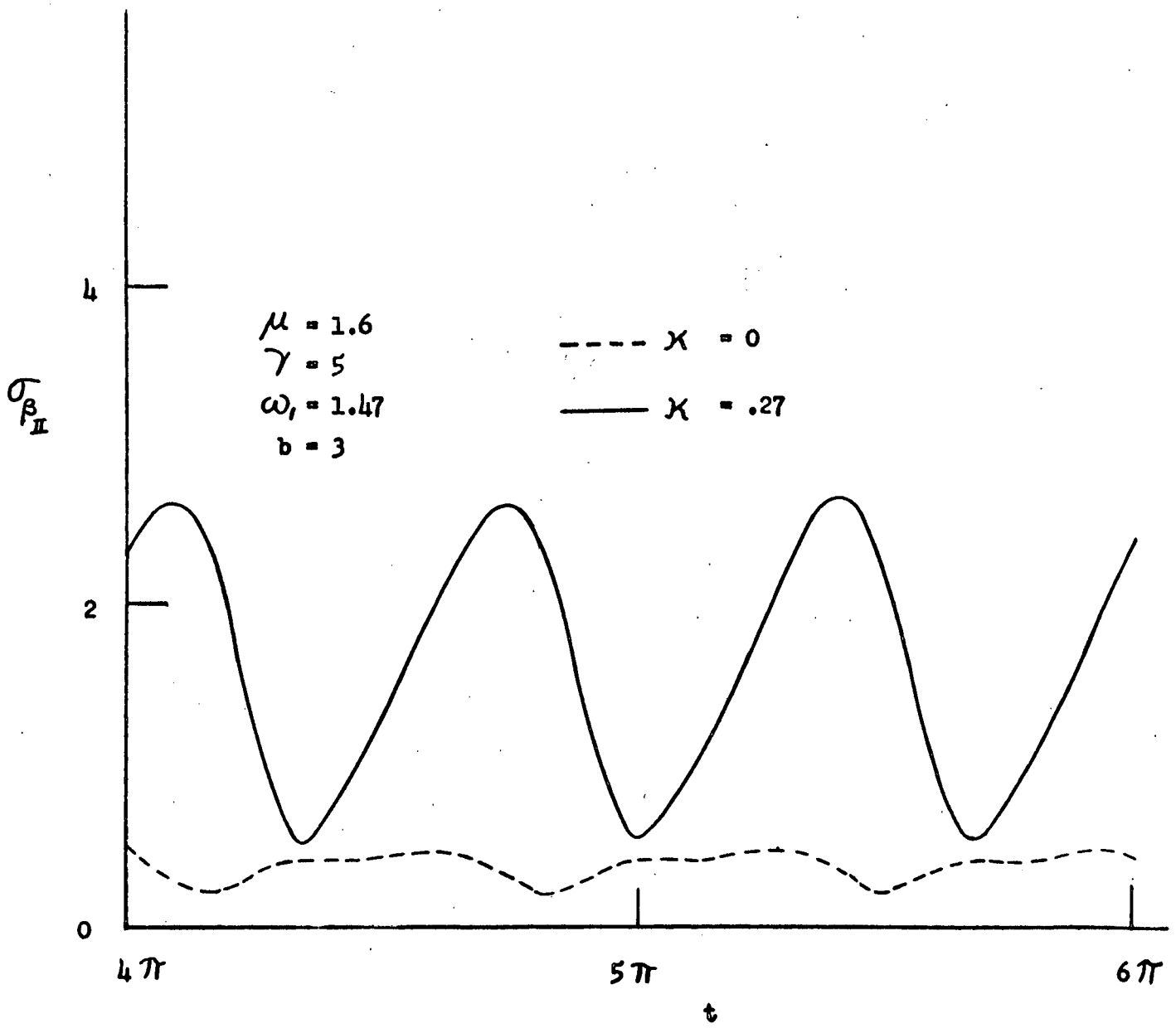
4
2
0
$\sigma_{\beta_{II}}$
μ = 1.6
γ = 5
ω_1 = 1.47
b = 3
---- $\varkappa$ = 0
—— $\varkappa$ = .27
4π
5π
6π
t

Fig. 15

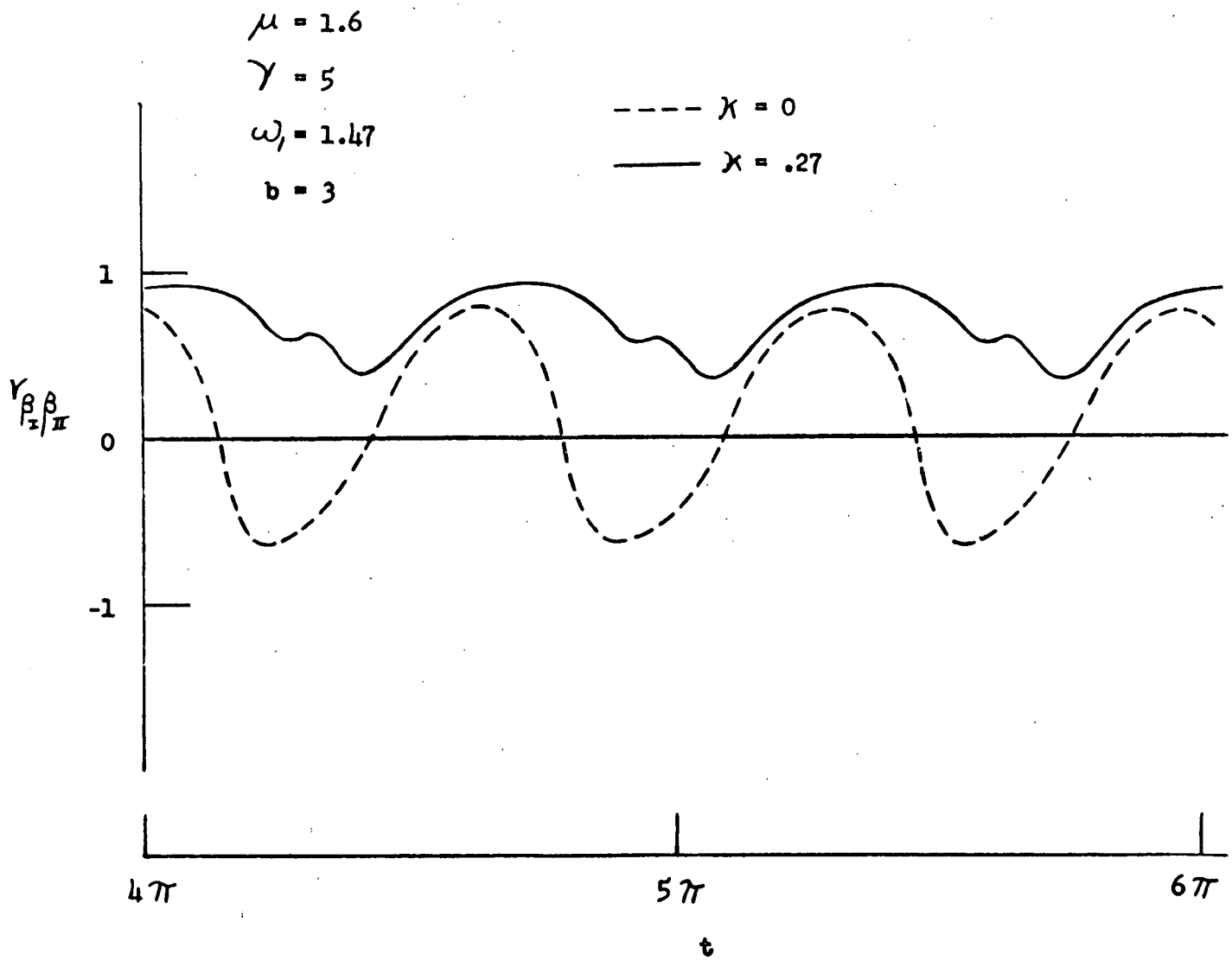

Fig. 16

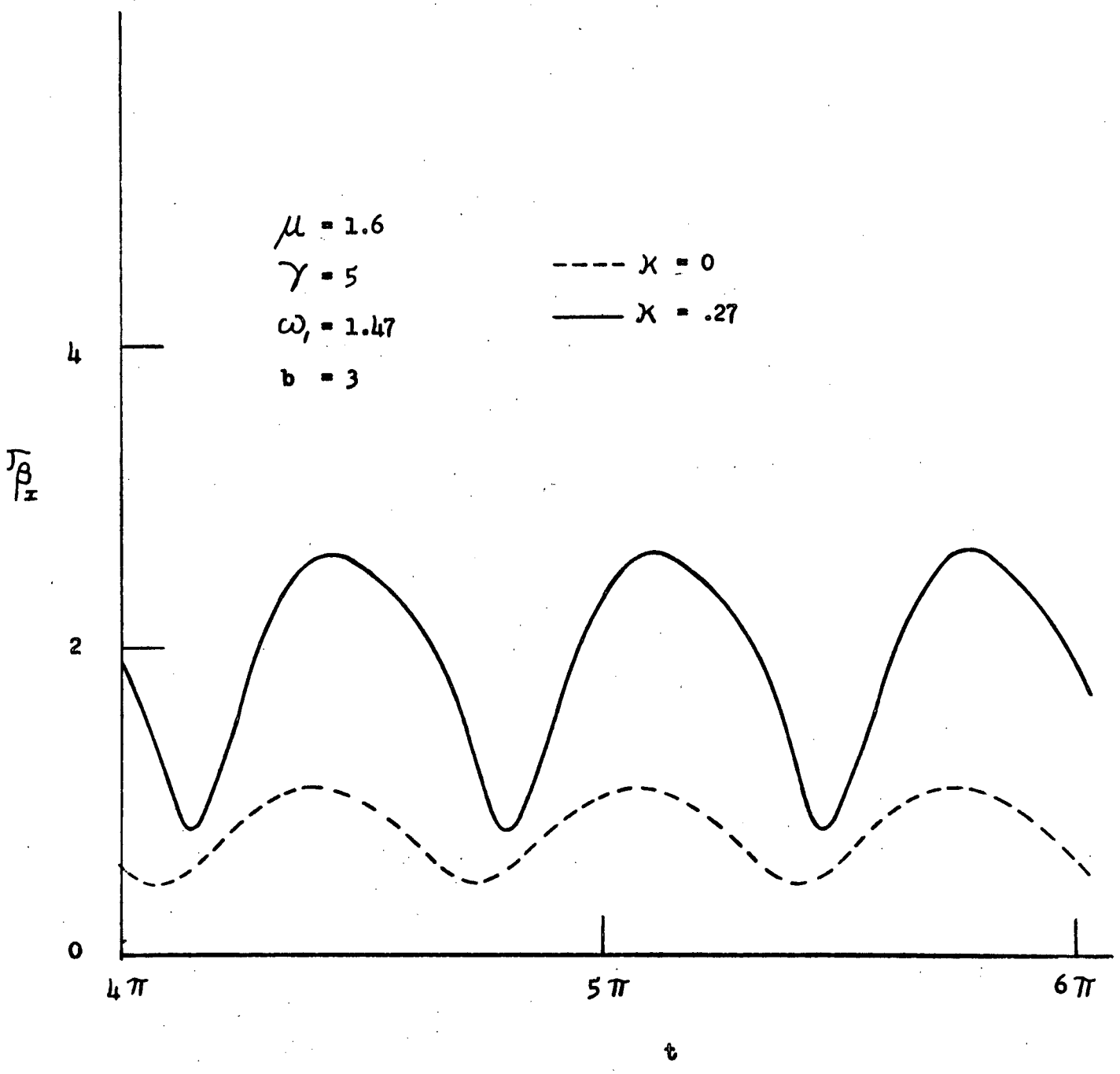

Fig. 17

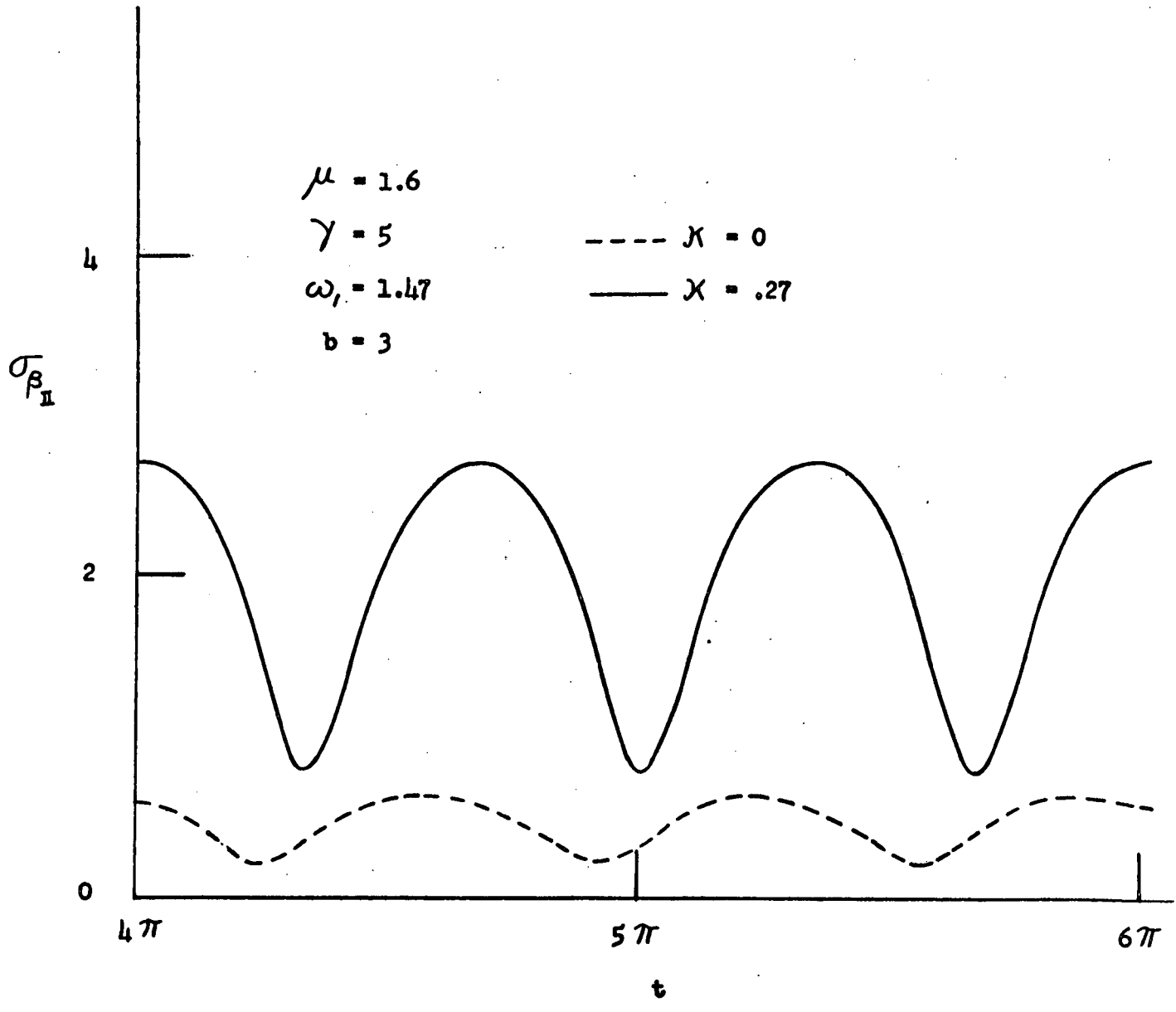

Fig. 18

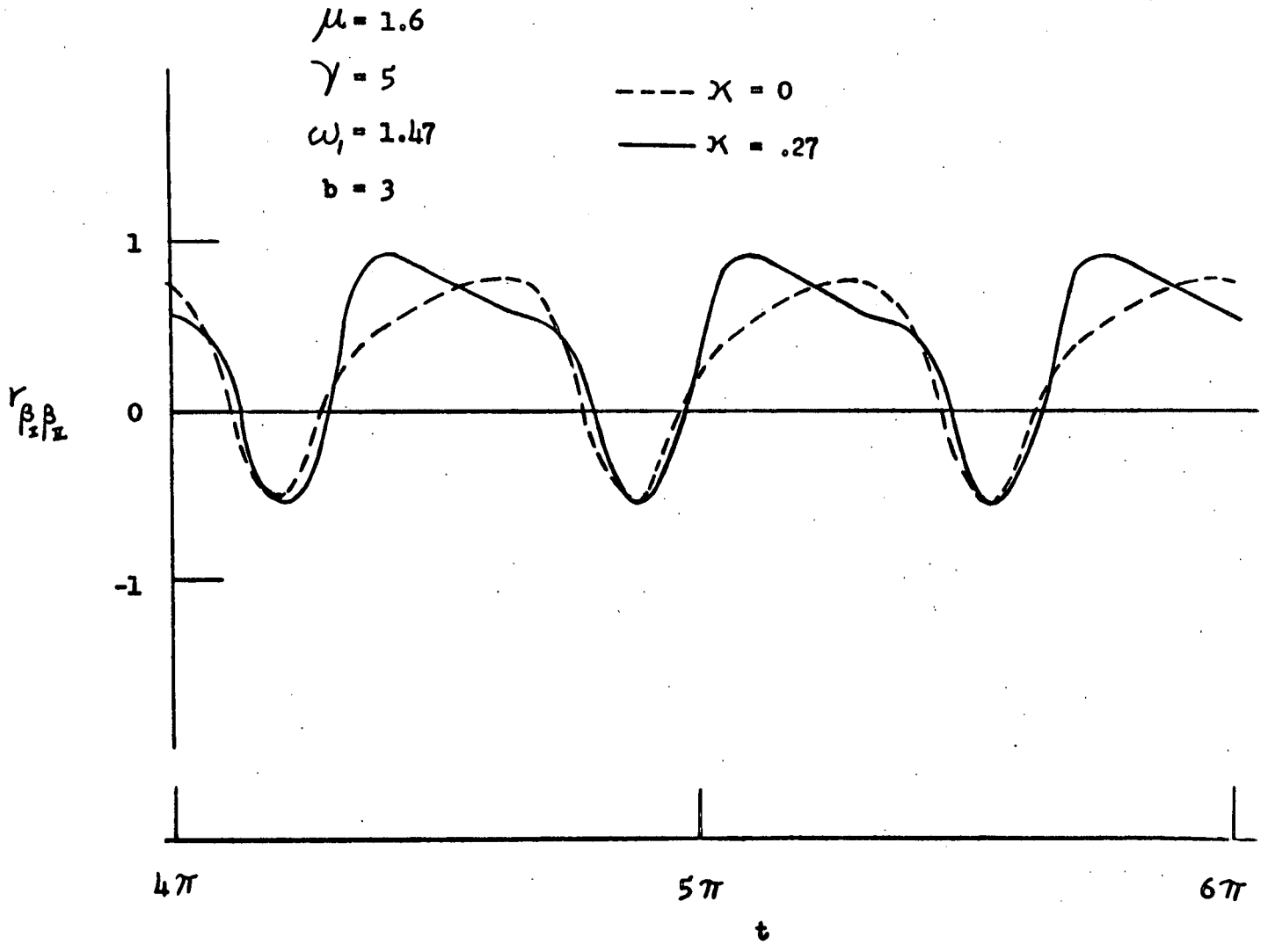

Fig. 19

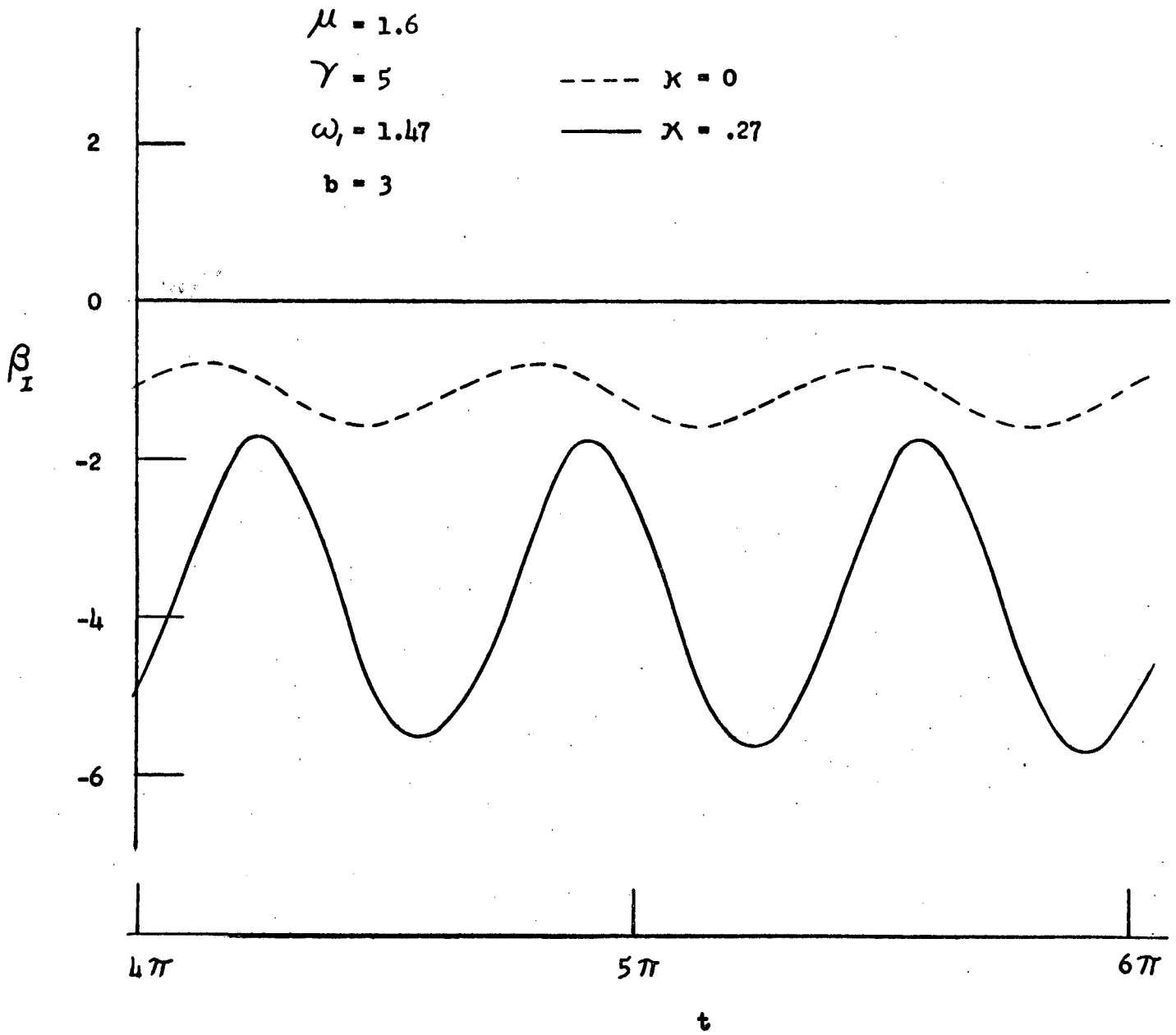

Fig. 20

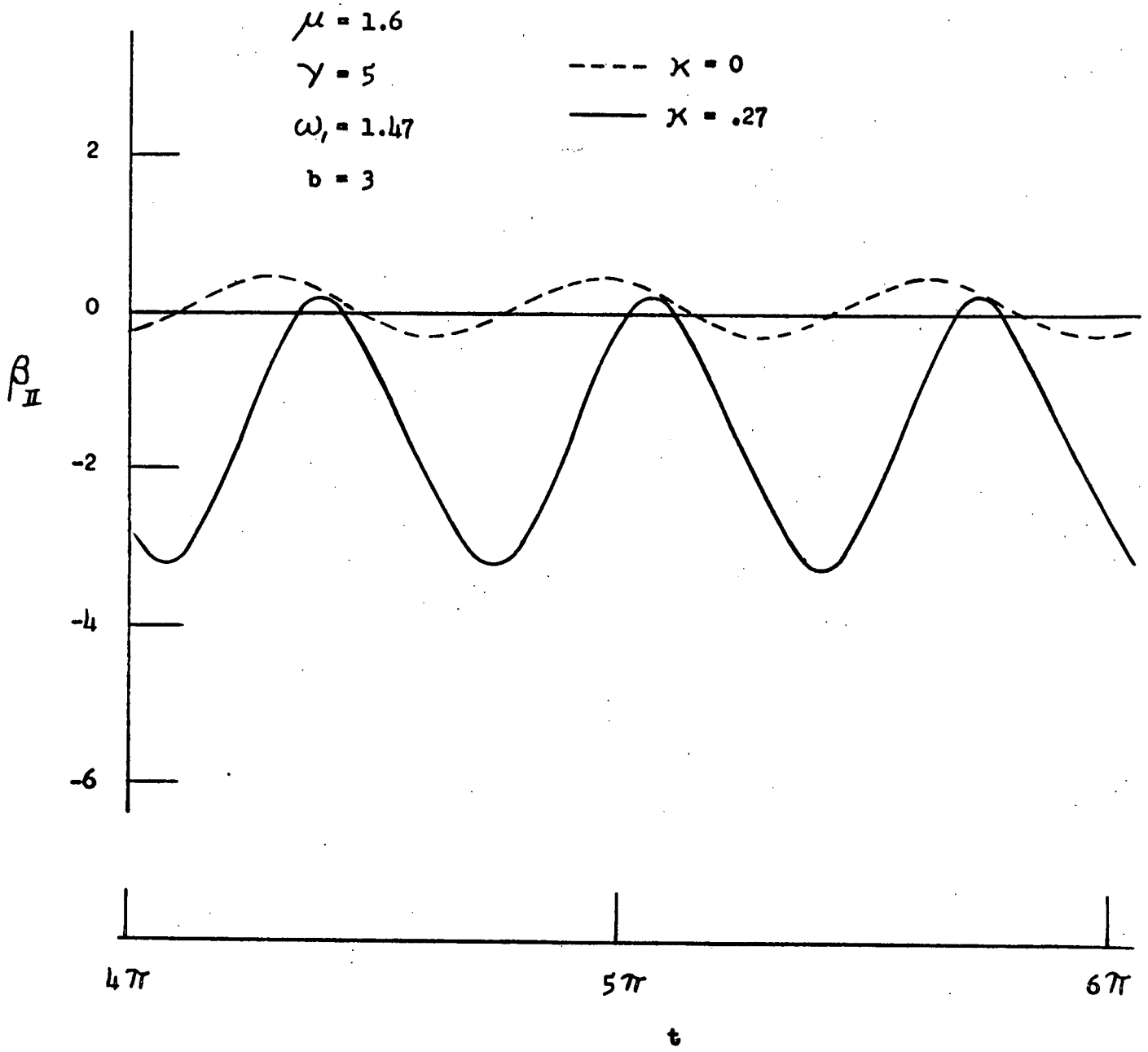

Fig. 21

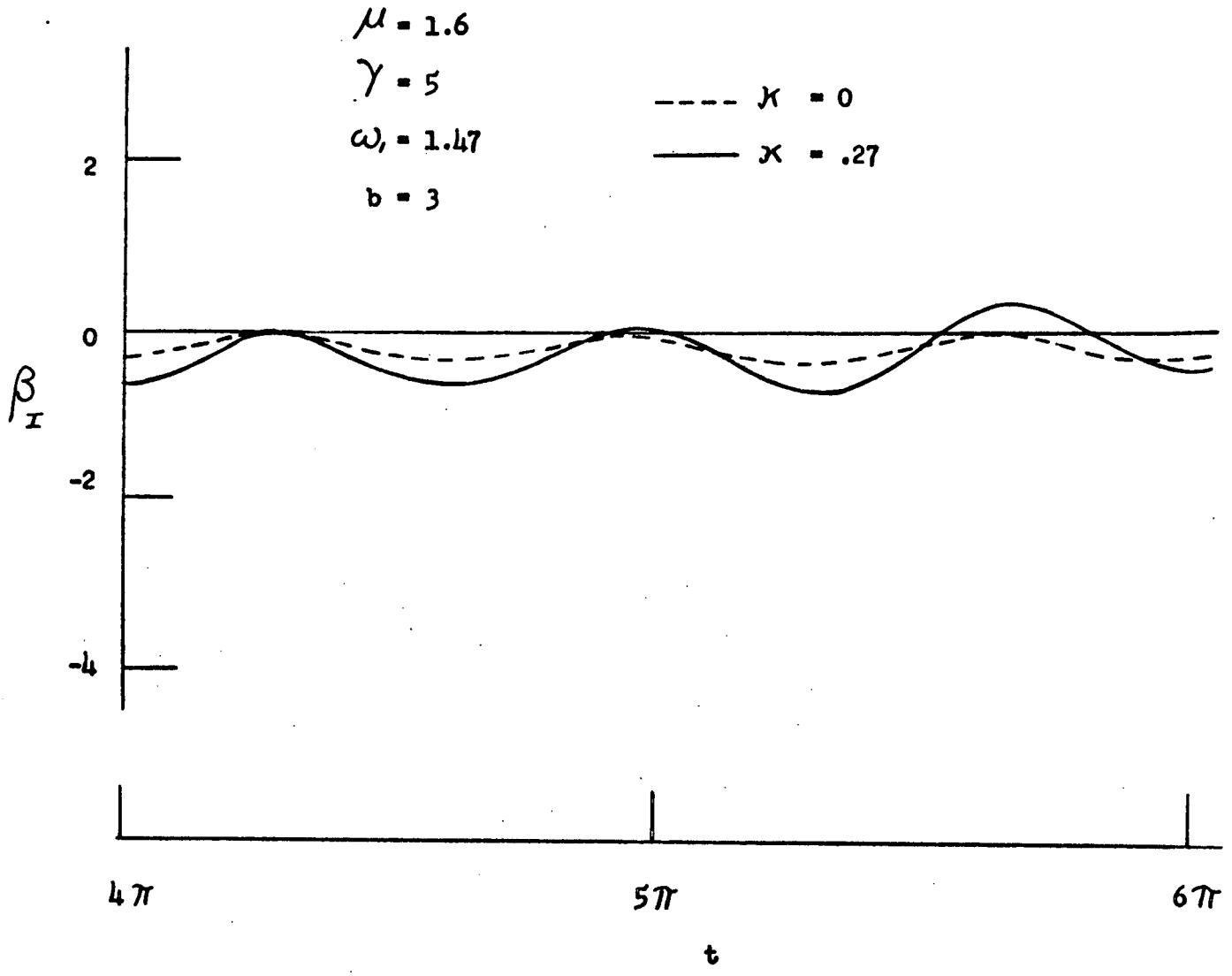

Fig. 22

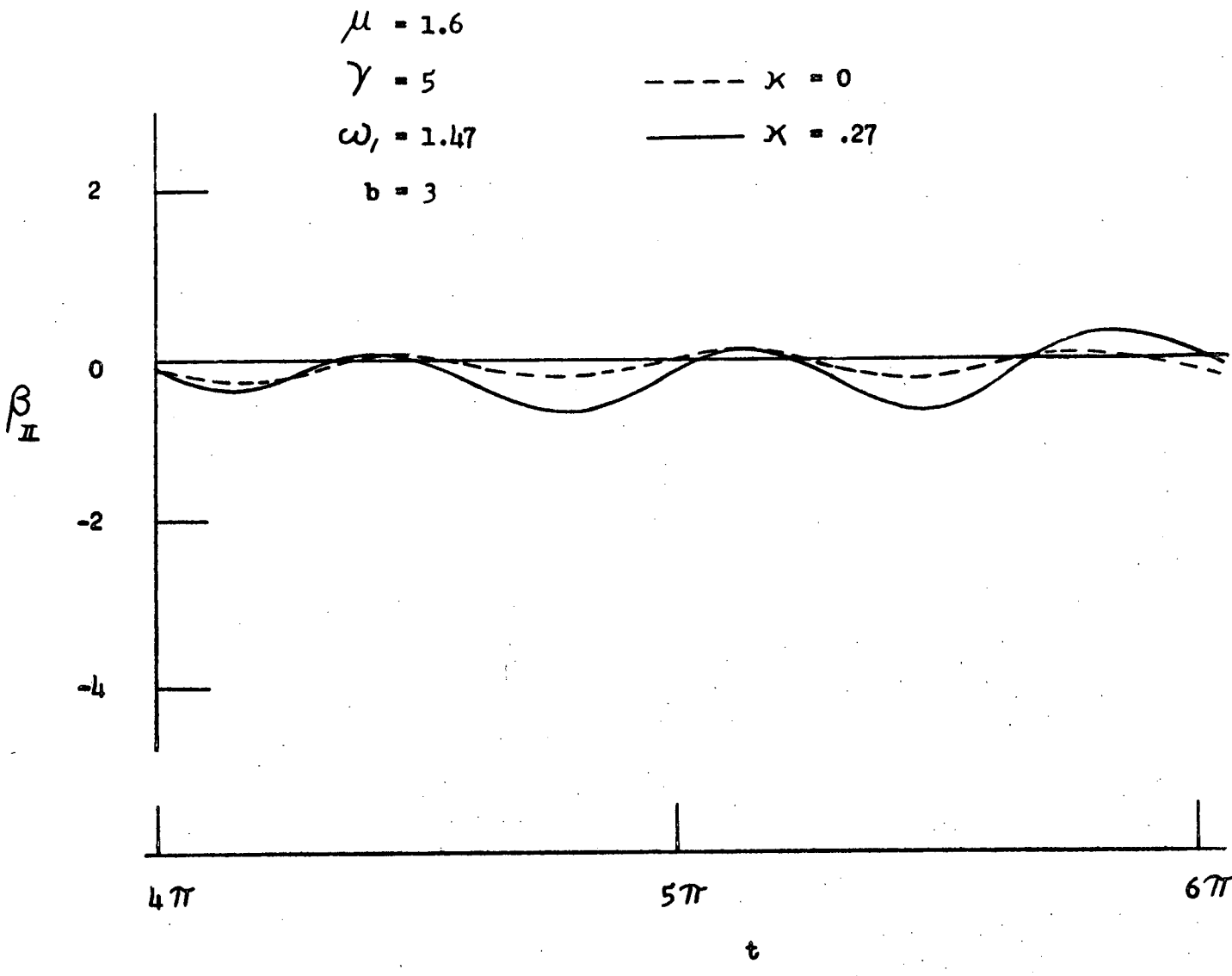

Fig. 23

Appendix A

Computation of Undamped Blade Modes

Nomenclature

Ω	rotor angular speed ($1/\Omega$ is the time unit)
R	rotor radius (length unit)
m_o	mass per unit length of blade root
$m_o R$	mass unit
$m_o R^2\Omega^2$	force unit
$T_i m_o R^2\Omega^2$	centrifugal force in ith massless segment
$m_i\ m_o R$	point mass between massless segments
$x_i\ R$	distance of m_i from rotor center
$\Delta T_i m_o R^2\Omega^2$	centrifugal force of ith point mass
$y_i\ R$	up deflection of m_i
ψ_i	slope of deflection curve at m_i
$l_i\ R$	length of ith segment
$(EI_i)\ q\ m_o R^4\Omega^2$	bending stiffness of ith segment assumed constant
EI_o	bending stiffness at blade root
$M_i m_o R^3\Omega^2$	bending moment at m_i
$S_i m_o R^2\Omega^2$	shear force to the left of m_i
$\omega\Omega$	frequency of harmonic oscillation of blade
$q = EI_o/m_o R^4\Omega^2$	non-dimensional bending stiffness of blade root
X_i	state vector at m_i with the 4 components y_i, ψ_i, M_i, S_i
ϕ_i	state transition matrix relating X_i to X_{i+1}

$x_i^{(1)}$ state vector for free end conditions $y_1 = 1$, $\psi_1 = M_1 = S_1 = 0$

$x_i^{(2)}$ state vector for free end conditions $\psi_1 = 1$, $y_1 = M_1 = S_1 = 0$

Fig. A-1 shows a massless blade segment with point mass at the left end in its maximum up position during a harmonic oscillation with circular frequency ω. The centrifugal force T_i along the element is assumed to be constant and to change only at the mass:

$$T_i = T_{i-1} + \Delta T_i \tag{A-1}$$

where

$$\Delta T_i = m_i x_i \tag{A-2}$$

Since the blade tip is to the left

$$T_i = \sum_{k=1}^{i} \Delta T_k \tag{A-3}$$

We resolve the centrifugal force T_i at the left end of the segment - but to the right of the mass - into a component along the deflected blade axis and a component $\psi_i T_i$ perpendicular to it. Deflection and slope at i+1 are

$$y_{i+1} = y_i + \psi_i \ell_i + M_i \ell_i^2/2qEI_i + (S_i + y_i m_i \omega^2 + \psi_i T_i)\ell_i^3/6qEI_i \tag{A-4}$$

$$\psi_{i+1} = \psi_i + M_i \ell_i/qEI_i + (S_i + y_i m_i \omega^2 + \psi_i T_i)\, \ell_i^2/2qEI_i \tag{A-5}$$

The moment equilibrium about the right end of the segment yields

$$M_{i+1} = M_i + (S_i + y_i m_i \omega^2 + \psi_i T_i)\, \ell_i \tag{A-6}$$

The vertical force equilibrium yields

$$S_{i+1} = S_i + m_i y_i \omega^2 \qquad \text{(A-7)}$$

Using the state vector

$$X_i = \begin{Bmatrix} Y_i \\ \psi_i \\ M_i \\ S_i \end{Bmatrix} \qquad \text{(A-8)}$$

the transition from X_i to X_{i+1} is according to Eqs. (A-4) to (A-7)

$$X_{i+1} = \phi_i X_i \qquad \text{(A-9)}$$

with the state transition matrix

$$\phi_i = \begin{bmatrix} 1 + m_i\omega^2 \ell_i^3/6qEI_i & \ell_i + T_i\ell_i^3/6qEI_i & \ell_i^2/2qEI_i & \ell_i^3/6qEI_i \\ m_i\omega^2\ell_i^2/2qEI_i & 1 + T_i\ell_i^2/2qEI_i & \ell_i/qEI_i & \ell_i^2/2qEI_i \\ m_i\omega^2\ell_i & T_i\ell_i & 1 & \ell_i \\ m_i\omega^2 & 0 & 0 & 1 \end{bmatrix} \qquad \text{(A-10)}$$

Combining the n fields:

$$X_{n+1} = \phi_n \phi_{n-1} \cdots \phi_1 X_1 \qquad \text{(A-11)}$$

X_1 at the tip of the blade has the unknowns y_1, ψ_1, while $M_1 = S_1 = 0$. We compute $X_{n+1}^{(1)}$ and $X_{n+1}^{(2)}$ for free end conditions $X_1^{(1)} = \begin{Bmatrix} 1 \\ 0 \\ 0 \\ 0 \end{Bmatrix}$, and $X_1^{(2)} = \begin{Bmatrix} 0 \\ 1 \\ 0 \\ 0 \end{Bmatrix}$.

$$Y_1 \, Y^{(1)}_{n+1} + \psi_1 \, Y^{(2)}_{n+1} = 0$$
$$Y_1 \, \psi^{(1)}_{n+1} + \psi_1 \, \psi^{(2)}_{n+1} = 0 \qquad \text{(A-12)}$$

The frequency equation is

$$\begin{vmatrix} Y^{(1)}_{n+1} & Y^{(2)}_{n+1} \\ \psi^{(1)}_{n+1} & \psi^{(2)}_{n+1} \end{vmatrix} = 0 \qquad \text{(A-13)}$$

The only unknown in Eq. (A-13) is ω. By iterating ω until Eq. (A-13) is satisfied, one obtains the natural frequencies. For each natural frequency one obtains for y = 1 from the first of Eqs. (A-12)

$$\psi_1 = - Y^{(1)}_{n+1} / Y^{(2)}_{n+1} \qquad \text{(A-14)}$$

so that now X_i can be computed for each i beginning with the known state vector

$$X_1 = \begin{Bmatrix} 1 \\ \psi_1 \\ 0 \\ 0 \end{Bmatrix} \qquad \text{(A-15)}$$

For regions of large curvature small segments ℓ_i are required, while for regions with little curvature the lengths ℓ_i can be larger. Using 20 segments the computation of two natural frequencies with associated modes takes on the IBM 360-50 computer about 10 CPU seconds. For given m_i and EI_i the natural frequencies depend only on q. For small q we have $\omega_1 = 1.0$, for large q we have

$$\omega_1 / q^{1/2} = \alpha \qquad \text{(A-16)}$$

whereby

$$\omega_1 \Omega = \frac{a}{R^2}\left(\frac{EI_o}{m_o}\right)^{1/2} \qquad \text{(A-17)}$$

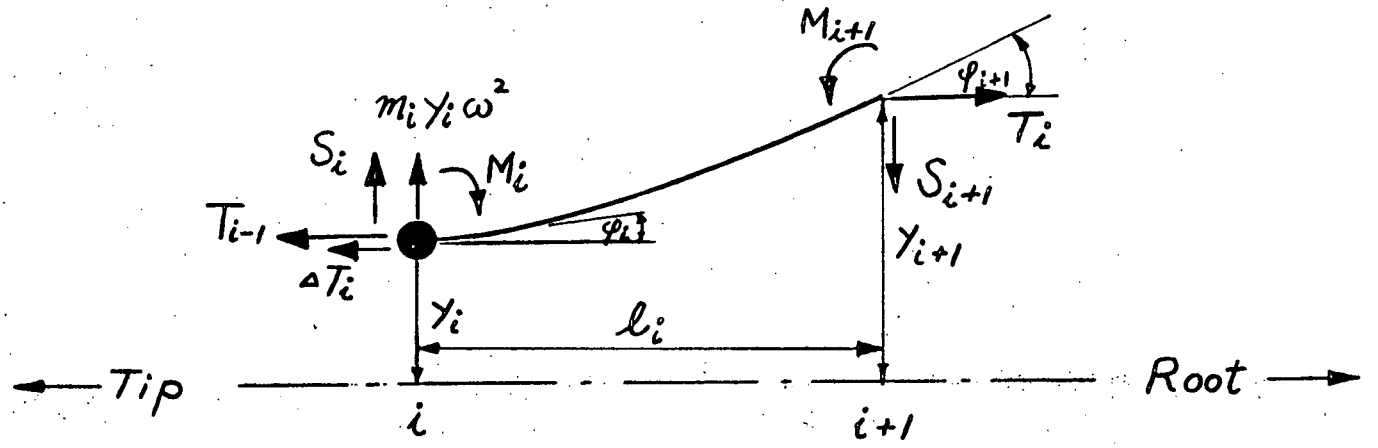

Fig. A-1

Appendix B

Fourier Coefficients of Reversed Flow Blade Analysis

For reversed flow, zero root cut out, tip loss factor B = .97 the expressions of Eq. (40) are replaced by the following truncated Fourier series:

$\mu = 0.8$

$$m_\lambda = .340 - .043 \cos 2t + .006 \cos 4t + .312 \sin t + .021 \sin 3t$$

$$m_\theta = .359 - .134 \cos 2t - .004 \cos 4t + .510 \sin t - .010 \sin 3t$$

$$m_{\theta_1} = .265 - .092 \cos 2t - .002 \cos 4t + .361 \sin t - .004 \sin 3t$$

$$K_1 = .255 \cos t - .015 \cos 3t + .003 \cos 5t + .133 \sin 2t + .008 \sin 4t$$

$$K_2 = .700 \cos t + .005 \cos 3t + .007 \cos 5t + .353 \sin 2t + .003 \sin 4t$$

$$C_1 = .234 - .017 \cos 2t + .004 \cos 4t + .220 \sin t + .010 \sin 3t$$

$$C_2 = .009 + .022 \cos 2t - .003 \cos 4t + .010 \sin t - .011 \sin 3t$$

$\mu = 1.6$

$$m_\lambda = .524 - .237 \cos 2t - .001 \cos 4t + .013 \cos 6t + .372 \sin t + .089 \sin 3t + .024 \sin 5t$$

$$m_\theta = .642 - .370 \cos 2t - .045 \cos 4t - .007 \cos 6t + 1.297 \sin t - .128 \sin 3t$$

$$m_{\theta_1} = .469 - .266 \cos 2t - .030 \cos 4t + .874 \sin t - .074 \sin 3t + .005 \sin 5t$$

$$K_1 = .648 \cos t - .190 \cos 3t + .009 \cos 5t + .014 \cos 7t + .369 \sin 2t + .091 \sin 4t + .021 \sin 6t$$

$$K_2 = 1.611 \cos t - .327 \cos 3t + .084 \cos 5t + .057 \cos 7t$$
$$+ 1.053 \sin 2t + .227 \sin 4t + .024 \sin 6t - .028 \sin 8t$$

$$C_1 = .345 - .143 \cos 2t + .006 \cos 4t + .011 \cos 6t$$
$$+ .270 \sin t + .062 \sin 3t + .014 \sin 5t$$

$$C_2 = - .019 + .035 \cos 2t + .013 \cos 4t + .004 \cos 6t$$
$$+ .031 \sin t - .006 \sin 5t$$

Appendix C

Multiblade Equations for Four Bladed Rotor without Reversed Flow Effects

For a 4 bladed rotor without reversed flow effects the multiblade equations are as follows. Terms originating from elastic flap bending are underlined.

$$\ddot{\beta}_o + \frac{\gamma_m}{2}(.221 + \underline{.028\kappa})\dot{\beta}_o + \omega_1^2\beta_o + \frac{\gamma_m}{2}(.152\mu \underline{-.014\mu\kappa})\dot{\beta}_{II}$$

$$+ \frac{\gamma_m}{2}(\underline{.457\mu\kappa})\beta_I - \frac{\gamma_m}{2}(.235\mu^2 + \underline{.535\mu^2\kappa})\beta_d = \frac{\gamma_m}{2}(.221 + .235\mu^2)\theta_o$$

$$- \frac{\gamma_m}{2}(.304\mu)\theta_I + \frac{\gamma_m}{2}(.304)\lambda \qquad \text{(C-1)}$$

$$\ddot{\beta}_I + 2\dot{\beta}_{II} + (\omega_1^2 - 1)\beta_I + \frac{\gamma_m}{2}(.221 + \underline{.028\kappa})(\dot{\beta}_I + \beta_{II})$$

$$+ \frac{\gamma_m}{2}(.304\mu + \underline{.886\mu\kappa})\beta_o + \frac{\gamma_m}{2}(.118\mu^2 + \underline{.268\mu^2\kappa})\beta_I \sin 4t$$

$$+ \frac{\gamma_m}{2}(.118\mu^2 + \underline{.268\mu^2\kappa})(1 - \cos 4t)\beta_{II} - \frac{\gamma_m}{2}(.304\mu$$

$$- \underline{.028\mu\kappa})\dot{\beta}_d \sin 2t - \frac{\gamma_m}{2}(.304\mu + \underline{.886\mu\kappa})\beta_d \cos 2t$$

$$= \frac{\gamma_m}{2}(.118\mu^2)\theta_I \sin 4t + \frac{\gamma_m}{2}(.221 + .118\mu^2 - .118\mu^2 \cos 4t)\theta_{II}$$

$$\text{(C-2)}$$

$$\ddot{\beta}_{II} - 2\dot{\beta}_I + (\omega_1^2 - 1)\beta_{II} + \frac{\gamma_m}{2}(.304\mu - \underline{.028\mu\kappa})\dot{\beta}_o$$

$$+ \frac{\gamma_m}{2}(.221 + \underline{.028\kappa})(\dot{\beta}_{II} - \beta_I) + \frac{\gamma_m}{2}(.118\mu^2 + \underline{.268\mu^2\kappa})$$

$$(1 - \cos 4t)\beta_I - \frac{\gamma_m}{2}(.118\mu^2 + \underline{.268\mu^2\kappa})\beta_{II} \sin 4t$$

$$+ \frac{\gamma_m}{2}(.304\mu - \underline{.028\mu\kappa})\dot{\beta}_d \cos 2t - \frac{\gamma_m}{2}(.304\mu + \underline{.886\mu\kappa})$$

$$\beta_d \sin 2t = \frac{\gamma_m}{2}(.608\mu)\theta_o - \frac{\gamma_m}{2}(.221 + .354\mu^2 + .118\mu^2$$

$$\cos 4t)\theta_I - \frac{\gamma_m}{2}(.118\mu^2)\theta_{II} \sin 4t + \frac{\gamma_m}{2}(.470\mu)\lambda \qquad \text{(C-3)}$$

$$- \frac{\gamma_m}{2}(.152\mu - \underline{.014\mu\kappa})(\dot{\beta}_I + \beta_{II}) \sin 2t + \frac{\gamma_m}{2}(.152 -$$

$$\underline{.014\mu\kappa})(\dot{\beta}_{II} - \beta_I) \cos 2t - \frac{\gamma_m}{2}(.235\mu^2 + \underline{.535\mu^2\kappa})$$

$$\beta_o \sin 2t - \frac{\gamma_m}{2}(.152\mu + \underline{.443\mu\kappa})\beta_I \cos 2t$$

$$- \frac{\gamma_m}{2}(.152\mu + \underline{.443\mu\kappa})\beta_{II} \sin 2t + \ddot{\beta}_d + \frac{\gamma_m}{2}(.221 + \underline{.028\kappa})\dot{\beta}_d$$

$$+ \omega_1^2\beta_d = \frac{\gamma_m}{2}(.235\mu^2)\theta_o \cos 2t - \frac{\gamma_m}{2}(.304\mu)\theta_I \cos 2t$$

$$- \frac{\gamma_m}{2}(.304\mu)\theta_{II} \sin 2t \qquad \text{(C-4)}$$

Part III

Effects of Rotor Support Flexibility

Abstract

The multiblade stability and random loads Analysis of Phase V-B Report has been extended to include angular rotor support flexibility about the longitudinal and lateral axes. The stability analysis results in whirl flutter or divergence conditions which have previously been studied only for the constant coefficient case of prop-rotor axial flow. While stiffening of the rotor support results in the removal of a divergence condition, which occurs at high advance ratio, the regressing whirl flutter margin is reduced by the higher support stiffness. Blade flap-bending flexibility which has at high advance ratio a greatly destabilizing effect is included in the analysis. A constant coefficient approximation is possible up to .8 advance ratio. Pitch-flap coupling stabilizes the divergence mode but destabilizes the regressing whirl flutter mode. The results of a random load analysis reflect the reduction in stability margin of some of the multiblade modes because of the coupling with the flexible support.

Nomenclature

α_I	pitching angular deflection of rotor support, positive down
α_{II}	rolling angular deflection of rotor support, positive to the left
α_k	angular deflection of rotor support about flapping axis of kth blade, positive up
β_k	equivalent flapping angle of kth blade, defined by straight line through first mode deflection at .73R
η	first blade mode shape
$\gamma_m = \rho acR^2/\int x\eta dm$	flexible blade Lock number
$\gamma = \rho acR^2/\int x^2 dm$	rigid blade Lock number
ζ_I, ζ_{II}	damping ratio of rotor support less blades in pitch and roll
ω_I, ω_{II}	undamped natural frequencies of rotor support less blades in pitch and roll
b	blade number per rotor
$I_b = \int x^2 dm$	blade moment of inertia
I_I, I_{II}	Pitch and roll support moments of inertia
$I_b' = \int x\eta dm$	blade moment of inertia of first blade mode shape
θ_k	pitch angle of kth blade
K_f	pitch-flap coupling ratio
κ	blade flap-bending flexibility coefficient in first blade mode: $\eta = x + \kappa \eta_h$
ω_1	first natural blade frequency when rotating, time unit $1/\Omega$
ψ_k	azimuth of kth blade

Introduction

It is known from the literature[1] that in prop-rotor flight minimal rotor support stiffnesses are required to prevent whirl flutter or divergence. The required support stiffnesses are maximum if the natural frequencies for pitch and yaw of the rotor support are equal. In this case, assuming a rigid blade and realistic nacelle to blade inertia ratios, and assuming an advance ratio of one, a nacelle frequency of about 1.8 is required. For a blade flapping frequency of $\omega_1 = 1.3$ the minimal nacelle frequency at the whirl stability limit is reduced to .6. For the prop-rotor dynamic analysis constant coefficient dynamic equations are used. This is not possible for the corresponding problem of high advance ratio lifting rotor operation, for which no whirl flutter analysis exists as yet. The multiblade analysis of Phase V-B Report has, therefore, been extended to include elastic rotor supports, and the characteristic values of the Floquet state transition matrix have been determined vs. support stiffness. Blade flap-bending flexibility, using the concept of Part II, is included in the analysis.

Dynamic Equations

The rotor support is assumed to be capable of a pitching angular deflection α_I, positive downward, and a rolling angular deflection α_{II}, positive to the left. The Kth blade then experiences an angular support deflection

$$\alpha_k = \alpha_I \cos \psi_k + \alpha_{II} \sin \psi_k \qquad (1)$$

Horizontal and vertical linear hub deflections are neglected. The horizontal hub deflections couple essentially with the chordwise blade modes which are here omitted. The vertical hub deflections couple essentially with collective blade flapping, but only weakly with the progressing or regressing whirl modes and were considered of secondary importance. In a complete dynamic analysis they should be included.

Using a space fixed reference system, and applying the single mode analysis of Part II, Eq. (30) now becomes for the kth blade

$$(1/\gamma_m)[\ddot{\beta}_k + (\omega_1^2-1)(\beta_k - \alpha_k) + \beta_k] = \int x \, df \qquad (2)$$

As compared to Eq. (30) the term $-(\omega_1^2 -1)\alpha_k(1/\gamma_m)$ has been added to the left hand side to account for the change of the elastic blade root moment due to α_k. This term gives rise to terms with factors α_I and α_{II} when the transformation to multiblade coordinates is performed according to the section "Multiblade Analysis" of Part II. For example, the second and third of the 4 multiblade equations for the 4-bladed

rotor presented in Appendix C of Part II will now have the additional terms on the right hand side:

$$\begin{aligned} &\text{Eq. (C-2)} \quad -(\omega_1^2 - 1)\,\alpha_I \\ &\text{Eq. (C-3)} \quad -(\omega_1^2 - 1)\,\alpha_{II} \end{aligned} \tag{3}$$

Furthermore, there are two new dynamic equations expressing the pitching and rolling equilibrium of the rotor support

$$\ddot{\alpha}_I + 2\zeta_I \omega_I \dot{\alpha}_I + \omega_I^2 \alpha_I = (\omega_1^2 - 1)(b/2)(I_b'/I_I)(\beta_I - \alpha_I) \tag{4}$$

$$\ddot{\alpha}_{II} + 2\zeta_{II} \omega_{II} \dot{\alpha}_{II} + \omega_{II}^2 \alpha_{II} = (\omega_1^2 - 1)(b/2)(I_b'/I_{II})(\beta_{II} - \alpha_{II}) \tag{5}$$

For some cases flapping feedback is considered in the form

$$\theta_k = - K_f \beta_k \tag{6}$$

In this case we have the following additional multiblade equations:

$$\begin{aligned} \theta_o &= - K_f \beta_o \\ \theta_I - \alpha_I &= K_f(\beta_{II} - \alpha_{II}) \\ \theta_{II} - \alpha_{II} &= - K_f(\beta_I - \alpha_I) \end{aligned} \tag{7}$$

which reduce for $K_f = 0$ to $\theta_I = \alpha_I$, $\theta_{II} = \alpha_{II}$. The effect of blade flap-bending flexibility is included in the form of Eq. (36) of Part II for the first mode, whereby the coefficient κ is zero for a rigid blade analysis and assumes various non-zero values depending on blade characteristics and rotational speed. For some cases at advance ratio $\mu = .8$ the multiblade equations were simplified to constant

coefficient equations by omitting the periodic terms in the coefficients. For an advance ratio of 1.6 the constant coefficient system of equations is invalid and the full system of equations with periodic coefficients must be used. Reversed flow effects are included in all numerical examples.

Applications to Stability Problems

We will apply the preceding theory to three cases.

Case I

Stability of a 3 bladed rotor with uniform rigid blades, $I_b/I_I = I_b/I_{II} = .20$, $\zeta_I = \zeta_{II} = 0$, $\mu = .8$ and 1.6, $\gamma = 5$ and 8, $K_f = 0$ and 1.5, $\omega_1 = 1.15$ and 1.30. $\omega_I = \omega_{II}$ variable.

The characteristic values of the Floquet state transition matrix are determined vs. $\omega_I = \omega_{II}$. The study provides data on the effect of blade natural frequency ($\omega_1 = 1.15$ and 1.30), of Lock number ($\gamma = 5$ and 8), of pitch flap coupling ($K_f = 0$ and 1.5), of advance ratio ($\mu = .8$ and 1.6) and of omitting the periodic terms for a case at $\mu = .8$.

Case II

Stability of a 3 bladed rotor with tapered elastic blades. $I_b/I_I = I_b/I_I = .20$, $\zeta_I = \zeta_{II} = 0$, $\mu = .8$ and 1.6, $\gamma = 5$, $\omega_1 = 1.47$, $K_f = 0$, $\kappa = 0$ and .27. $\omega_I = \omega_{II}$ variable. Again the characteristic values are determined vs. $\omega_I = \omega_{II}$. The study gives data on the effect of advance ratio ($\mu = .8$ and 1.6) and of blade flexibility ($\kappa = 0$ and .27).

Case III

Stability margins of a 4 bladed rotor with thickness tapered elastic blades when slowly reducing rotor speed from $\mu = .30$. Here μ is used as the parameter for the characteristic values. $\gamma = 4.5$, $I_b/I_I = .10$, $I_b/I_{II} = .16$,

$\zeta_I = \zeta_{II} = 0$. The value of κ varies with μ. $\kappa = .27$ for $\mu = .30$, $\kappa = .33$ for $\mu = .80$, $\kappa = .36$ for $\mu = 1.6$, the values of ω_I and ω_{II} also vary with μ. $\omega_I = .5, 1.33, 2.66$, $\omega_{II} = .6, 1.6, 3.2$, respectively for $\mu = .3, .8, 1.6$.

Figures 1 to 5 show the characteristic curves in the complex plane for the case I. The only modes affected by support stiffness are zero or low frequency modes, which can be interpreted as regressing flapping modes. They indicate that an increase in rotor support stiffness results in improved stability of the zero frequency mode and in reduced stability of the next higher modes. Figure 1 shows for $\mu = .8$, $\gamma = 5$ the effect of blade stiffness. The minimum support stiffness ω_I for avoiding divergence is slightly less than 0.4 for the case $\omega_1 = 1.15$ and is slightly larger than 0.4 for $\omega_1 = 1.3$. At $\omega_I = 0.6$ the regressing mode has less damping for $\omega_1 = 1.15$. Figure 2 shows for $\mu = .8$, $\omega_1 = 1.15$ the effect of blade Lock number. The minimum support stiffness ω_I is slightly less than 0.4 for $\gamma = 5$ and is 0.4 for $\gamma = 8$. Figure 3 shows that the constant coefficient approximation is at $\mu = .8$, $\gamma = 8$, $\omega_1 = 1.15$ and $\omega_I = 0.6$ approximately correct. The effect of pitch-flap coupling is shown in Figure 4. With $K_f = 1.5$ divergence is avoided even for a very low support stiffness, $\omega_I = 0.2$. However, the next higher mode has less damping. Figure 5 shows the effect of advance ratio. At $\mu = 1.6$ a support stiffness ω_I of slightly larger than 0.8 is required to avoid divergence.

At this ω_I value the next mode has little damping. It is interesting to note that the rotor support stiffness requirements for the lifting rotor are at the same advance ratio roughly the same as for the prop rotor, and the whirl flutter problem appears to be equally critical.

Figures 6 and 7 show the characteristic curves in the complex plane for the case II. At $\mu = .8$, as shown in Figure 6, the minimum support stiffness for avoiding divergence is close to $\omega_I = 0.4$ when rigid blades are assumed. If blade flexibility is included in the analysis, the minimum support stiffness required for stability is increased to a value larger than $\omega_I = 0.5$. Figure 7 shows the effect of blade flexibility on the required minimum support stiffness at $\mu = 1.6$. It is seen that when rigid blades are assumed, $\omega_I = 1.0$ or even less is satisfactory to avoid divergence. However, as blade flexibility is considered, it appears that the instability cannot be prevented in the entire region $1 < \omega_I < 1.4$.

Figure 8 shows the characteristic curves in the complex plane for the case III. It indicates that during the rotor stopping process, as μ increases from 0.3 to 1.6, the stability margins improve. Although not shown in the figure, the analysis also reveals no instability, as μ is further increased to 3.2, so that stopping the rotor appears to be safe.

Applications to Random Load Problems

One point of Case III of the preceding section pertaining to the thickness tapered elastic blades at advance ratio $\mu = .8$ was selected for a random loads analysis, comparing the rigid rotor support with the flexible rotor support. The method described in Part I Eqs. (4) to (7) was used to determine the variance matrix with the components $\sigma_{(\beta_I - \alpha_I)}$, $\sigma_{(\beta_{II} - \alpha_{II})}$ and $r_{(\beta_I - \alpha_I),(\beta_{II} - \alpha_{II})}$. Multiblade coordinates for the 4 bladed rotor, as described in Reference (2) were used. For rigid rotor support $\alpha_I = \alpha_{II} = 0$. For flexible rotor support the quantities $\beta_I - \alpha_I$, $\beta_{II} - \alpha_{II}$ are proportional to the rotor pitching and rolling moments.

Fig. 9 shows the time variable standard deviation $\sigma_{(\beta_I - \alpha_I)}$ for rigid and flexible rotor support. It is periodic with 4 per rev. Support flexibility increases the maximum standard deviation by about 20%. Fig. 10 shows the time variable standard deviation $\sigma_{(\beta_{II} - \alpha_{II})}$, also with and without support flexibility. Finally, Fig. 11 shows the time variable cross correlation coefficient between $\beta_I - \alpha_I$ and $\beta_{II} - \alpha_{II}$. As can be seen from Fig. 8, the case analyzed here has ample stability margin which is the reason why only modest increases of random load levels with support flexibility occur.

Conclusion

1. Whirl flutter of hingeless lifting rotors at high advance ratio appears to be as critical as for prop rotors, though the whirl modes are different.
2. For a rotor support with high angular flexibility divergence occurs. As the rotor support is stiffened, the divergence disappears, but a whirl flutter mode becomes unstable.
3. A hingeless rotor with a good stability margin when operating on an elastic support experiences only minor increases in random rotor loads due to the support flexibility.
4. A refinement of the analysis by including axial motion of the rotor support is desirable.
5. So far only flapwise whirl flutter at high advance ratio was studied. It is desirable to extend the analysis to include edgewise and combined edgewise and flapwise whirl flutter and divergence.

References

1. Young, M. I. and Lytwyn, R. T., "The Influence of Blade Flapping Restraint on the Dynamic Stability of Low Disk Loading Propeller Rotors", Journal American Helicopter Society, Vol. 12, No. 4, October 1967, pp. 38-54.

2. Hohenemser, K. H. and Yin, S. K., "Some Applications of the Method of Multiblade Coordinates", Journal American Helicopter Society, Vol. 17, No. 3, July 1972.

Figure Captions

Fig. 1 Stability for $b = 3$, $\gamma = 5$, $\mu = .8$, vs. Support Frequency $\omega_I = \omega_{II}$, Rigid Uniform Blade, Effect of Blade Frequency

Fig. 2 Stability for $b = 3$, $\mu = .8$, $\omega_1 = 1.15$ vs. Support Frequency $\omega_I = \omega_{II}$, Rigid Uniform Blade, Effect of γ

Fig. 3 Stability for $b = 3$, $\gamma = 8$, $\mu = .8$, $\omega_1 = 1.15$ vs. Support Frequency $\omega_I = \omega_{II}$, Rigid Uniform Blade, Constant and Periodic Coefficient Comparison

Fig. 4 Stability for $b = 3$, $\gamma = 5$, $\mu = .8$, $\omega_1 = 1.3$, vs. Support Frequency $\omega_I = \omega_{II}$, Rigid Uniform Blade, Effect of Pitch Flap Ratio K_f

Fig. 5 Stability for $b = 3$, $\gamma = 5$, $\omega_1 = 1.3$, vs. Support Frequency $\omega_I = \omega_{II}$, Rigid Uniform Blade, Effect of Advance Ratio

Fig. 6 Stability for $b = 3$, $\gamma = 5$, $\mu = .8$, $\omega_1 = 1.47$, vs. Support Frequency $\omega_I = \omega_{II}$, Thickness Tapered Blade, Effect of Blade Flexibility

Fig. 7 Stability for $b = 3$, $\gamma = 5$, $\mu = 1.6$, $\omega_1 = 1.47$, vs. Support Frequency $\omega_I = \omega_{II}$, Thickness Tapered Blade, Effect of Blade Flexibility

Fig. 8 Stability for $b = 4$, $\gamma = 4.5$, of Stopping Rotor with Thickness Tapered Flexible Blades vs. μ.

Fig. 9 Standard Deviation $\sigma_{(\beta_I - \alpha_I)}$ vs. Time for $b = 4$, $\gamma = 4.5$, $\omega_1 = 2.57$, $\mu = .8$, Thickness Tapered Flexible Blade, Effect of Support Flexibility

Fig. 10 Standard Deviation $\sigma_{(\beta_{II} - \alpha_{II})}$ vs. Time for $b = 4$, $\gamma = 4.5$, $\omega_1 = 2.57$, $\mu = .8$, Thickness Tapered Flexible Blade, Effect of Support Flexibility

Fig. 11 Cross correlation Coefficient, $r_{(\beta_I - \alpha_I),(\beta_{II} - \alpha_{II})}$ vs. Time for $b = 4$, $\gamma = 4.5$, $\omega_1 = 2.57$, $\mu = .8$, Thickness Tapered Flexible Blade, Effect of Support Flexibility

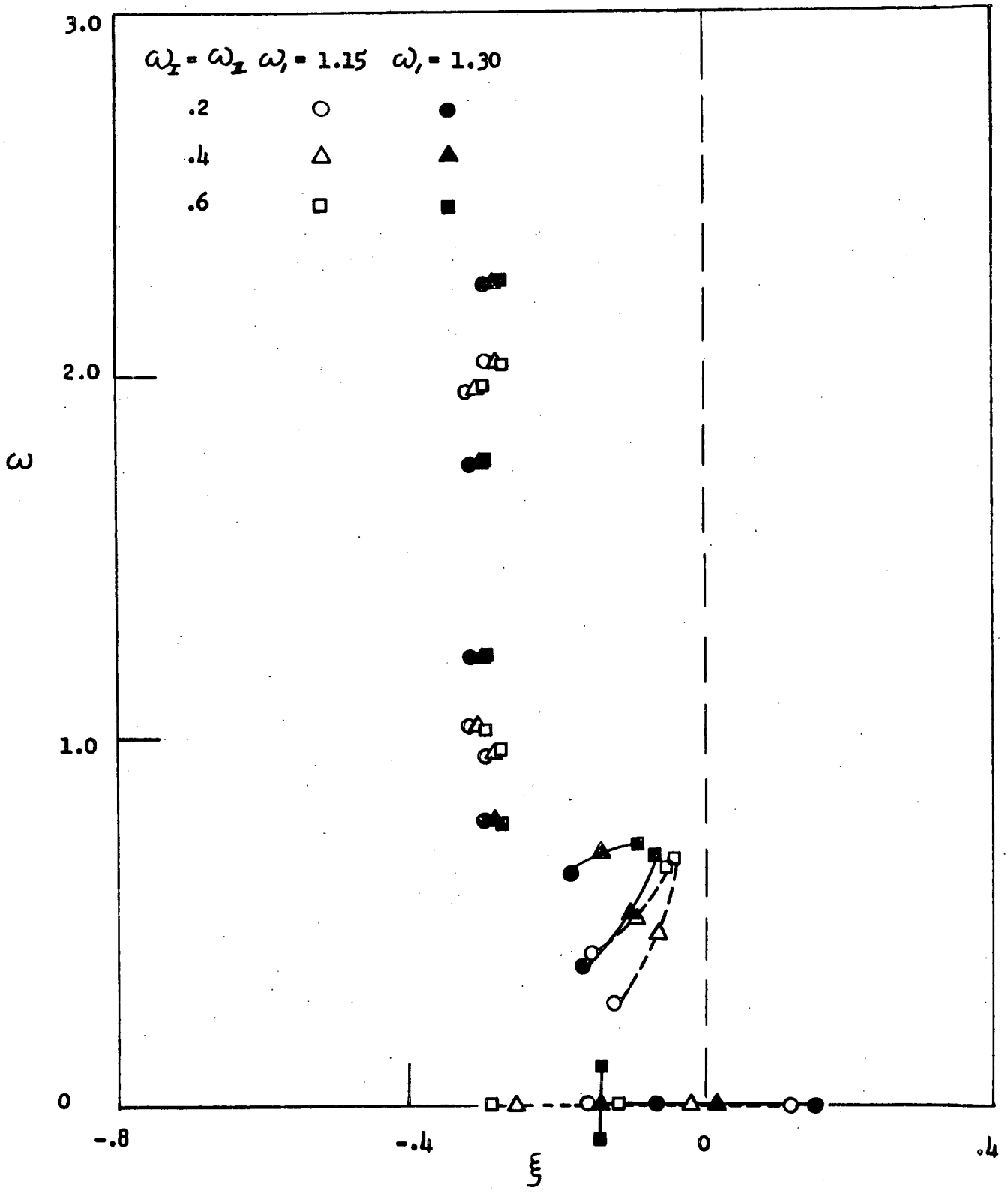
3.0
$\omega_r = \omega_i$ $\omega_1 = 1.15$ $\omega_1 = 1.30$
.2
.4
.6
2.0
ω
1.0
0
-.8
-.4
0
.4
ξ

Fig. 1

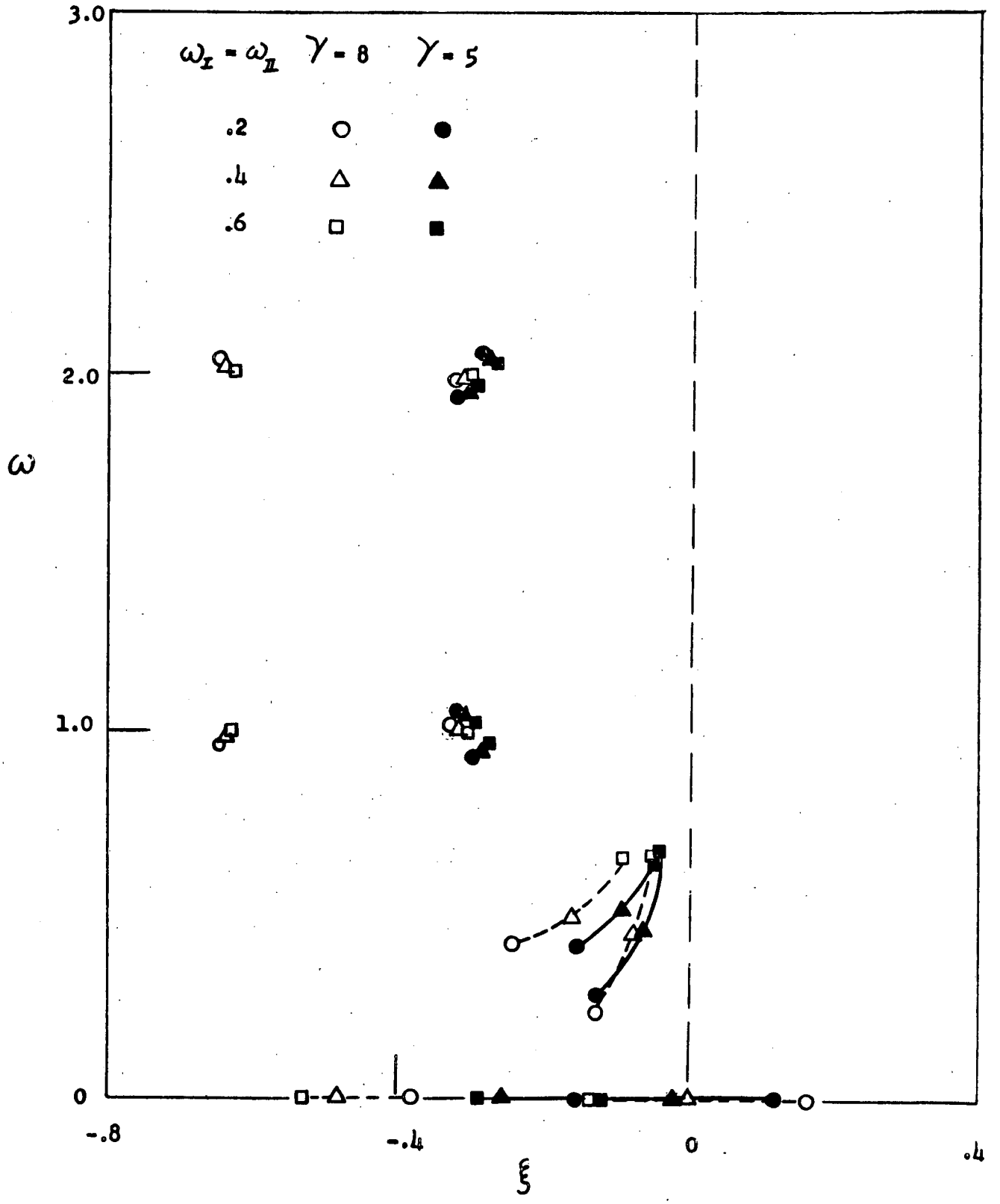

Fig. 2

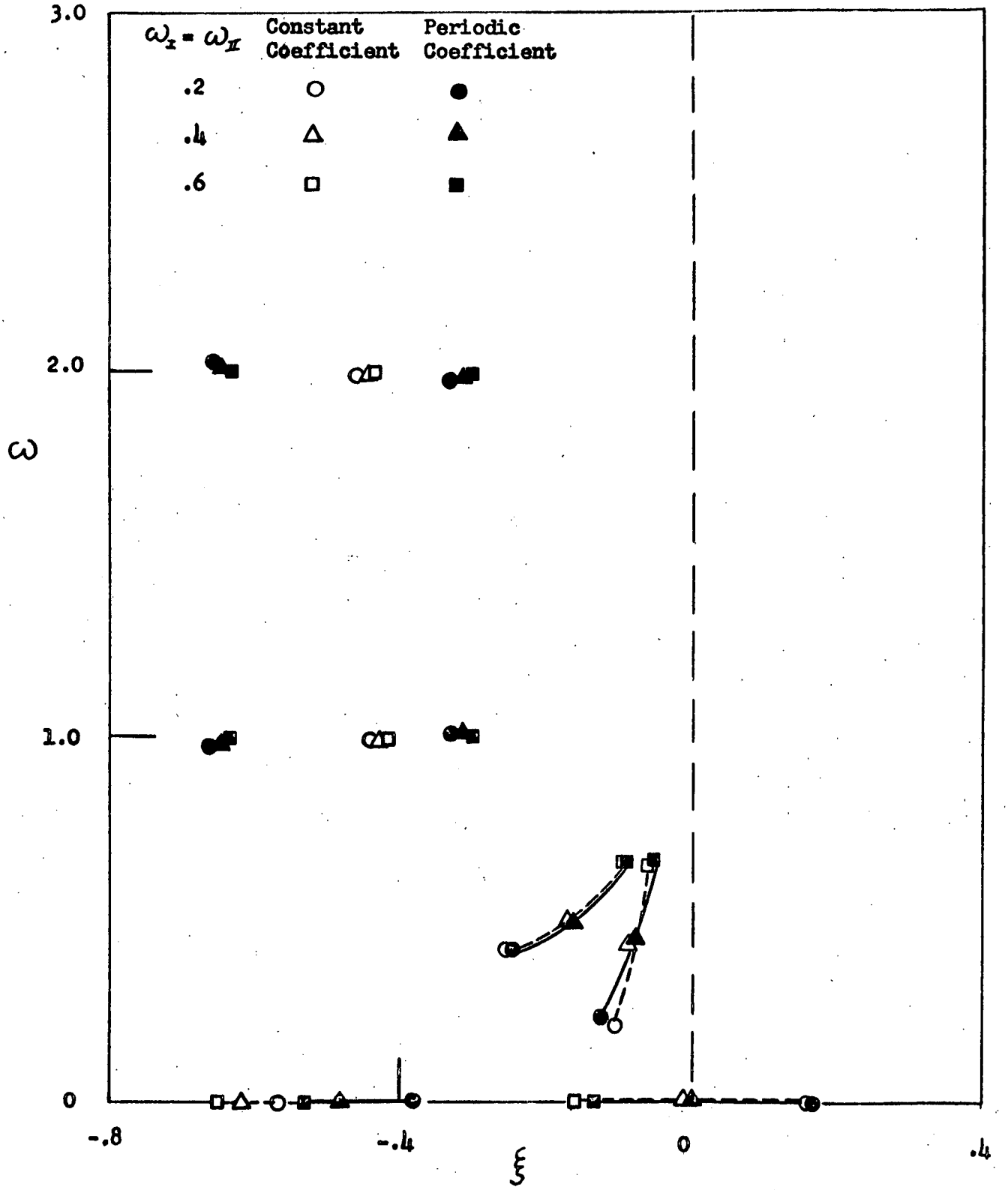
3.0
2.0
1.0
0
ω
$\omega_I = \omega_{II}$
Constant Coefficient
Periodic Coefficient
.2
.4
.6
-.8
-.4
0
.4
ξ

Fig. 3

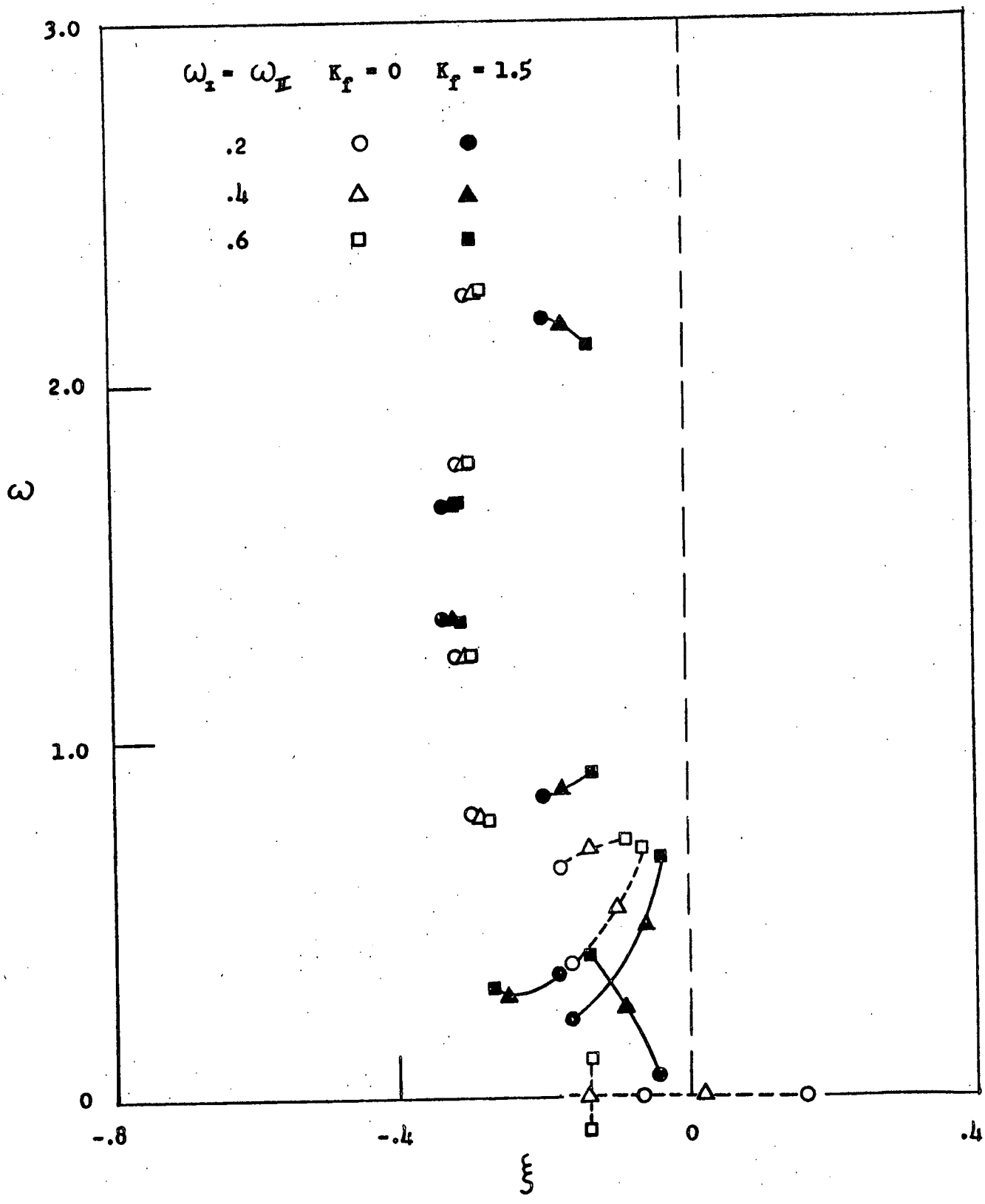

Fig. 4

C3

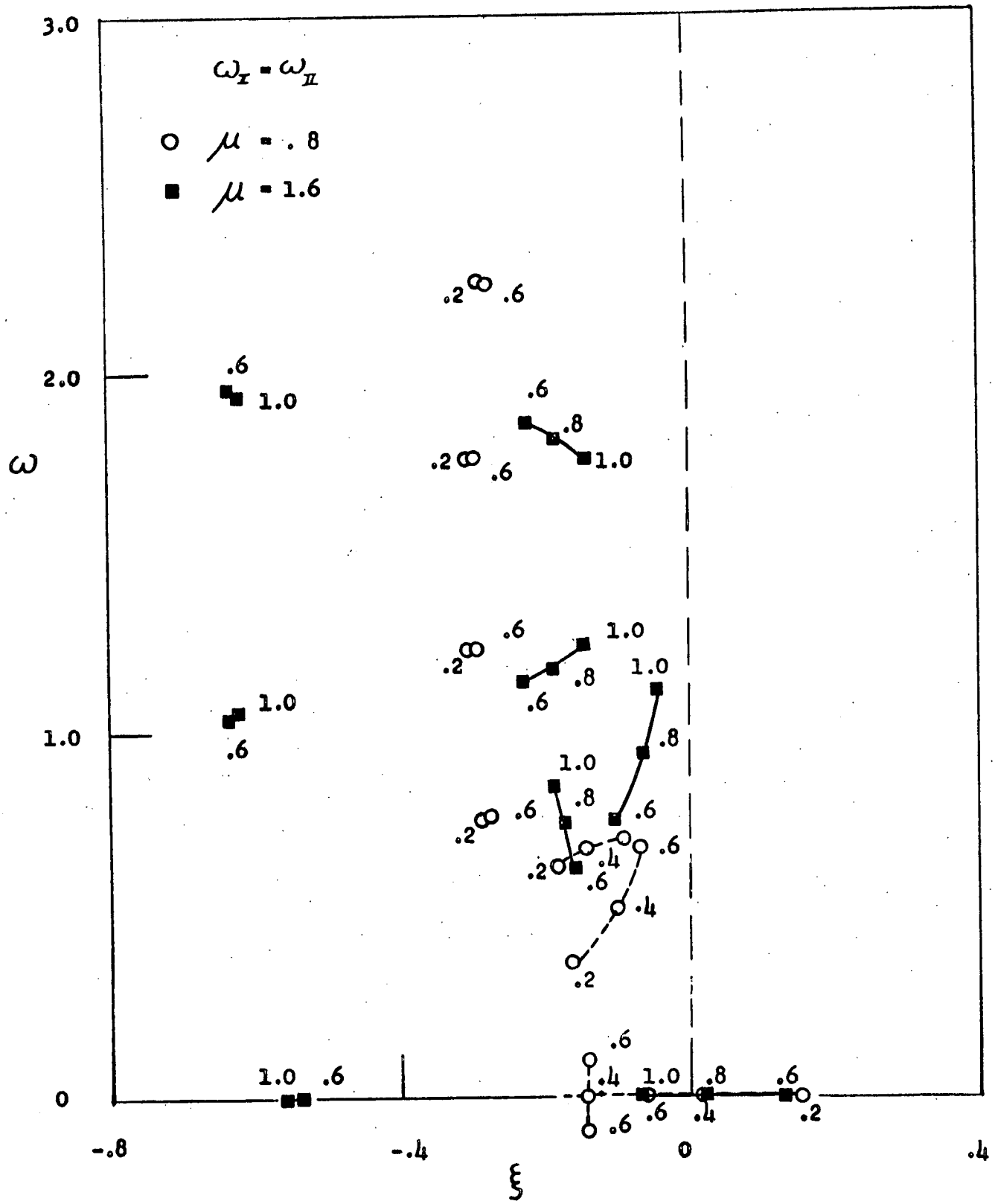

Fig. 5

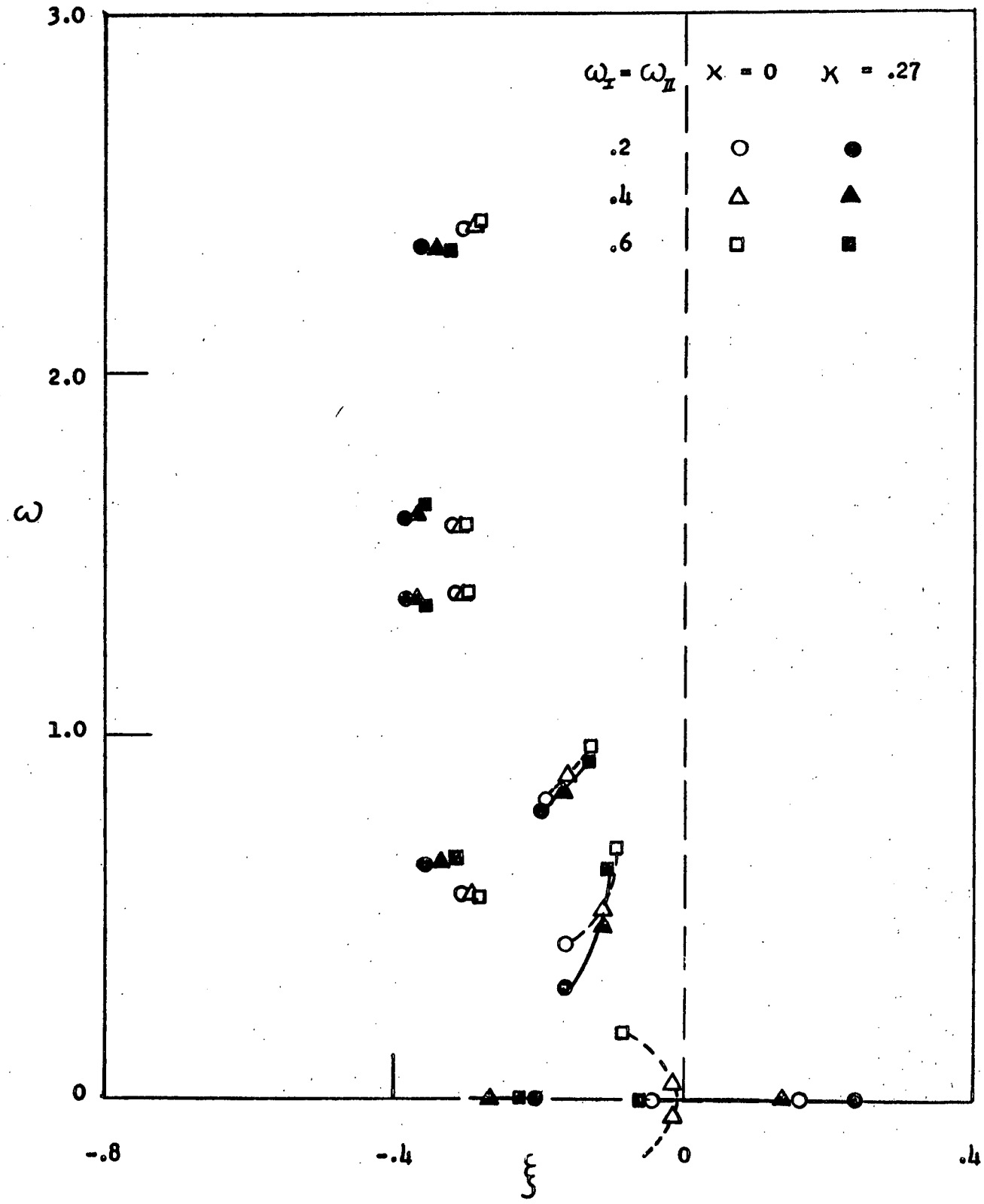

Fig. 6

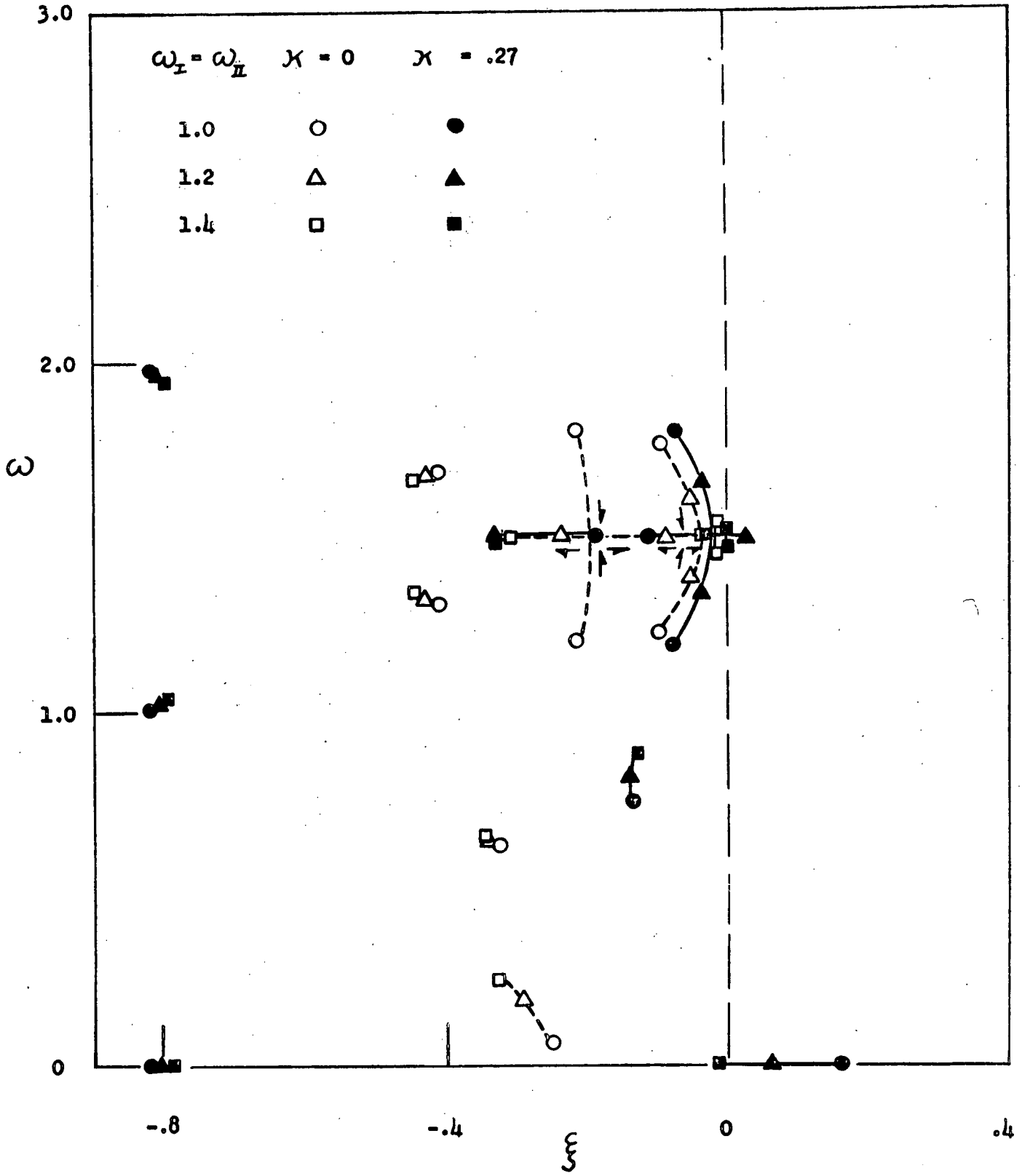
3.0
$\omega_I = \omega_{II}$ $\varkappa = 0$ $\varkappa = .27$
1.0
1.2
1.4
2.0
ω
1.0
0
-.8
-.4
0
.4
ξ

Fig. 7

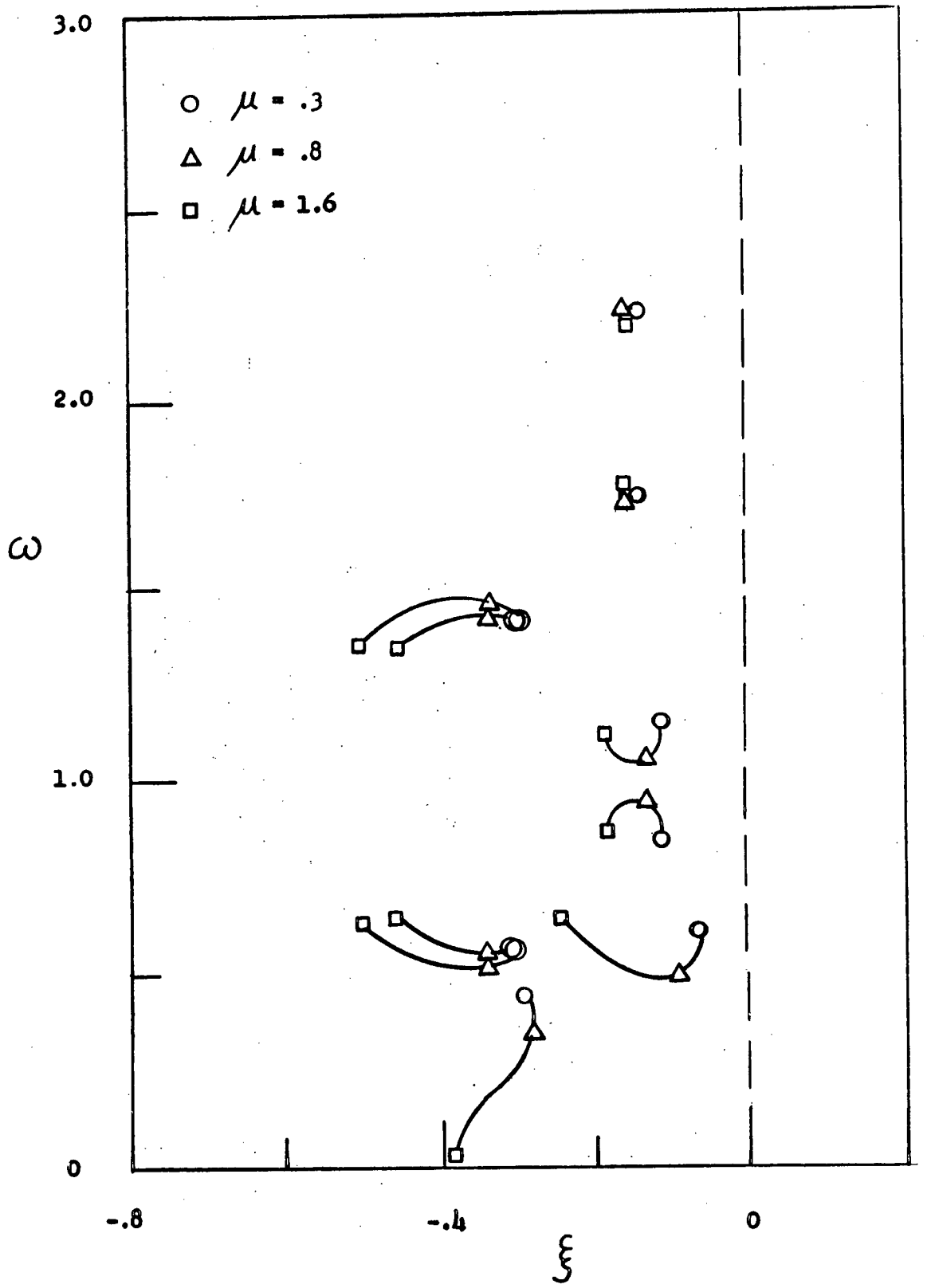

Fig. 8

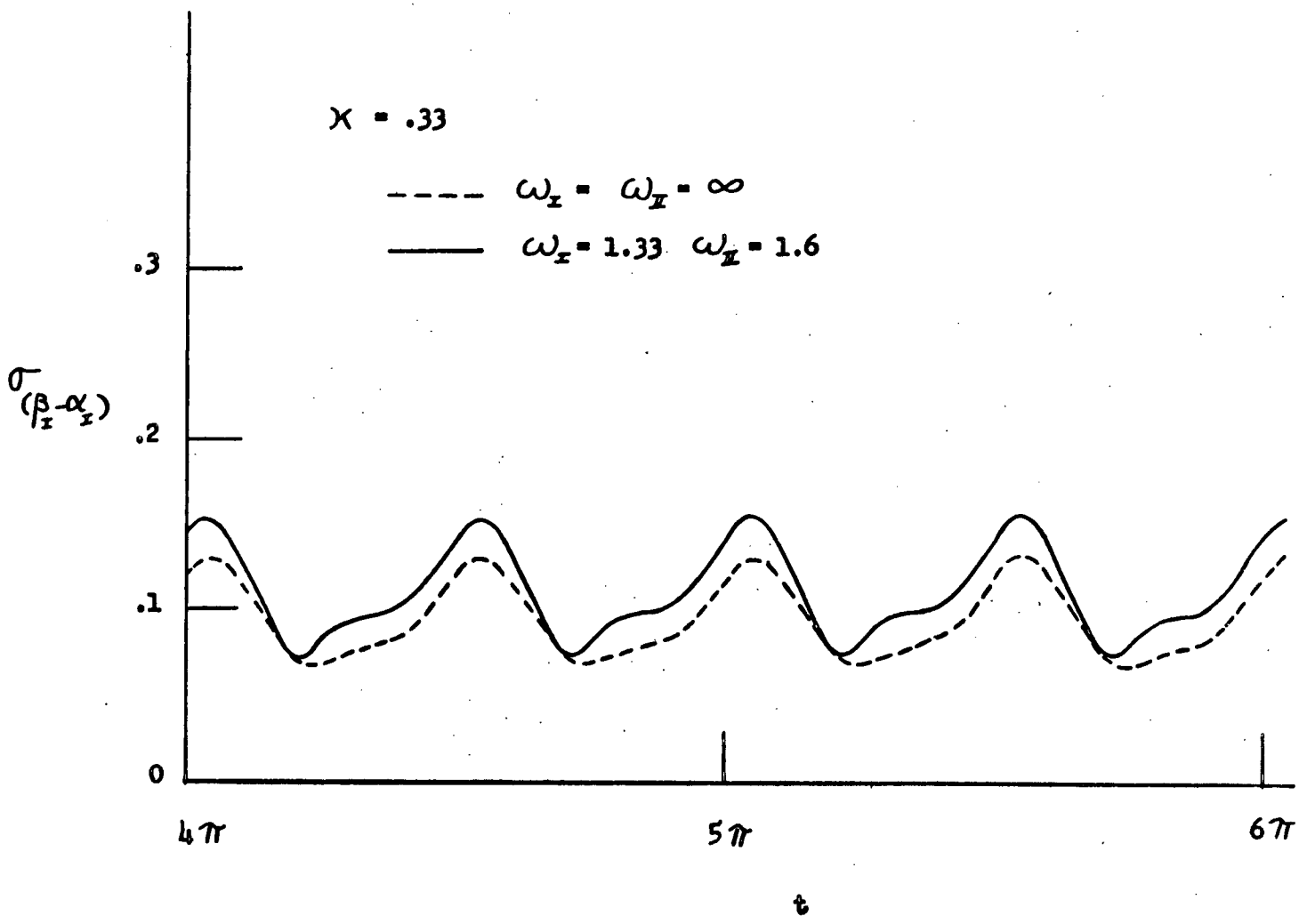
X = .33
$\omega_x = \omega_y = \infty$
$\omega_x = 1.33$ $\omega_y = 1.6$
$\sigma_{(\beta_x - \alpha_x)}$
.3
.2
.1
0
4π
5π
6π
t

Fig. 9

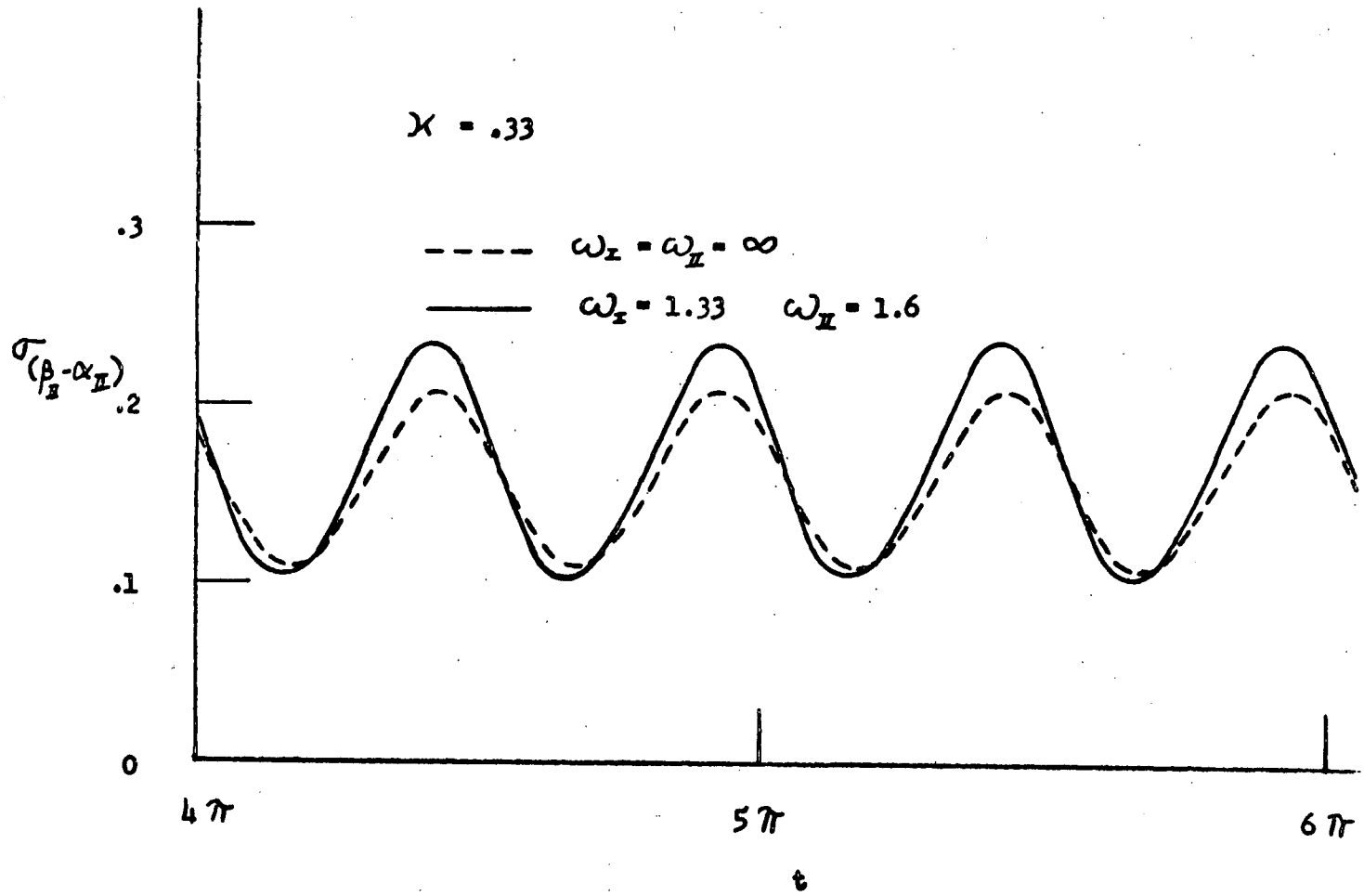
χ = .33
$\omega_I = \omega_{II} = \infty$
$\omega_I = 1.33$ $\omega_{II} = 1.6$
$\sigma_{(\beta_{II}-\alpha_{II})}$
.3
.2
.1
0
4π
5π
6π
t

Fig. 10

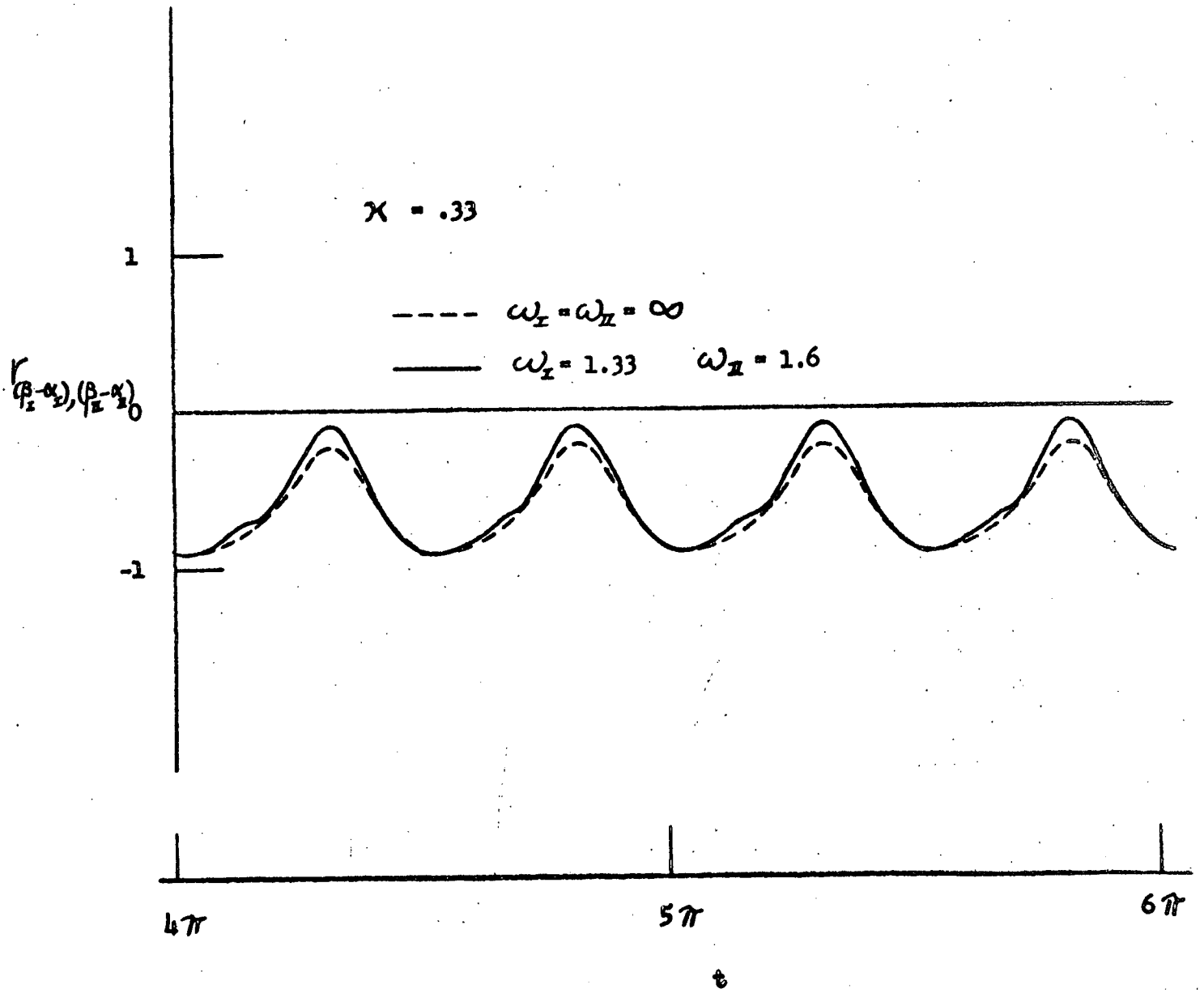
χ = .33
1
-1
---- $\omega_I = \omega_{II} = \infty$
——— $\omega_I = 1.33$ $\omega_{II} = 1.6$
$r_{(\beta_I-\alpha_I),(\beta_{II}-\alpha_{II})_0}$
4π
5π
6π
t

Fig. 11

Addendum

RESPONSE OF LINEAR PERIODICALLY TIME VARYING SYSTEMS TO RANDOM EXCITATION

D.A. Prelewicz[1]

Washington University, St. Louis, Missouri

INTRODUCTION

Recently developed stochastic models for the flapping vibration of helicopter rotor blades [1][2] give rise to the problem of determining the response of periodically time varying linear systems to random excitation. Mathematically, the problem is to determine the statistical properties of a response process $\bar{x}(t)$ satisfying

$$\left.\begin{aligned} \frac{d\bar{x}}{dt} &= A(t)\bar{x} + \bar{f} \\ A(t) &= A(t+T) \end{aligned}\right\} \qquad (1)$$

where $f(t)$ is a random input process and the matrix $A(t)$ is given in terms of system parameters.

In this note, the class of weakly periodic nonstationary processes is shown to arise in a natural way in connection with the system (1). In particular, it is shown that the steady state response of the system (1), if it exists, to a weakly periodic nonstationary process with period T is also a weakly periodic nonstationary process with period T.

[1]Assistant Professor
Associate Member AIAA

[2]Numbers in brackets designate references at end of Note

In references [1-4] both time domain and mixed time frequency domain methods have been used to calculate response statistics for (1). These relations are generalized within the framework of weakly periodic nonstationary processes.

DETERMINISTIC CASE

A solution of (1) for $t > t_0$ is [5].

$$\bar{x}(t) = Z(t,t_0)\bar{x}(t_0) + \int_{t_0}^{t} Z(t,s)\bar{f}(s)ds \tag{2}$$

where $Z(t,t_0)$ is the transition matrix satisfying

$$\left.\begin{aligned} \frac{dZ}{dt} &= A(t)Z \quad , \; t > t_0 \\ Z(t_0,t_0) &= I \text{ (identity matrix)} \end{aligned}\right\} \tag{3}$$

Furthermore, the periodicity of $A(t)$ implies that [6]

$$Z(t,t_0) = P(t)e^{C(t-t_0)}P^{-1}(t_0) \quad , \; t > t_0 \tag{4}$$

where C is a constant matrix and $P(t+T) = P(t)$. The steady state response is given by

$$\bar{x}(t) = \int_{-\infty}^{t} Z(t,s)\bar{f}(s)ds \tag{5}$$

RANDOM EXCITATION

Letting $u = t-s$ in equation (5), using (4) and taking expectations gives the following expressions for the steady state mean and autocorrelation of the output process

$$E\{\bar{x}(t)\}=\bar{\mu}_x(t) = \int_0^{\infty} P(t)e^{Cu}P^{-1}(t-u)\bar{\mu}_f(t-u)du \tag{6}$$

$$E\{\bar{x}(t_1)\bar{x}^T(t_2)\}=R_{xx}(t_1,t_2) = \int_0^{\infty}\int_0^{\infty} P(t_1)e^{Cu_1}P^{-1}(t_1-u_1) \tag{7}$$

$$R_{ff}(t_1-u_1,t_2-u_2)P^{-1T}(t_2-u_2)e^{C^Tu_2}P^T(t_2)du_1du_2$$

Suppose that $\bar{f}(t)$ exists in a mean square sense and that

$$\bar{\mu}_f(t) = \bar{\mu}_f(t+T) \tag{8}$$

$$R_{ff}(t_1,t_2) = R_{ff}(t_1+T,t_2+T) \tag{9}$$

Such a process is said to be weakly period nonstationary with period T. It is precisely these processes which are of interest in the rotor vibration problem. From (6), (7) and the periodicity of P(t) it is apparent that if the steady state response exists then it is also weakly periodic nonstationary of period T. Hence linear periodically time varying systems with period T "preserve" weakly periodic nonstationary processes of period T in the same sense that linear time invariant systems "preserve" weakly stationary processes.

The periodicity can now be used to simplify the calculation of the mean and the autocorrelation. From (2)

$$\bar{\mu}_x(t) = Z(t,t_0)\bar{\mu}_x(t_0) + \int_{t_0}^{t} Z(t,s)\bar{\mu}_f(s)ds \tag{10}$$

Using the periodicity of $\bar{\mu}_x(t_0)$

$$\bar{\mu}_x(t_0)=\bar{\mu}_x(t_0+T)= Z(t_0+T,t_0)\bar{\mu}_x(t_0)+\int_{t_0}^{t_0+T} Z(t_0+T,s)\bar{\mu}_f(s)ds \tag{11}$$

Solving for $\bar{\mu}_x(t_0)$ gives

$$\bar{\mu}_x(t_0) = [I-Z(t_0+T,t_0)]^{-1}\int_{t_0}^{t_0+T} Z(t_0+T,s)\mu_f(s)ds \tag{12}$$

Now from (2) we obtain

$$R_{xx}(t_1+T,t_2+T)=Z(t_1+T,t_1)R_{xx}(t_1,t_2+T)+\int_{t_1}^{t_1+T} Z(t_1+T,s_1)\,R_{fx}(s_1,t_2+T)\,ds_1 \tag{13}$$

$$R_{xx}(t_1,t_2+T)=R_{xx}(t_1,t_2)Z^T(t_2+T,t_2)+\int_{t_2}^{t_2+T} R_{xf}(t_1,s_2)\,Z^T(t_2+T,s_2)\,ds_2 \tag{14}$$

Substituting (14) into (13) and using the periodicity of $R_{xx}(t_1,t_2)$ gives

$$\begin{aligned} &Z^{-1}(t_1+T,t_1)R_{xx}(t_1,t_2)-R_{xx}(t_1,t_2)Z^T(t_2+T,t_2) = \\ &\int_{t_2}^{t_2+T} R_{xf}(t_1,s_2)Z^T(t_2+T,s_2)\,ds_2 \\ &+\int_{t_1}^{t_1+T} Z^{-1}(t_1+T,t_1)Z(t_1+T,s_1)R_{fx}(s_1,t_2+T)\,ds_1 \end{aligned} \tag{15}$$

where in the steady state

$$\left.\begin{aligned} R_{xf}(t_1,s_2) &= \int_{-\infty}^{t_1} Z(t_1,s_1)R_{ff}(s_1,s_2)\,ds_1 \\ R_{fx}(s_1,t_2+T) &= \int_{-\infty}^{t_2+T} R_{ff}(s_1,s_2)Z^T(t_2+T,s_2)\,ds_2 \end{aligned}\right\} \tag{16}$$

Combining (15) and (16)

$$\begin{aligned} &Z^{-1}(t_1+T,t_1)R_{xx}(t_1,t_2)-R_{xx}(t_1,t_2)Z^T(t_2+T,t_2) = \\ &\int_{t_2}^{t_2+T}\int_{-\infty}^{t_1} Z(t_1,s_1)R_{ff}(s_1,s_2)Z^T(t_2+T,s_2)\,ds_1\,ds_2 \\ &\int_{t_1}^{t_1+T}\int_{-\infty}^{t_2+T} Z(t_1,s_1)R_{ff}(s_1,s_2)Z^T(t_2+T,s_2)\,ds_2\,ds_1 \end{aligned} \tag{17}$$

where $Z(t_1,s_1)$ in the second integral on the right is

$$Z(t_1,s_1)=Z^{-1}(t_1+T,t_1)Z(t_1+T,s_1)=P(t_1)e^{C(t_1-s_1)}P^{-1}(s_1) \qquad (18)$$

It is convenient to use (17) to obtain the instantaneous autocorrelation matrix $R_{xx}(t,t)$ and to determine $R_{xx}(t_1,t_2)$ from

$$R_{xx}(t_1,t_2)=Z(t_1,t_2)R_{xx}(t_2,t_2)+\int_{t_2}^{t_1}\int_{-\infty}^{t_2} Z(t_1,s_1)R_{ff}(s_1,s_2)$$
$$Z^T(t_2,s_2)ds_2ds_1 \quad , \quad t_1 > t_2 \qquad (19)$$

obtained from (2) by letting $t_0=t_2$, postmultiplying by $\bar{x}^T(t_2)$, taking the expectation and then using the second of (16). This approach gives an explicit expression for $R_{xx}(t_1,t_2)$.

In the variables $\tau=t_1-t_2$ and $\zeta=t_1+t_2$ it is apparent that, for fixed τ, $R_{xx}(\tau,\zeta)$ is periodic in ζ with period $2T$. Also, using (7) it is easy to show that

$$R_{xx}(\tau,\zeta) = R_{xx}^T(-\tau,\zeta) \qquad (20)$$

Hence $R_{xx}(\tau,\zeta)$ is completely determined if it is known on a strip $0 \leq \tau < \infty$, $t \leq \zeta < t + 2T$.

In the special case of weakly periodic nonstationary white noise excitation, i.e.

$$R_{ff}(t_1,t_2) = F(t_1)\delta(t_1-t_2) \qquad (21)$$

where $F(t_1)=F(t_1+T)$ and $\delta(\ )$ is the Dirac delta function, (17) gives

$$Z^{-1}(t+T,t)R_{xx}(t,t)-R_{xx}(t,t)Z^{T}(t+T,t)=\int_{t}^{t+T} Z(t,s)F(s)\,Z^{T}(t+T,s)\,ds \qquad (22)$$

and (19) reduces to

$$R_{xx}(t_1,t_2) = Z(t_1,t_2)R_{xx}(t_2,t_2),\ t_1 > t_2 \qquad (23)$$

For the white noise case, a differential equation satisfied by $R_{xx}(t,t)$ is given in [3,4]. Equation (22) gives the periodic solution of that equation. Also, the above analysis shows that the direct time domain approach is not limited to white noise excitation.

SPECTRAL DENSITY

$R_{ff}(\tau,\zeta)$ is, for fixed τ, periodic in ζ with period $2T$. Hence, if $R_{ff}(\tau,\zeta)$ is absolutely integrable in τ, then it is apparent that $R_{ff}(\tau,\zeta)$ has the spectral representation

$$R_{ff}(\tau,\zeta) = \sum_{n=-\infty}^{\infty}\int_{-\infty}^{\infty} \Phi_{ff}(\omega,n)e^{i\omega\tau}e^{\frac{in\pi\zeta}{T}}\,d\omega \qquad (24)$$

Inversion yields

$$\Phi_{ff}(\omega,n) = \frac{1}{4\pi T}\int_{-\infty}^{\infty}\int_{-T}^{T} R_{ff}(\tau,\zeta)e^{-i\omega\tau}e^{-\frac{in\pi\zeta}{T}}\,d\zeta\,d\tau \qquad (25)$$

Substituting (24) into (7), using (4) and rearranging terms gives

$$R_{xx}(t_1,t_2) = \sum_{n=-\infty}^{\infty}\int_{\infty} H(t_1,\tfrac{n\pi}{T}-\omega)\Phi_{ff}(\omega,n)H^{T}(t_2,\tfrac{n\pi}{T}+\omega)\,d\omega \qquad (26)$$

where

$$H(t,\lambda) = \int_{-\infty}^{t} Z(t,s)e^{i\lambda s}\,ds \qquad (27)$$

Equation (26) is a generalization of the mixed time frequency relation used in [1] to include weakly period nonstationary excitation.

If $R_{ff}(t_1,t_2)$ can be expressed in the product form

$$R_{ff}(t_1,t_2) = F(t_1)R(t_1-t_2)G^T(t_2) \tag{28}$$

where $R(t_1,t_2)$ has a Fourier transform $\Phi(\omega)$, then

$$R_{xx}(t_1,t_2) = \int_{-\infty}^{\infty} H_1(t_1,-\omega)\Phi(\omega)H_2^T(t_2,\omega)d\omega \tag{29}$$

where

$$\begin{aligned} H_1(t,\lambda) &= \int_{-\infty}^{t} Z(t,s)F(s)e^{i\lambda s}\,ds \\ H_2(t,\lambda) &= \int_{-\infty}^{t} Z(t,s)G(s)e^{i\lambda s}ds \end{aligned} \tag{30}$$

Excitation satisfying (28) is treated in Reference [3].

It is interesting to note that a direct relationship exists between the spectral densities of the input and output processes. First notice that for fixed τ, $Z(\tau,\zeta)$ is periodic in ζ with period 2T. Hence assuming that $Z(\tau,\zeta)$ is absolutely integrable in τ, it has the same type of spectral representation as $R_{ff}(\tau,\zeta)$ namely

$$Z(\tau,\zeta) = \sum_{n=-\infty}^{\infty} \int_{-\infty}^{\infty} \Phi_z(\omega,n)e^{i\omega\tau}e^{\frac{in\pi\zeta}{T}}\,d\omega \tag{31}$$

Inverting gives

$$\Phi_z(\omega,n) = \frac{1}{4\pi T}\int_{-\infty}^{\infty}\int_{-T}^{T} Z(\zeta,\tau)e^{i\omega\tau}e^{-\frac{in\pi\zeta}{T}}\,d\zeta d\tau \tag{32}$$

Substituting (31) into (7), changing variables t_1, t_2 to τ, ζ and simplifying using the appropriate Fourier orthogonality relations yields

$$R_{xx}(\tau,\zeta) = 4\pi^2 \sum_{j,k,\ell=-\infty}^{\infty} \int_{-\infty}^{\infty} \Phi_z(\lambda+(\ell+j)\tfrac{\pi}{T},j)\Phi_{ff}(\lambda,\ell)$$
$$\Phi_z^T(-\lambda+(\ell+k)\tfrac{\pi}{T},k)e^{i\tau[(j-k)\frac{\pi}{T}+\lambda]}e^{i\zeta(j+k+\ell)\frac{\pi}{T}}\,d\lambda \qquad (33)$$

Now substituting (33) into the expression for $\Phi_{xx}(\omega,n)$ (equation (24) with f replaced by x) yields after simplification

$$\Phi_{xx}(\omega,n) = 4\pi^2 \sum_{j,k=-\infty}^{\infty} \Phi_z(\omega+(n-j)\tfrac{\pi}{T},j)\Phi_{ff}(\omega+(k-j)\tfrac{\pi}{T},n-k-j)$$
$$\Phi_z^T(-\omega+(n-k)\tfrac{\pi}{T},k) \qquad (34)$$

CONCLUSIONS

When viewed within the framework of weakly periodic nonstationary processes, the steady state analysis of the random response of periodically time varying systems is quite similar to the well known analysis of time invariant systems subject to weakly stationary excitation. That is, all of the results derived herein reduce to well known results for linear time invariant systems subject to weakly stationary excitation. These results should prove useful in the further development of rotor vibration models.

REFERENCES

1. Gaonkar, G.H. and Hohenemser, K.H., "Stochastic Properties of Turbulence Excited Rotor Blade Vibrations," AIAA Journal, Vol. 9, No. 3, March 1971, pp. 419-424.
2. Gaonkar, G.H. and Hohenemser, K.H., "Comparison of Two Stochastic Models for Threshold Crossing Studies of Rotor Blade Flapping Vibrations," AIAA Paper No. 71-389.
3. Gaonkar, G.H. and Hohenemser, K.H., "An Advanced Stochastic Model for Threshold Crossing Studies of Rotor Blade Vibrations," to appear in the AIAA Journal.
4. Wan, F.Y.M. and Lakshmikantham, C., "Rotor Blade Response to Random Loads: A Direct Time Domain Approach," AIAA Paper No. 72-169.
5. Struble, R.A., "Nonlinear Differential Equations," McGraw-Hill, New York (1962) pp. 97.
6. Ibid, pp. 106.